
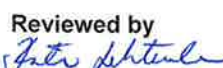



## Black carbon emissions from a ship engine in laboratory (SEA-EFFECTS BC WP1)

Authors: Päivi Aakko-Saksa<sup>1</sup>, Timo Murtonen<sup>1</sup>, Hannu Vesala<sup>1</sup>, Päivi Koponen<sup>1</sup>, Hilikka Timonen<sup>2</sup>, Kimmo Teinilä<sup>2</sup>, Minna Aurela<sup>2</sup>, Panu Karjalainen<sup>3</sup>, Niina Kuittinen<sup>3</sup>, Harri Puustinen<sup>1</sup>, Pekka Piimäkorpi<sup>1</sup>, Sami Nyysönen<sup>1</sup>, Jarno Martikainen<sup>1</sup>, Jarmo Kuusisto<sup>1</sup>, Matti Niinistö<sup>1</sup>, Tuula Pellikka<sup>1</sup>, Sanna Saarikoski<sup>2</sup>, Jesse Jokela<sup>2</sup>, Pauli Simonen<sup>3</sup>, Fanni Mylläri<sup>3</sup>, Hugo Wihersaari<sup>3</sup>, Topi Rönkkö<sup>3</sup>, Monica Tutuianu<sup>4</sup>, Liisa Pirjola<sup>5</sup>, Alekski Malinen<sup>5</sup>

<sup>1</sup>VTT, <sup>2</sup>FMI, <sup>3</sup>TUT, <sup>4</sup>AVL, <sup>5</sup>Metropolia

Confidentiality: Public

<b>Report's title</b>	
Black carbon emissions from a ship engine in laboratory (SEA-EFFECTS BC WP1)	
<b>Customer, contact person, address</b>	<b>Order reference</b>
SEA-EFFECTS BC within the Tekes Arctic Seas program	
<b>Project name</b>	<b>Project number/Short name</b>
Shipping Emissions in the Arctic – Black Carbon	SEA-EFFECTS BC
<b>Author(s)</b>	<b>Pages</b>
Päivi Aakko-Saksa <sup>1</sup> , Timo Murtonen <sup>1</sup> , Hannu Vesala <sup>1</sup> , Päivi Koponen <sup>1</sup> , Hilikka Timonen <sup>2</sup> , Kimmo Teinilä <sup>2</sup> , Minna Aurela <sup>2</sup> , Panu Karjalainen <sup>3</sup> , Niina Kuittinen <sup>3</sup> , Harri Puustinen <sup>1</sup> , Pekka Piimäkorpi <sup>1</sup> , Sami Nyysönen <sup>1</sup> , Jarno Martikainen <sup>1</sup> , Jarmo Kuusisto <sup>1</sup> , Matti Niinistö <sup>1</sup> , Tuula Pellikka <sup>1</sup> , Sanna Saarikoski <sup>2</sup> , Jesse Jokela <sup>2</sup> , Pauli Simonen <sup>3</sup> , Fanni Mylläri <sup>3</sup> , Hugo Wihersaari <sup>3</sup> , Topi Rönkkö <sup>3</sup> , Monica Tutuianu <sup>4</sup> , Liisa Pirjola <sup>5</sup> , Aleksi Malinen <sup>5</sup> <sup>1</sup> VTT, <sup>2</sup> FMI, <sup>3</sup> TUT, <sup>4</sup> AVL, <sup>5</sup> Metropolia	112 p.
<b>Keywords</b>	<b>Report identification code</b>
Black carbon, BC, EC, ship, marine, emission	VTT-R-02075-17
<b>Summary</b>	
<p>The SEA-EFFECTS BC project aims at more reliable BC evaluation for ships, and towards new on-line monitoring techniques. In WP1, the exhaust emissions of a 1.6-MW marine engine at 75% and 25% engine loads were studied in the VTT laboratory. Fuels with varying sulphur contents (0.1%, 0.5%, 2.5%) and with a biocomponent were used. From the four IMO's candidate methods, Photo-Acoustic Spectroscopy (PAS, AVL MSS), Multiangle Absorption Photometer (MAAP) and Filter Smoke Number (Smoke Meters AVL 415S and AVL 415SE) methods were covered. In addition, BC with aethalometers (AE33, AE42) and EC from filter samples were analysed. Pegasor PPS was used for on-line PM measurement. To complement these measurements, a comprehensive setup of state-of-the-art instrumentation was used to characterize chemical composition and physical properties of the exhaust gas. The most critical issue for reliable BC measurements proved to be the test set-up. MAAP designed for ambient measurements needs high dilution ratios (DR) at high BC concentrations. An extensive instrumentation and procedures are needed for adjustment, determination and verification of the high DRs, and uncertainty in DR is directly reflected in the BC results. The measurement range of MAAP is also narrow. Overall, MAAP proved not to be practical for routine measurements from marine engines. Many challenges in the BC measurements can be alleviated using instruments capable to operate at low DRs or without dilution, such as Filter Smoke Meters (FSN based BC) and AVL MSS (PAS principle). When all requirements were met, instruments rated the BC emissions in the same order despite of different measurement principles. The results also unveiled dependences between the BC emissions, fuels and loads for the engine studied. For example, reduced sulphur content of the fuel efficiently reduced the PM emission, but not necessarily the BC emission.</p>	
<b>Confidentiality</b>	Public
Espoo, 17.8.2017	
<b>Written by</b>	<b>Reviewed by</b>
 Päivi Aakko-Saksa et al. Principal Scientist	 Kati Lehtoranta Senior Scientist
	<b>Accepted by</b>
	 Jukka Lehtomäki Research Team Leader
<b>VTT's contact address</b>	
P.O.Box 1000, FI-02044 VTT	
<b>Distribution (customer and VTT)</b>	
Distribution through VTT's publication database.	
<p><i>The use of the name of VTT Technical Research Centre of Finland Ltd in advertising or publishing of a part of this report is only permissible with written authorisation from VTT Technical Research Centre of Finland Ltd.</i></p>	

## Preface

---

With the expected rise in commercial shipping in the Arctic, increased ship emissions are anticipated. International Maritime Organisation (IMO) is evaluating the needs for regional and global control of Black Carbon (BC), which increases global warming and ice melting through deposition on ice and snow. IMO has also called for voluntary measurement studies to collect data and to gain experiences with the BC measurement methods.

The SEA-EFFECTS BC project (2015-2016) aims at more reliable BC evaluation from ships, and towards new on-line monitoring techniques by using various measurement techniques in laboratory and on-board a ship. Definitions of sampling and sample treatment are essential for reliable measurements, particularly when using new fuels and emission control technologies. The first measurement campaign (WP1) of the SEA-EFFECTS BC project was conducted in 2015 with a 1.6 MW Wärtsilä Vasa 4R32 LN engine at VTT's engine laboratory. The test matrix comprised fuels with 0.1%, 0.5% and 2.5% sulphur contents and a biofuel blend. For each fuel, two engine loads corresponding to 75% and 25% were tested. Ten different BC instruments covering various methods (optical, thermal-optical and refractive) were employed. The SEA-EFFECTS BC project consists of three working packages: the first one (WP1) focused on measurements of Black carbon emissions from a marine engine in the laboratory, the second (WP2) is dedicated to the BC measurements performed on-board of ship equipped with scrubber, and finally the WP3 has the objective to assess the impact of anticipated emission regulations on business potential. This report includes the results of WP1. The results are also published as scientific articles.

SEA-EFFECTS BC partners cover four research organisations and eight industrial partners: VTT Technical Research Centre of Finland Ltd. (VTT), Finnish Meteorological Institute (FMI), Tampere University of Technology (TUT), University of Turku (UTU), Wärtsilä Finland Oy, HaminaKotka Satama Oy, VG-Shipping Oy, Pegasor Oy, Spectral Engines Oy, Gasmot Technologies Oy, Oiltanking Finland Oy and Kine Robot Solutions Oy. Invited experts in the Steering Group are Jorma Kämäräinen (Trafi), Kaarle Kupiainen (SYKE), Jukka-Pekka Jalkanen (FMI). The responsible research organisations of work within the project are VTT, FMI, TUT and UTU.

The WP1 measurements were carried out by VTT, FMI, TUT and non-partner research organisations Helsinki Metropolia University of Applied Sciences, the University of Eastern Finland (UEF). In addition, companies Pegasor Oy (Erkka Saukko), Wärtsilä Finland Oy (Juha Heikkilä), Spectral Engines Oy (Matti Tammi), AVL List GmbH (Monica Tutuianu, Austria) and Gasera contributed to the actual measurements. Acknowledgements are given to Neste and VG Shipping Oy for donation of two test fuels. The SEA-EFFECTS BC project belongs to the Arctic Seas programme of Tekes in Finland.

Financial support from Tekes (40356/14), Trafi (172834/2016) and from industrial partners, Wärtsilä, Pegasor, Spectral Engines, Gasmot, VG-Shipping, HaminaKotka Satama Oy, Oiltanking Finland Oy and Kine Robotics, and the in-kind support from AVL and Neste is gratefully acknowledged. Authors thank personnel at the research organisations and companies of the project.

Espoo, 17 August 2017

Authors

## Contents

---

Preface .....	3
Contents .....	4
1. Abbreviations .....	6
2. Introduction .....	7
3. Test set-up and protocol .....	13
3.1 Overview .....	13
3.2 Engine .....	15
3.3 Test fuels .....	16
3.4 Engine oil .....	18
3.5 Test matrix and daily protocol .....	19
3.6 Probes, dilution .....	20
3.6.1 Test set-up .....	20
3.6.2 Probes .....	21
3.6.3 Diluters .....	21
3.6.4 Determination of dilution ratio .....	22
3.6.5 Dilution ratios and their uncertainties .....	24
3.6.6 Summary of sampling, flows, residence times and sample temperatures .....	25
4. Methods .....	27
4.1 Gaseous emissions and parameters .....	27
4.2 Filter Smoke Number, AVL 415S and AVL 415SE .....	28
4.3 Photo acoustic method: AVL Micro Soot Sensor (MSS) .....	29
4.4 Multiangle Absorption Photometer, MAAP .....	29
4.5 Aethalometers .....	30
4.6 The Soot Particle Aerosol Mass Spectrometer, SP-AMS .....	31
4.7 Pegasor Particle Sensor (PPS-M) .....	32
4.8 SMPS, CPC, ELPI+ and HDTMA .....	33
4.9 Catalytic strippers and thermodenuder .....	34
4.10 Potential Aerosol Mass (PAM) chamber .....	35
4.11 PM sampling .....	35
4.12 EC analysis .....	38
4.13 Metal analysis .....	42
4.14 Anions in PM .....	42
4.15 PAHs and SOF associated with PM .....	43
4.16 Fuel/lube originating constituents in PM .....	43
4.17 Units of the results .....	43

5	Results .....	45
5.1	Stability of the test engine .....	45
5.2	Engine parameters with different fuels .....	47
5.3	Gaseous emissions .....	48
5.3.1	CO, HC, NO <sub>x</sub> and CO <sub>2</sub> .....	48
5.3.2	SO <sub>2</sub> and other gases measured with FTIR .....	50
5.3.3	Hydrocarbon measurements – new options for on-line analyses .....	52
5.4	Primary PM and its composition .....	53
5.4.1	PM emission .....	53
5.4.2	Organic carbon .....	55
5.4.3	SO <sub>4</sub> , NO <sub>3</sub> , PO <sub>4</sub> , Br, Cl, F .....	56
5.4.4	Oxygen .....	57
5.4.5	Metals in PM and fuel/lube .....	58
5.4.6	PAHs in PM .....	60
5.4.7	Summary of the PM composition .....	61
5.5	EC results .....	63
5.5.1	Possible artefacts and interpretation of the thermograms .....	63
5.5.2	Validity of samples .....	68
5.5.3	Pre-studies on sample pre-treatment and temperature programs .....	69
5.5.4	EC round-robin in three laboratories .....	74
5.6	BC results .....	77
5.6.1	Comparison of instruments .....	77
5.6.2	Summary of BC and impact of fuels and engine loads on BC .....	81
5.6.3	Standard deviations .....	84
5.7	Brown carbon .....	85
5.8	Aged aerosol .....	89
5.9	Particle sizing and volatility .....	91
5.9.1	Particle number size distributions .....	91
5.9.2	Total particle number .....	93
5.9.3	Particle volatility .....	94
5.9.4	Emission factors for soot mode particle number .....	97
6	Discussion and conclusions .....	100
	References .....	103
	Appendix 1. Results in different units .....	108
	Appendix 2. Example of thermograms using NIOSH 5040 .....	111
	Appendix 3. Yellow punch after the EC/OC analysis .....	112

## 1. Abbreviations

---

AE	Aethalometer
BC	Black carbon
CI	Compression Ignition (Diesel)
CO <sub>2</sub>	Carbon dioxide
CO	Carbon monoxide
CPC	Condensation Particle Counter
eBC	Equivalent black carbon
EC	Elemental carbon
ELPI	Electric Low Pressure Impactor
FID	Flame ionization detector
FFV	Flexible-fuel vehicles
FMPS	Fast Mobility Particle Sizer
FSN	Filter Smoke Number
FTIR	Fourier transformation infrared
H <sub>2</sub> SO <sub>4</sub>	Sulphuric acid
H/C	Hydrogen to carbon ratio
HC	Hydrocarbons
HCLD	Heated Chemiluminescence
HFID	Heated Flame Ionisation Detector
IMO	International Maritime Organisation
IOF	Insoluble Organic Fraction
IR	Infrared
kg <sub>oe</sub>	Kilogram(s) of oil equivalent (kgoe), equivalent to 41 868 kJ/kg.
LAC	Light absorbing carbon
LII	Laser Induced Incandescence
MAAP	Multi-Angle Absorption Photometry
MT	Microtroll, partial flow mini dilution tunnel, ISO 8178 compliant PM sampling
mSO <sub>4</sub>	Sulphates associated in metal and non-metal compounds (no sulphuric acid)
NDIR	Nondispersive Infrared
NH <sub>3</sub>	Ammonia
NO	Nitrogen oxide
NO <sub>2</sub>	Nitrogen dioxide
N <sub>2</sub> O	Nitrous oxide
NO <sub>x</sub>	Nitrogen oxides (NO and NO <sub>2</sub> )
OC	Organic carbon
PAH	Polyaromatic hydrocarbons
PAM	Potential Aerosol Mass chamber
PAS	Photoacoustic Spectroscopy
PM	Particulate matter
PN	Particle number
PPS-M	Pegasor Particle Sensor
Sm <sup>3</sup>	Volumetric flow in standardized conditions, 273.15 K and 101325 Pa <sup>1</sup>
SMPS	Scanning Mobility Particle Sizer
SOA	Secondary organic aerosols
SPC	AVL Smart Sampler, ISO 8178 compliant partial flow dilution PM sampling
TC	Total carbon
TC	Turbo charger
TOR	Thermal optical reflectance
TOT	Thermal optical transmittance
UV	Ultraviolet
VOC	Volatile organic compounds

<sup>1</sup> Since 1997, IUPAC standard T, P (STP) 273.15 K (0 °C) and 10<sup>5</sup> Pa. A. D. McNaught & A. Wilkinson, 1997, Compendium of Chem. Terminology ("Gold Book"). Normal T, P (NTP) 293.15 K (20 °C) and 101 325 Pa.

## 2. Introduction

---

Shipping represents 9% of the global SO<sub>x</sub> emissions and 18-30% of the global NO<sub>x</sub> emissions (Suominen 2011). The share of shipping in the global BC emissions is less than 2%, however, in the north of 70° latitude BC mostly originate from shipping (Quinn et al. 2011). BC emissions into atmosphere increases global warming directly by affecting radiative forcing of atmosphere and indirectly by increasing ice melting through deposition on ice and snow. These are of concern especially in the Arctic where ship traffic and consequently the ship emissions are anticipated to increase (Winther et al. 2014). In 2012, the largest share of Arctic ships BC emissions originated from fishing ships (45%) followed by passenger ships (20%), tankers (9%), general cargo (8%) and container ships (5%). Maritime ships also have a significant influence on the net warming in the Bay of Bengal (Ramana & Devi 2016).

IMO is currently evaluating the needs for regional and global control of BC, and work is launched to establish a methodology for the BC measurements in shipping environment. There are many items open at IMO regarding possible BC regulation, for example, if BC should be regulated from “only shipping inside the Arctic” or also from “international shipping”. It is not clear if the regulation should be for certification at test bed or “alarm” at sea. Test conditions and reference conditions are not defined, nor the measurement method/system. Development of a base line and reduction target or the control measures are not fixed, either. IMO’s Marine Environment Protection Committee (MEPC), 68th session, 11 to 15 May 2015, agreed to the need for voluntary BC measurement studies and invited interested parties to participate in voluntary data collection.

IMO has agreed on a technology-neutral definition for BC covering different properties according to Bond et al. (Bond et al. 2013): *“Black Carbon is a distinct type of carbonaceous material, formed only in flames during combustion of carbon-based fuels. It is distinguishable from other forms of carbon and carbon compounds contained in atmospheric aerosol because it has a unique combination of the following properties:*

- *It strongly absorbs visible light with a mass absorption cross section of at least 5 m<sup>2</sup>g<sup>-1</sup> at a wavelength of 550 nm;*
- *It is refractory; that is, it retains its basic form at very high temperatures, with vaporization temperature near 4000 K;*
- *It is insoluble in water, in organic solvents including methanol and acetone, and in other components of atmospheric aerosol; and*
- *It exists as an aggregate of small carbon spherules”*

One measurement method addressing all properties given in the definition does not exist. IMO has defined four candidate methods for the BC measurements: Photoacoustic Spectroscopy (PAS), Multiangle Absorption Photometry (MAAP), Laser Induced Incandescence (LII) and Filter Smoke Number (FSN) (Hellen 2015). PAS, MAAP and LII are not covered by any international standards, and dilution stage is necessary for these methods. FSN is a robust, well-known method, and the only candidate method that is currently standardised (ISO 5040). A number of intercomparisons between MAAP, aethalometers and PAS have shown good correlations but variable regression slopes (Collaud Coen et al. 2010). In addition to instrument and measurement method choices, definitions of exhaust sampling and sample treatment before actual measurements are essential, particularly when using new fuels and emission control technologies. Sampling and sample treatment can affect e.g. condensation of sulphuric acid and hydrocarbon compounds on particle surfaces and thus optical properties of exhaust aerosol and particle size distribution. Techniques for characterization of EC and BC are reviewed for example by Lack et al. (Lack et al. 2014). Recommendations for reporting of BC are given by Petzold et al. (Petzold et al. 2013).

**Special emission control areas are defined to reduce airborne emissions from ships.**

The sulphur content of shipping fuels is below 0.1%, or scrubber is used, in the SO<sub>x</sub> emission control area (SECA) of Baltic Sea, North Sea and English Channel starting from 1.1.2015. Furthermore, fuel sulphur content will be reduced globally to 0.5% from today's 3.5% in 2020 or 2025. Tier III NO<sub>x</sub> regulation is applied for new builds in 2016 in NECA areas of North America and the United States Caribbean Sea. Methane emissions are getting more attention with increasing use of LNG. Other emissions of importance may be regulated from medium to long term, such as short-lived climatic forcers, SLCF (BC, methane, ozone, HFCs), N<sub>2</sub>O, ammonia, particles, formaldehyde, and noise. These emissions have impact on climate change, environment and health. There are different technological options to meet current and anticipated emissions requirements. For example, in SECA regions ships can use 0.1%S marine fuels, scrubbers or LNG. Capability of these technological options to reduce emissions vary. LNG is a low-emission fuel having also negligible BC emissions, whereas 0.1%S diesel does not necessarily reduce NO<sub>x</sub> or BC emissions (Sippula et al. 2014). Capability of scrubbers or methanol to reduce to BC emissions has not been evidenced.

**Most of the emission species are fuel- and engine-dependent and some of them are formed in emission control devices.**

Complete combustion of hydrocarbons produces only carbon dioxide (CO<sub>2</sub>) and water, while constituents called traditionally "emissions" represent only a small share, less than 0.5% (V/V), of the total exhaust gas. Air to fuel ratio (AFR) is one of the parameters affecting the exhaust emissions from the internal combustion engines. Diesel engines use excess air (lean, AFR>1), and therefore inexpensive three-way catalysts cannot be used to reduce nitrogen oxide emissions (NO<sub>x</sub>) simultaneously with emissions of total hydrocarbons (HC) and carbon monoxide (CO). Particulate matter (PM) emissions tend to be elevated due to characteristics of diesel spray and its combustion. Emissions of THC and CO are typically at low level from diesel combustion. Emission control systems consisting of e.g. SCR are required for diesel engines to achieve low NO<sub>x</sub> emissions.

"Emissions" other than CO<sub>2</sub>

- CO, HC
- NO<sub>x</sub> consisting of nitrogen monoxide (NO) and nitrogen dioxide (NO<sub>2</sub>)
- PM consisting of BC, organic compounds, sulphates, nitrates, metals and water, amongst others
- Methane (CH<sub>4</sub>)
- Ammonia (NH<sub>3</sub>) and nitrous oxide (N<sub>2</sub>O)
- Hundreds of gaseous/semivolatle compounds, such as HCs, carbonyls, polycyclic aromatic compounds (PACs)

Engine design, operating conditions and characteristics of catalyst affect the engine-out NO<sub>x</sub> and PM emissions. Engine can be designed to minimise NO<sub>x</sub> or PM emissions, but their simultaneous control is challenging as engine design techniques reducing PM typically increases NO<sub>x</sub> emissions and vice versa. This is illustrated in Figure 2.1 for heavy-duty diesel engines (Needham 1991 in Dieselnet). Emission control devices may enhance formation of for example NH<sub>3</sub> and N<sub>2</sub>O (Mejía-Centeno et al. 2007).



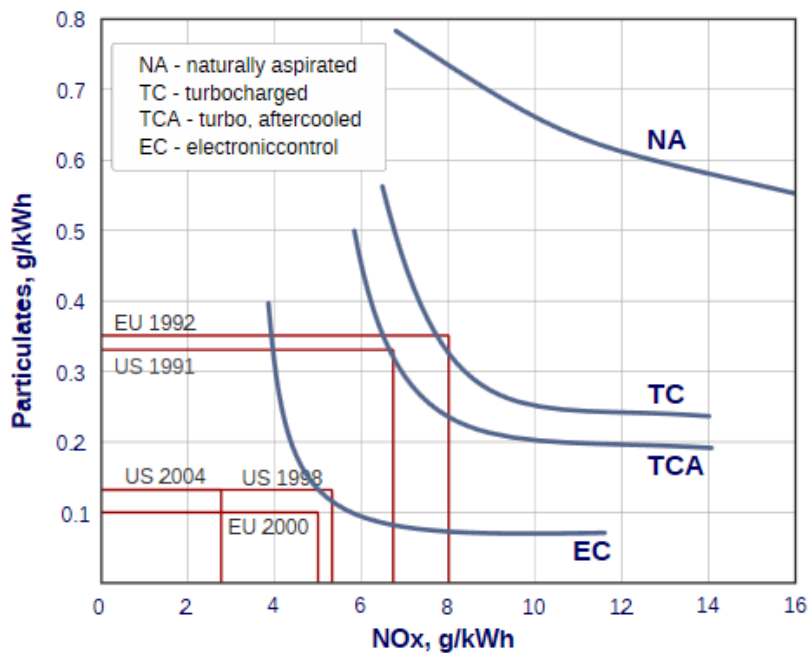


Figure 2.1.  $\text{NO}_x$ -PM trade-off for heavy-duty diesel engines (Needham 1991)

**PM in engine exhaust consists typically of carbonaceous compounds** (organic carbon=OC, black carbon=BC, brown carbon=BrC), inorganic ions (sulphates, nitrates, ammonium), metals (e.g. V, Fe, Ca, Na) and bound water. Particles containing mostly inorganic ions and/or organic carbon are typically light in color and they scatter solar radiation, and thus they are considered to cool the climate (IPCC 2013). Particles containing mostly BC, BrC and/or metals typically have dark color and they absorb light, and thus they are considered to warm the climate. Total absorbance of aerosols is linked to their chemical composition, which is dependent on the source and atmospheric ageing processes. (Bond et al. 2013; Lim et al. 2014; Collaud Coen et al. 2010; Yang et al. 2009).

In the diesel exhaust, BC and BrC are the most important light absorbing components. BC (optically determined with e.g. MAAP, aethalometer), elemental carbon (EC; determination based on thermal or thermal-optical methods e.g. Sunset OC/EC carbon analyser) or soot carbon are often used synonymously for the major light-absorbing component that forms in incomplete combustion process. However, EC, which is refractory, non-volatile material of PM measured with thermal methods is not commensurable with BC. BrC comprises of light absorbing organic compounds, such as refractory PACs originating from unburned or incompletely combusted fuel and engine oil.

The light absorption of BC is predominant in the mid-visible/long wavelength (550-950nm) where the contribution of other absorbing species is low. Soot particles are mostly insoluble in water and organic solvents (Andreae and Gelencser, 2006).

A large variety of particle phase organic compounds are typically observed in exhaust emissions; hydrocarbons, aromatic compounds etc. Mostly these compounds are colorless or light color and thus light scattering. However, recent studies have indicated that a subgroup of coloured organic compounds (e.g. long-chain, polymeric, aromatic organic compounds) that absorb solar radiation in UV wavelengths exists (Andreae and Gelencser, 2006). This spectral dependence causes the material, or its solution, to appear brown (or yellow) and thus it has been named as Brown carbon as an analogy to Black carbon. BrC contributes in shorter wavelengths than BC, absorption of BrC is strongest in UV wavelengths (300nm). BrC shows stronger wavelength-dependence than BC so its absorption steeply decreases into visible wavelengths (Andreae and Gelencser 2006). (Figure 2.2). BrC is typically formed in combustion processes, but can also form via

heterogeneous or multiphase reactions e.g. when sulphate react with organic compounds in low relative humidity (RH) (Andreae and Gelencser 2006, Yang 2009, Lim 2014)(Bond et al. 2013).

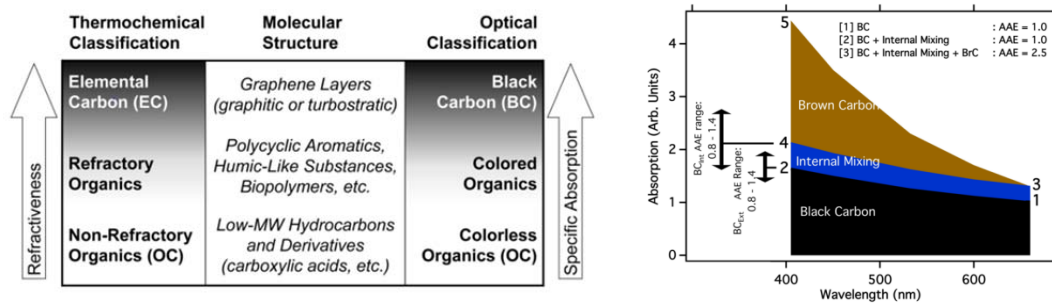


Figure 2.2 a) Classification and molecular structure of carbonaceous aerosol components (from Pöschl, 2003), b) absorption of Brown carbon as a function of wavelength (Lack and Langridge, 2013)

Optical instruments measure absorption which is converted to BC mass, by dividing the results using a “mass absorption cross section” (MAC) value. In MAAP value  $6.6 \text{ m}^2 \text{ g}^{-1}$  for BC (670nm) is used (Petzold and Schönlinner, 2004). In eathalometer value  $\sigma_{\text{air}} = 7.77 \text{ m}^2 \text{ g}^{-1}$  for BC (880nm) is used (Drinovec et al., 2015). For other wavelengths MAC values ranging from 7.19 to  $18.47 \text{ m}^2 \text{ g}^{-1}$  are used. Both “BC” and “EC” can only be regarded as “proxies” for the concentration of soot carbon, whose accuracies depend on the similarity between measured soot particles and the species used for instrument calibration.

Most filter-based techniques suffer from artefacts due to multiple scattering by the filter fibers and aerosols embedded in the filter, and by the light absorbing particles accumulation in the filter (filter-loading). (Bond et al. 2013; Hyvärinen et al. 2013). Compounds condensed on BC (coating), such as semivolatiles and water vapor, may enhance absorption by 30–50%. BrC may account for 30% of total absorption at 370nm, and even still more than 10% at mid-visible wavelengths. Most sulphates and nitrates scatter light, and thus they have a direct cooling effect. Sulphate coatings likely contribute to the longer visible light. Organonitrates can absorb light in short wavelengths (Zhang et al., 2011).

Primary BC particles, 10–90 nm spherules, do not exist by themselves in ambient air—instead they cluster together immediately after their formation in a flame to form aggregates (Wentzel et al. 2003). Small aerosol particles tend to absorb more near the UV than near the longer wavelengths. Increase in total absorption increase of 30% has been observed when loose aggregates were compared with primary spherules. (Yang et al. 2009, Andreae and Gelencser 2006, Lim et al. 2014, Collaud Coen et al. 2010, Yang et al. 2009).

Ageing of aerosol may change absorption for example due to the formation of secondary organic aerosols (SOA) (Lim et al. 2014; Collaud Coen et al. 2010; Yang et al. 2009). Kanaya et al. (Kanaya et al. 2008) estimated that coating of particles become thicker in an aged air mass, which may lead to overestimated BC due to lensing effect.

## Fuels

Heavy fuel oils (HFO) are colloidal liquids containing heavy aromatics, asphaltenes, resins, sulphur, nitrogen, oxygen and metals. “Ash” of HFO typically contains vanadium and nickel. Fuel properties affect combustion in a diesel engine, and consequently also on the efficiency and exhaust emissions. Paraffins are aliphatic hydrocarbons with excellent combustion properties. Naphthenes are also easily combustible. Aromatics have lower heating value than paraffins or naphthenes, and combustion of aromatics is also slower. Asphaltenes and resins tend to form soot through pyrolysis in combustion. Vanadium and iron together with

some other metals have been found to improve combustion. Vanadium pentoxide ( $V_2O_5$ ) catalyses formation of  $SO_3$  and  $H_2SO_4$ . Sodium (Na) leads to corrosion at temperatures above 550-600 °C (Neste 1987). In modern engines the effect of metals on combustion is presumably less important.

HFO is residual of oil refinery and thereby it contains heavy constituents with high distillation points (Figure 2.3), while distillates are substantially lighter fractions of crude oil consisting of for example C10-C12 hydrocarbons distilling from 170 °C to 250 °C. Hydrocarbon molecules of HFO may contain over 40 carbon atoms, for example asphaltenes are polar, aromatic compounds with molecular masses from 300 g/mol to 10 000 g/mol (Figure 2.4). Asphaltenes are surrounded by resin, which is also aromatic, but lighter in molecular mass and distillation than asphaltenes. Hydrogen to carbon ratio of aromatics and asphaltenes is lower than that of lighter hydrocarbons, and so is their energy content. Carbon to hydrogen ratio of HFO is for example 1.2, while that of distillates is in the range of 1.05 to 1.1.

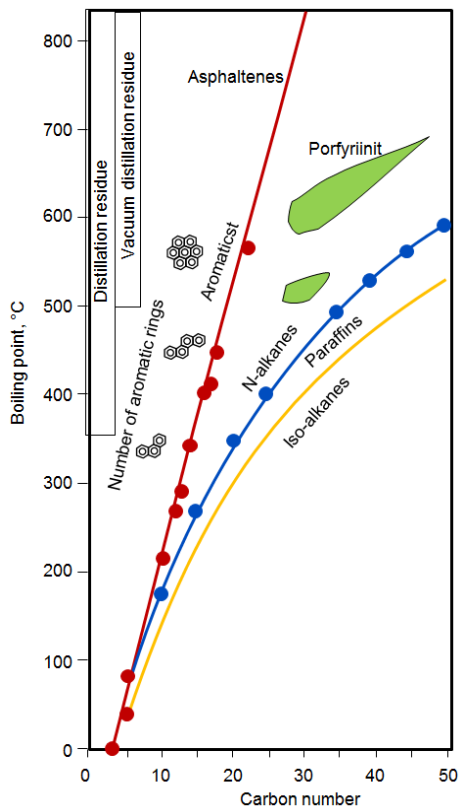


Figure 2.3. Distillation temperatures of some hydrocarbons present in HFO (Neste 1987).

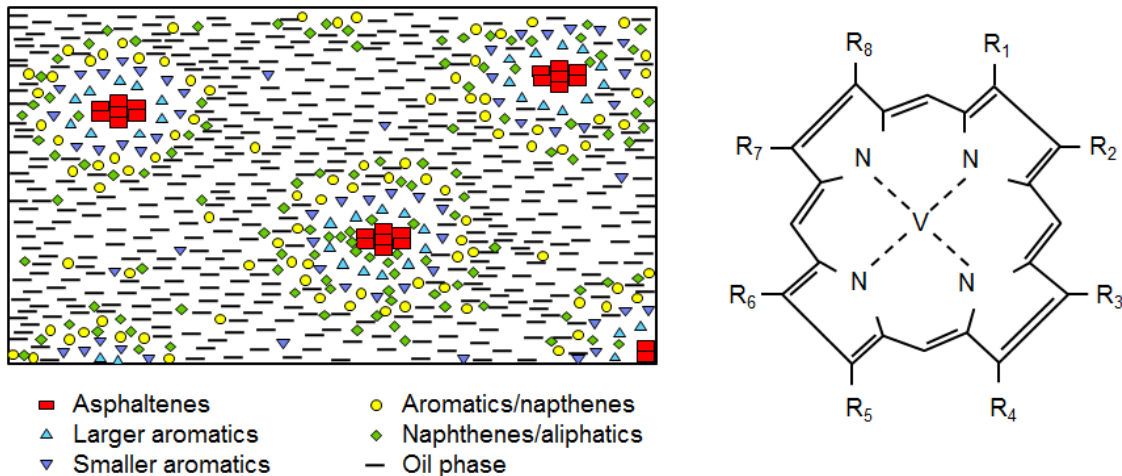


Figure 2.4. Presentation of HFO (left) and a schematic example of an asphaltene molecule (right) (Neste 1987).

Concentrations of sulphur, nitrogen and metals are highest in the asphaltene fraction of HFO (Table 2.1) (Neste 1987).

Table 2.1. Concentrations of sulphur, nitrogen and metals is the highest in the asphaltene fraction of HFO. An example by Neste (1987).

HFO composition	Share of HFO, %	Sulphur %	Nitrogen %	V ppm	Ni ppm	Carbon residue, %
Asphaltenes	11.5	4.0	1.5	740	230	50
Resins, hard	5.6	3.2	0.8	275	47	35
Resins, soft	17.0	2.6	1.0	57	33	18
Oil phase	65.9	2.0	0.3	0.2	0.1	0.5
<b>HFO</b>	<b>100</b>	<b>2.4</b>	<b>0.6</b>	<b>110</b>	<b>35</b>	<b>11.1</b>

Sulphur in fuel is combusted almost completely to  $\text{SO}_2$ , and a small share (a few percent) of fuel sulphur may be oxidised to  $\text{SO}_3$ . Elevated AFR ratio or presence of vanadium and iron may increase conversion of  $\text{SO}_2$  to  $\text{SO}_3$ . (Stuart 2010)(Neste 1987).  $\text{SO}_3$  is present as condensed  $\text{H}_2\text{SO}_4$  below its dew point<sup>2</sup>. These aerosol droplets, typically around  $1 \mu\text{m}$ , scatter light forming a “blue plume”. Dew point temperatures calculated for different sampling systems and fuels used in this project are presented in Chapter 5.4.3.

Besides condensed sulphuric acid, “sulphates” in PM may be in a form of other inorganic or organic sulphates. All of these have different capability to combine water (Chapter 4.14).

**For marine fuels with sulphur contents below 0.5% or below 0.1%**, constituents resembling those of the residual fuels may be present depending on the blending strategies and refinery processes. These “sulphur-limited” marine fuels cannot be assumed to resemble diesel fuels for high-speed diesel engines, nor does PM generated in their combustion resemble each other.

In our study, an **oxygenated biofuel** was studied. Although this biocomponent was not esterified, its implications on emissions may resemble those observed for fatty acid methyl

<sup>2</sup> A film of  $\text{H}_2\text{SO}_4$  may be deposited on surfaces and when adsorbed with PM, acidic, corrosive smuts may be formed (preventing fuel additives e.g. MgO or MgOH form solid salts). (Stuart 2010).

esters (FAME biodiesel) in earlier studies. Oils and fats have low sulphur content and they do not contain aromatics. Some stability and material problems may occur with these unsaturated polar compounds. Energy contents of oils and fats are low when compared to the distillate fuels due to their oxygen content. High density compensates this to some extent (ACEA et al. 2006; Graboski & McCormick 1998). FAME generally reduces CO, HC and PM emissions, but increases NO<sub>x</sub> emissions (McCormick et al. 2001; Sharp et al. 2000; Chang & Gerpen 1997). However, the engine, load conditions, diesel fuel used for comparison, and properties of FAME affect the results. NO<sub>x</sub> increase with FAME is assumed to be related to its high density, high distillation temperature, high oxygen content and number of double bonds. Reduction of PM emission with FAME is believed to be due to presence of oxygen. (McCormick et al. 2001; Durbin & Norbeck 2002; Grimaldi et al. 2002). FAME reduces soot (BC) portion of PM, while it may increase the organic fraction of PM. (McGill et al. 2003; Aakko & Nylund 2003; Murtonen et al. 2010). Oxidation catalyst removes soluble organic fraction (SOF) of PM efficiently, and thus a combination of FAME and oxidation catalyst can result in a substantial benefit in PM and BC emission. Mutagenic effect tested with Ames strains are typically lower for FAME than for fossil diesel fuel (low PAH content).

**This report of the SEA-EFFECTS BC project covers the results of the laboratory measurement campaign (WP1) conducted with a marine diesel engine at VTT's engine laboratory. Different BC instruments representing optical, thermal-optical and refractive methods were used. From the IMO's candidate methods, PAS, MAAP and FSN methods were covered, and a Soot-Particle Aerosol Mass Spectrometer (SP-AMS) was also included. In addition, particle sizing, composition and physical properties were analysed to increase understanding of the BC results from different instruments. This project provides data for the further evaluation of the BC measurement methods. The measurements will continue on-board of a ship equipped with scrubber (WP2).**

### **3. Test set-up and protocol**

---

#### **3.1 Overview**

The first measurement campaign of the SEA-EFFECTS BC project was conducted in 2015 with a 1.6 MW Wärtsilä Vasa 4R32 LN medium-speed engine at VTT's engine laboratory. Test fuels comprised fuels with 0.1%, 0.5% and 2.5% sulphur contents and a biofuel blend. Two engine loads used were 75% and 25%. Ten different BC instruments represented optical, refractive and thermal-optical methods. From the IMO's candidate methods, PAS, MAAP and FSN methods were covered. In addition, PM composition and physical properties were analysed as well as characteristics of particles using several state-of-the-art online instruments. The following instruments were covered:

- BC based on FSN measured with two Smoke Meters (AVL 415S and AVL 415SE). Light absorption based on measurement of the relative change in optical reflectance of visible light from a filter.
- AVL Micro Soot Sensor, the photo acoustic (PAS) method. A modulated laser beam (heating) causes a sound pressure wave detected by a microphone.
- MAAP 5012. MAAP measures relative change in optical transmission and reflectance of scattered light with multiple detectors simultaneously as particles are collected.
- Two aethalometers (MAGEE AE42 and AE33). Change in absorption of transmitted light as particles are collected.
- Elemental and organic carbon (EC/OC). The thermal-optical analysis.

- Soot Particle Aerosol Mass Spectrometer (SP-AMS). Combines the technologies from Aerosol Mass Spectrometer (AMS) for quantitative aerosol mass loadings and Single Particle Soot Photometer (SP2) for BC, organics, ions and metal analysis. Refractory carbon, rBC.
- Pegasor Particle Sensor (PPS-M), continuous monitoring. Based on electrical charge of particles.
- In-depth PM analysis with SMPS, CPC, ELPI+, HTDMA. Scanning mobility particle sizer (SMPS) measures mobility particle size distribution. Condensation particle counter (CPC) measures particle number concentration. EEPS measures the mobility particle size distribution. Electrical Low Pressure Impactor (ELPI) measures the particle size distribution according to their aerodynamic diameter. Hygroscopic Tandem Differential Mobility Analyzer (HTDMA) measures the change in particle mobility size distribution after the sample is subjected to chosen relative humidity
- Filter sampling using in-stack (EN 13284-1a) and partial flow dilution (ISO 8178) methods. Particulate mass was collected with two parallel ISO 8178 compliant collection systems (AVL Smart Sampler SPC 472 and Microtroll (MT)) to provide sufficient number of samples for compositional analyses.
- PM composition including SOF, anions, elements and analysis of polyaromatic hydrocarbons (PAHs).
- The effect of sample treatment on BC emissions was studied by using catalytic strippers (CS), thermodenuder (TD) and potential aerosol mass (PAM) chamber in front of aethalometers, MAAP, SP-AMS, Nano-SMPS, Long-SMPS and CPC according to a pre-defined program.
- Gaseous emissions with traditional techniques and real-time by using FTIR (Gaset DX-4000).

Two high dilution ratio (DR) systems were built up to meet requirements of the instruments designed for the measurements of ambient aerosols, such as MAAP and aethalometers, and for other instruments demanding high DR at high exhaust particle concentrations.

Protocol for the measurement campaign to achieve representative results was defined (e.g. fuel change, engine warm-up and load change procedures). A number of parameters related to engine, fuel and lube oil were adjusted and recorded, for example, engine speed, power, fuel mass flow rate, pressures, temperatures and humidity in different locations. Fuel containing 0.1% sulphur was tested before and after the measurement campaign to monitor stability of the set-up. Properties of all used fuels and lube oil were analysed.

## 3.2 Engine

VTT's medium-speed engine, Wärtsilä Vasa 4R32 LN with a modified configuration, was used in the tests (Figure 3.1). Table 3.1 shows basic characteristics of the engine. This engine is in the size range of auxiliary power engines in ships.



Figure 3.1. VTT's medium-speed engine, Wärtsilä Vasa 4R32 LN.

Test engine was equipped with a mechanical injection system, and consequently it is sensitive towards fuel properties, mainly viscosity and density, through their impact on start of injection and spray formation. For example, early start of injection resulted by high density and viscosity tends to

increase combustion temperature and thereby increase fuel efficiency and  $\text{NO}_x$ , while PM decreases. (Nylund et al. 1997). Modern engines equipped with common rail systems are by default less sensitive towards fuel properties than the engines with mechanical injection systems.

The engine test cell is equipped with a versatile fuel handling system for light and heavy fuel oils. In these tests, system designed for heavy fuel oil was used. Temperature of heavier fuels was adjusted to reach manufacturer's recommended viscosity for the Wärtsilä Vasa 4R32 engine (about  $16 \text{ mm}^2/\text{s}$ ). The temperatures of the fuels were adjusted to  $28\text{--}34 \text{ }^\circ\text{C}$  for the 0.1%S (fuel containing 0.1% sulphur) and Bio30 fuels, to  $100 \text{ }^\circ\text{C}$  for the 0.5%S fuel and to  $134 \text{ }^\circ\text{C}$  for the 2.5%S fuel. The fuel supply pressures varied from 9.6 to 12 bar. These differences may also have an impact on engine operation. The test engine was not specifically adjusted for each fuel in this study.

Table 3.1. Specifications of the test engine.

<b>Wärtsilä Vasa 4R32 LN E</b>	
Serial number	6399
Nominal power, kW	1640
Number of cylinders	4
Speed, rpm	750 rpm
Bore, mm	320 mm
Stroke, mm	350 mm
Compression ratio	13.8
Rotating direction	clockwise
Firing order	1-3-4-2
Exhaust valve opens / closes	56 deg bbdc / 44 deg atdc
Inlet valve opens / closes	52 deg bt dc / 28 deg abdc
Injection pump	LOrange PEO-G052
Injection valve	LOrange VUO-G186C
Injection nozzle	Wärtsilä part number 009422407; 9 x 0.53 mm x 150°
Injection nozzle opening pressure	520 bar
Static injection advance	12.3 deg
Turbocharger	BBC VTR 254 VA12 VC1 VG13 HA06 HF11 WA52 WC2 WG06 EA03 EC2 EF13

### 3.3 Test fuels

Fuels with different sulphur contents were selected for the tests: 0.1%S, 0.5%S and 2.5%S, as well as the biofuel blend. The four fuels of the measurement campaign were as follows:

- “0.1%S fuel” Marine Diesel Oil (MDO DMB)
- “0.5%S fuel” Fuel oil representing the intermediate fuel oil (IFO)
- “2.5%S fuel”, Heavy fuel oil (HFO)
- “Bio30”, Biofuel blend with Marine diesel oil in ratio of 30/70



*Figure 3.2. Tanker truck for HFO delivery and an IBC container.*

The 0.1%S and 0.5%S fuels arrived by tanker, and they were stored in 1 m<sup>3</sup> IBC containers at 40-50 °C (Figure 3.2). 2.5%S fuel was used directly from a tanker truck. Biofuel arrived in 1 m<sup>3</sup> IBC containers.

Samples from each fuel container were analysed for densities to verify that fuels were homogenous and not contaminated. Fuel samples were analysed by ASG Analytik-Service GmbH. Fuel properties are shown in Table 3.2.



Table 3.2. Properties of the test fuels analysed by ASG Analytik-Service GmbH.

Parameter	Method	Unit	0.1%S fuel	0.5%S fuel IFO	2.5%S fuel HFO	Bio30
Density (15 °C)	DIN EN ISO 12185	kg/m <sup>3</sup>	869,6	-	-	866,2
Density (50 °C)		kg/m <sup>3</sup>	-	905,7	979,1	-
Kin. viscosity (40 °C)	DIN EN ISO 3104	mm <sup>2</sup> /s	4,806	-	-	6,689
Kin. viscosity (50 °C)		mm <sup>2</sup> /s	-	126,8	-	-
Kin. viscosity (80 °C)		mm <sup>2</sup> /s	-	-	186,8	-
Carbon residue (10 % D.)	DIN EN ISO 10370	% (m/m)	<0,10	-	-	2,41
Carbon residue (100 %)		% (m/m)	-	3,67	18,3	-
Hydrogen Sulfide	IP 570	mg/kg	<10	<10	<10	<10
Water content (K.-F.)	DIN EN 12937	mg/kg	53	-	-	197
Water content	DIN ISO 3733	% (V/V)	-	0.22	0.54	-
Total sediment content	ISO 10307-1	% (m/m)	<0,01	0,25	0,37	<0,01
Ash content (775 °C)	DIN EN ISO 6245	% (m/m)	<0,00 5	0,038	0,094	<0,005
Flash point	DIN EN ISO 2719	°C	86,5	206,0	103,0	67,5
Pour point	DIN ISO 3016	°C	0	+30	-5	-9
Cloud point	DIN EN 23015	°C	+3	-	-	-3
Cetane Index	DIN EN ISO 4264	-	49,9	-	-	46,4
10 % (V/V) recovery	DIN EN ISO 3405	°C	261,0	-	-	229,0
50 % (V/V) recovery		°C	311,0	-	-	310,0
90 % (V/V) recovery		°C	357,7	-	-	333,8
Cetane Number (DCN)	DIN EN 15195	-	-	-	-	-
Cetane Number	IP 541-06	-	-	44,5	26,1	-
CCAI	DIN ISO 8217 annex F	-	-	780	848	-
Acid number (TAN)	ASTM D 664	mg KOH/g	0,025	0,619	0,776	3,33
Strong acid number		mg KOH/g	-	-	<0,1	<0,1
Oxidation stability	DIN EN ISO 12205	mg/m <sup>3</sup>	10	*	*	9
HFRR (Lubricity)	DIN EN ISO 12156-1	µm	349	178	154	220
Copper strip corrosion	ASTM D 130	Corr.degree	1	1	1	1
Steel corrosion	ASTM D 665	Corr.degree	1	1	intensive rust	1
Iodine value	DIN ISO 3961	g Iodine/100g	-	-	-	49
Calorific value, lower	DIN 51900-2 mod.	kJ/kg	42,53	42,10	40,25	40,74
Sulphur (S)		mg/kg	781	3750	22 200	4.3
Silver (Ag)		mg/kg	<0,5	<0,5	<0,5	<0,5
Copper (Cu)		mg/kg	<0,5	<0,5	<0,5	<0,5
Aluminium (Al)		mg/kg	<0,5	<0,5	0,9	<0,5
Cadmium (Cd)		mg/kg	<0,5	<0,5	<0,5	<0,5
Sodium (Na)		mg/kg	<0,5	6,5	24	2,0
Potassium (K)		mg/kg	<0,5	0,6	1,9	1,2
Chromium (Cr)		mg/kg	<0,5	<0,5	<0,5	<0,5
Manganese (Mn)		mg/kg	<0,5	<0,5	<0,5	<0,5
Nickel (Ni)		mg/kg	<0,5	6,6	75	<0,5
Iron (Fe)		mg/kg	<0,5	3,8	6,4	<0,5
Molybdenum (Mo)		mg/kg	<0,5	<0,5	0,8	<0,5
Barium (Ba)	ASG 1917-ICP-OES	mg/kg	<0,5	<0,5	0,5	<0,5
Boron (B)		mg/kg	<0,5	<0,5	1,2	<0,5
Calcium (Ca)		mg/kg	<0,5	0,7	19	<0,5
Magnesium (Mg)		mg/kg	<0,5	<0,5	4,1	<0,5
Lead (Pb)		mg/kg	<0,5	<0,5	0,8	<0,5
Vanadium (V)		mg/kg	<0,5	2,3	430	<0,5
Tin (Sn)		mg/kg	<0,5	<0,5	<0,5	<0,5
Zinc (Zn)		mg/kg	<0,5	<0,5	0,5	<0,5
Silicon (Si)		mg/kg	<0,5	<0,5	1,4	<0,5
Titanium (Ti)		mg/kg	<0,5	<0,5	1,7	<0,5
Phosphorous (P)	mg/kg	<0,5	1,5	1,1	<0,5	
Cobalt (Co)	mg/kg	<0,5	0,8	0,5	<0,5	
Lithium (Li)	mg/kg	<0,5	<0,5	<0,5	<0,5	

Carbon, hydrogen, nitrogen, oxygen and ash results from ASG did not cover 100% of the fuel composition, and therefore carbon and hydrogen contents were adjusted (Table 3.3).

Table 3.3. Composition of the test fuels. Carbon and hydrogen contents analysed by ASG Analytik-Service GmbH are adjusted to achieve 100% fuel composition.

	0.1%S DMB	0.5%S IFO	2.5%S HFO	Bio30
Carbon content, % (m/m)	87,0	86,8	86,2	83,0
Hydrogen content, % (m/m)	12,9	12,5	10,4	13,1
Nitrogen content, % (m/m)	0,013	0,228	0,541	0,003
Oxygen content, % (m/m)	0	0	0,5	3,9
Sulfur content, % (m/m)	0,078	0,375	2,22	0,00043
Ash, % (m/m)	0	0,038	0,094	0
SUM	100,0	100,0	100,0	100,0

In addition to sulphur content, many other fuel properties varied substantially. The 2.5%S fuel contained substantially less hydrogen than the other fuels leading to low H/C ratio (Figure 3.3). The Bio30 fuel was the only fuel containing a relatively high amount of oxygen, 3.9 % (m/m). Density, viscosity, nitrogen content, ash and metal contents of the fuels also vary substantially.

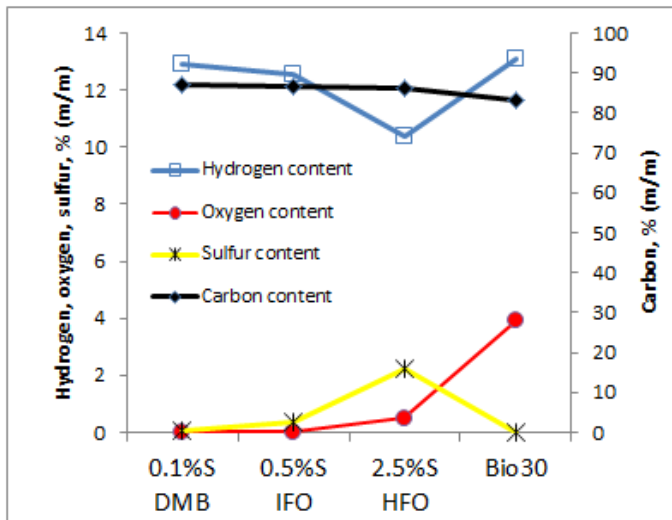


Figure 3.3. Carbon, hydrogen, sulphur and oxygen content of the test fuels.

### 3.4 Engine oil

The engine oil type Shell Argina XL 40 was employed. The engine oil was used for approximately 200 hours before the SEA-EFFECTS BC project started. Samples of engine oil were taken before the tests (sample 1) and after the tests (sample 2). Moreover, a fresh engine oil sample was also analysed (sample 3). The engine oil samples were analysed by ASG Analytik-Service Gesellschaft mbH. The results are shown in Table 3.4. The three engine oil samples were in good condition. The fresh engine oil (sample 3) showed the lowest metal contents.

Table 3.4. Engine oil properties. Samples 1 before and sample 2 at the end of the SEA-EFFECTS BC measurement campaign. Sample 3 is a fresh engine oil.

				Sample 1	Sample 2	Sample 3
				31.8.2015	29.9.2015	30.9.2015
Viscosity	+40 C	cSt	ASTM D445	132,83	133,74	131,84
	+100 C			14,39	14,42	14,25
Viscosity index		-		107	107	106
TBN		-	ISO 3771	50,98	50,97	51,52
TAN						
Oxidation		A / cm		2	2	1
Nitration		A / cm		3	3	0
Sulphating		A / cm		0	0	0
Dispersing		%		86	81	
Elements - ICP		ppm	ASTM D5185			
Calcium		ppm		15938	16085	16146
Magnesium		ppm		68	67	79
Boron		ppm		1	1	1
Zinc		ppm		421	425	419
Phosphorus		ppm		350	354	352
Barium		ppm		0	0	0
Sulfur		ppm		6160	6345	5603
Engine wear metals - ICP		ppm	ASTM D5185			
Iron				9	9	0
Chrome				0	0	0
Tin				0	0	0
Aluminium				5	5	0
Nickel				2	3	0
Copper				1	1	0
Lead				0	0	0
Molybden				0	0	0
PQ-index		-		OK	OK	OK
Contaminants - ICP		ppm				
Silicon		-		15	15	18
Potassium				4	4	4
Sodium				14	14	12
Water content		ppm	ADTM D6304 C	600	440	30
Glycol		-		negat	negat	negat
Fuel dilution		%		<0,30	<0,30	<0,30
Biodiesel content (FAME)		%		<0,30	<0,30	<0,30
Soot		%		<0,1	<0,1	<0,1
Flash point (PM)		C	ASTM D93	228	227	
Density		kg/m <sup>3</sup>	ASTM D4052	918	918	
Gravimetric analysis		g/l	in-house	0,6-1,0	0,7-1,4	

### 3.5 Test matrix and daily protocol

Emission measurements for each fuel were conducted for two days. The first fuel, 0.1%S, was tested also in the end of the program to ensure that engine emission level did not change over the measurement campaign. For each fuel, dilution ratio of approximately 100 was used on the first testing day and dilution ratio of over 600 (even close to 2000) on the

second testing day. Daily protocol is presented in Table 3.5. One day was reserved for fuel changes to assure sufficient time for adaptation for each fuel.

Table 3.5. Daily protocol.

Warm-up, one hour:	10 minutes at 50% load and 50 minutes at 75% load.
Tests at 75% load (morning session)	<ul style="list-style-type: none"> <li>In-stack: in minimum three collections, Munktell MK360 quartz filters</li> <li>Filter collections                             <ul style="list-style-type: none"> <li>Pallflex TX40 filters (prim., back-up): 7-8 collections (2 sampling systems)</li> <li>Munktell MK360 quartz filters, Pallflex TX40 back-up: min. 3 collections</li> </ul> </li> <li>AVL 415S and AVL 415SE synchronized with the PM collections</li> <li>Real-time instruments with continuous measurements</li> <li>Periodically ON/OFF: CS1, TD before AE33 and SP-AMS. CS2 before MAAP. CS3 before PPS-M. First day program: CS1, TD before aethalometers, MAAP and SP-AMS.</li> </ul>
Load change:	Stabilisation at least 0.5 hours
Tests at 25% load (evening session)	Same measurements as at 75% load

## 3.6 Probes, dilution

### 3.6.1 Test set-up

A schematic representation of the instrumentation used in the tests is shown in Figure 3.4 (see also cover page of this report).

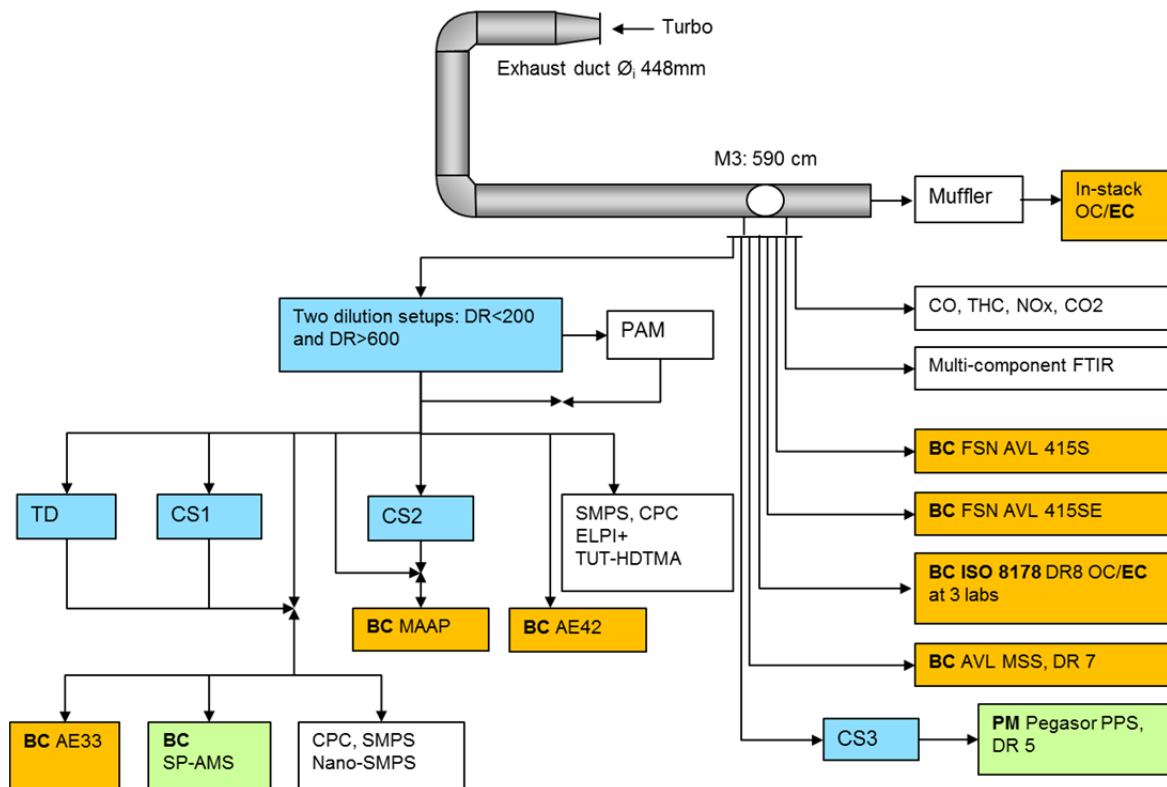


Figure 3.4. Overview of the instrumentation in the SEA-EFFECTS BC measurements.

### 3.6.2 Probes

For in-stack sampling, probe was available at the exhaust duct from the earlier experiments. The probes of Microtrol, AVL 415S FSN and gaseous emissions were also located in the usual position “M3” (Figure 3.5). Distance from M3 to the first bend of the exhaust duct was 167 cm and to the second bend 508 cm. Ratios of these distances to the i.d. of the exhaust duct were 3.8 and 11.4, respectively. Distance to muffler before the second bend was 78 cm and ratio between distance and i.d. of the exhaust duct 1.8.

A new probe was built up in position M3 using 8 mm (i.d.) tubes. This probe provided samples for Smart Sampler, AVL 415SE FSN, MSS, PPS-M and for the TUT dilution system (feeding sample to TUT and FMI instruments). In addition, temperature and pressure measurements of sampling point were conducted through the new probe.

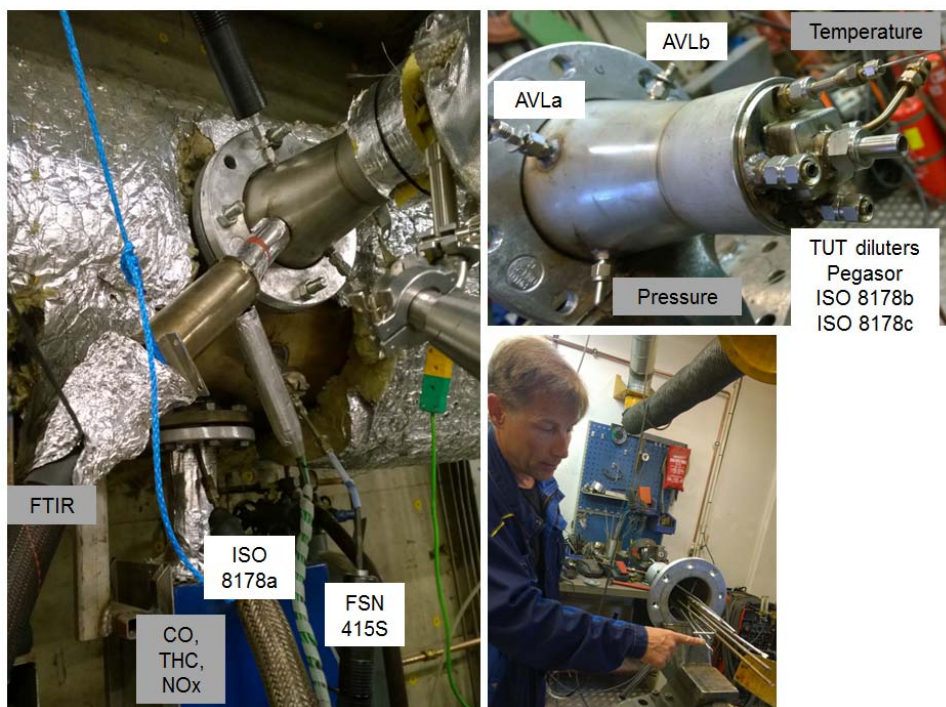


Figure 3.5. Probes for the sampling in the SEA-EFFCETS BC campaign.

### 3.6.3 Diluters

AVL Smoke Meter and in-stack sampling used raw exhaust without dilution. The AVL Smart Sampler and the Microtrol used partial flow dilution according to standardized procedure. AVL MSS and Pegasor PPS-M instruments used their own diluters.

Aethalometers, MAAP, SP-AMS, particle sizing instruments and SOA (PAM) measurements require high dilution ratios. TUT built two comprehensive dilution systems consisting of several heated and non-heated diluters to meet the needs of different instruments (Figure 3.6).

The first dilution setup consisted of two-diluters that resulted in a nominal dilution ratio of approximately 100. The primary dilution was executed with a porous tube diluter (PTD) where the dilution ratio was set to about 12. The secondary dilution was executed with an ejector diluter (Dekati diluter) with a nominal dilution ratio of 8.

The second DR setup was designed for the measurements where higher DR above 600 was necessary, namely for MAAP, and to adjust constant  $\text{NO}_x$  levels ( $\sim 11$  ppm) for PAM chamber where the secondary aerosol formation takes place. The second dilution system consisted of three diluters: a heated ejector diluter (modified Dekati diluter) with DR of about 4.5 and the temperature of dilution air about  $350^\circ\text{C}$ , secondary dilution with an ejector diluter (Dekati diluter) with a nominal dilution ratio of 8, an adjustable dilution with a mass flow controller and an ejector diluter (Dekati diluter) with a nominal dilution ratio of 8.

Dilution ratio of below 200 was used in the first measurement day with each test fuel. Higher dilution ratios of 600–1800 were used in the second measurement day with each fuel, when also PAM was used.

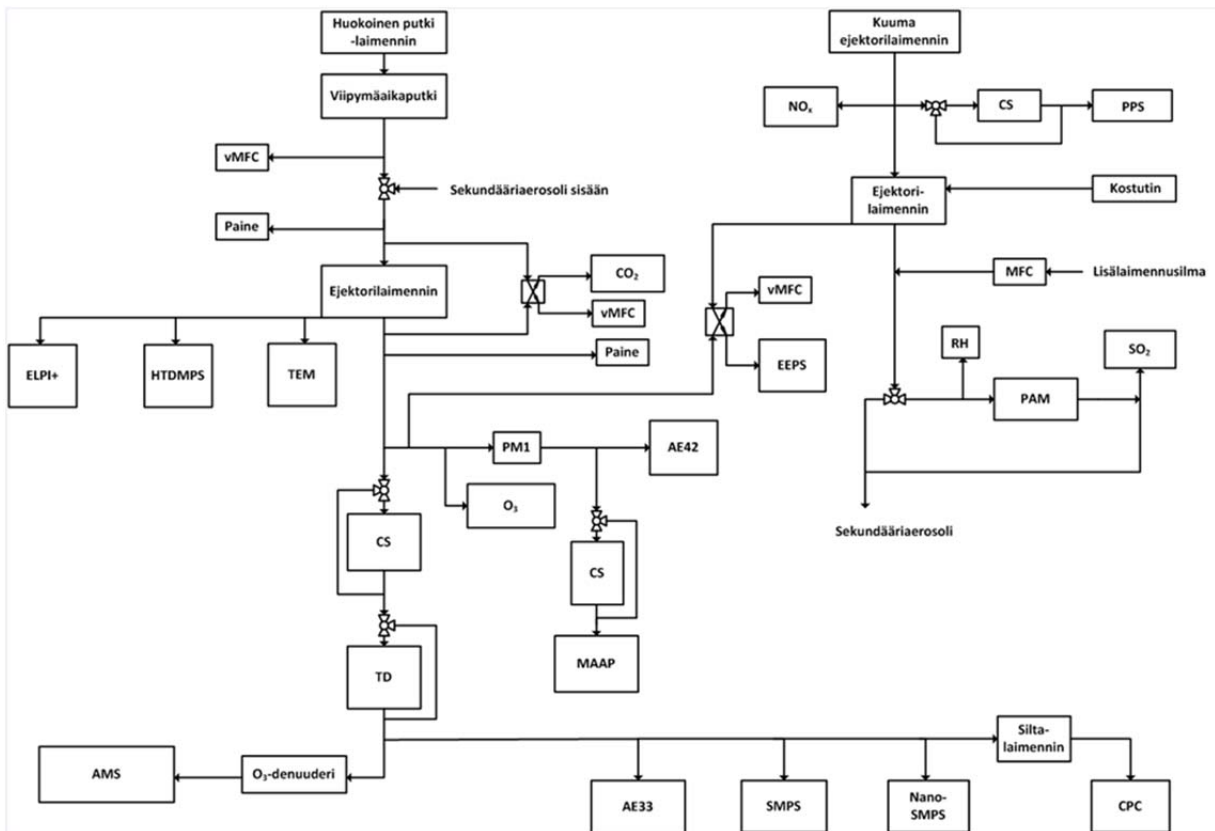


Figure 3.6. TUT dilution systems for Aethalometers, MAAP, SP-AMS and particle size instruments.

### 3.6.4 Determination of dilution ratio

The AVL Smart Sampler, the Microtroll, AVL MSS and Pegasor PPS-M used their own dilutions systems, and also determination of DR for these instruments is designed by manufacturers.

For TUT dilution system, the DR was verified on-line by using  $\text{CO}_2$  analysers at different locations for raw and diluted exhaust gas. Temperatures, pressures, humidity and dilution air impurities were also monitored.

DR was calculated based on equation (1).

$$DR = \frac{c_{raw\_wet} - c_{background}}{c_{dil\_wet} - c_{background}} \quad (1)$$

$C_{raw\_wet}$  = CO<sub>2</sub> concentration in raw, wet exhaust gas  
 $C_{dil\_wet}$  = CO<sub>2</sub> concentration in diluted, wet exhaust gas  
 $C_{background}$  = CO<sub>2</sub> concentration in dilution air

Raw exhaust CO<sub>2</sub> was measured on dry basis by cooling the sample to approximately 0–3 °C, whereas CO<sub>2</sub> from diluted exhaust was measured on wet basis. Therefore dry to wet correction of raw exhaust CO<sub>2</sub> is required. Water content of the wet exhaust gas was measured by FTIR (Chapter 4.1). According to ISO 8178 dry to wet correction is conducted using equation (2).

$$CO2_{wet} = CO2_{dry} * (1 - 1,85 * \frac{G_{fuel}}{G_{aird}}) \quad (2)$$

Dry to wet conversion can also be conducted using the general formula (3).

$$CO2_{wet} = CO2_{dry} * (1 - w) \quad (3)$$

w = water fraction, for example 0.1 represents 10% of water

Water fraction is calculated by using equations (4) and (5).

$$w = \frac{kg(water\ vapour)}{kg(dry\ air)} = \frac{M(water)*p}{M(dry\ air)*(P-p)} = 0.62 * 10^{-5} * p \quad (4)$$

$$p = \frac{e^{77.3450 + 0.0057 T - 7235 / T}}{T^{8.2}} \quad (5)$$

M = molar mass (g/mol), dry air 28.97 g/mol, water 18 g/mol  
 P = total atmospheric pressure (Pa); at room temperature P - p is nearly equal to P  
 p = water vapour saturation pressure (Pa)  
 e = Neper number (2.718)  
 T = dry bulb temperature of the moist air (K)

VTT analysed for CO<sub>2</sub> of the raw exhaust was with two analysers continuously (Chapter 4.1). TUT analysed CO<sub>2</sub> concentrations of the diluted exhaust gas thrice on most measurement days with a Sick Maihak SIDOR analyser. CO<sub>2</sub> concentrations of dilution air were measured with the same analyser. One sensor was used for concentrations higher than 5000 ppm, and the other sensor for concentrations lower than 5000 ppm. The Sick Maihak SIDOR analyser was calibrated before and after the measurement campaign with 3000 ppm and 11.9 % calibration gases. A drift of 35 ppm was observed at 3000 ppm concentration, which is approximately 1.3% of reading (Table 3.6).

*Table 3.6. Calibration of the Sick Maihak SIDOR analyser used for measurement of the CO<sub>2</sub> concentrations from the diluted exhaust gas.*

Calibration gas	Sensor 1		Sensor 2	
	25.8.2015	28.9.201	25.8.2015	28.9.201
<b>Zero gas</b>	-8	5	0,11	-0,01
<b>3000 ppm</b>	2885	2920	0,3	0,3
<b>11.9 %</b>	-	-	12,04	11,8

### 3.6.5 Dilution ratios and their uncertainties

The DR used for the AVL Smart Sampler was 8, while for the Microtroll approximately 30. DR used for AVL MSS was 7 and for Pegasor PPS-M DR was 5. AVL Smoke Meters sampled raw exhaust gas without dilution.

Aethalometers, MAAP, SP-AMS and particle sizing instruments used high DRs of the TUT dilution system (Figure 3.7). Target dilution ratios were readjusted when engine load changed. DR drifted in some cases substantially. True DR was used in the calculation of the results for real-time instruments. Variation on the DR emphasises the importance of using on-line measurements for determination of DR, particularly when in-house dilution systems are used.

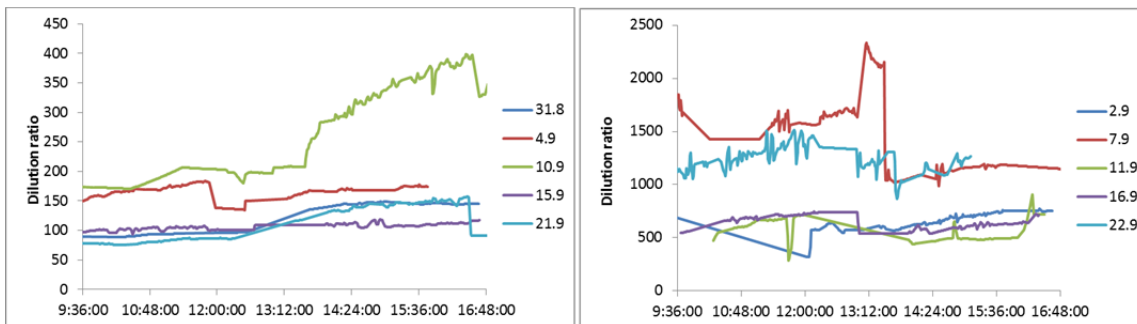


Figure 3.7. On the left hand-side measurement days with lower target DRs, and on the right-hand side higher target DRs.

Uncertainty in DR determination based on CO<sub>2</sub> concentration is dependent on the accuracy of the analysers. However, for high DRs in the engine environment, dilution air is also an important source of uncertainty. Two air compressors were used at VTT: the Garden Denver located on the ground floor and the Atlas Copco located below the heavy-duty chassis dynamometer. Both dilution air sources are subject to the CO<sub>2</sub> contaminations, which has also been evidenced (e.g. CO<sub>2</sub> peak during 16-17.12.2015, the Atlas Copco). TUT measured the CO<sub>2</sub> concentrations from dilution air typically thrice a day (once on 16<sup>th</sup> September 2015). CO<sub>2</sub> concentration was exceptionally high on 16<sup>th</sup> September and in the morning of 4<sup>th</sup> September. Systematic trend of reduced CO<sub>2</sub> concentrations towards evening may be due to analyser drift when the test cell temperature increased.

Depending on the load point and fuel, CO<sub>2</sub> raw (wet) exhaust concentrations varied from 4.85 to 6.33 %(v/v) in these measurements, and the CO<sub>2</sub> concentrations of the diluted exhaust gas from 650 to 1000 ppm when DR was below 200. When using DRs above 600, CO<sub>2</sub> concentrations of the diluted exhaust gas were in a range of 440-470 ppm, and in one test only 410 ppm (Figure 3.8). These concentrations are close to the typical CO<sub>2</sub> concentrations of 365-395 ppm in the dilution air.



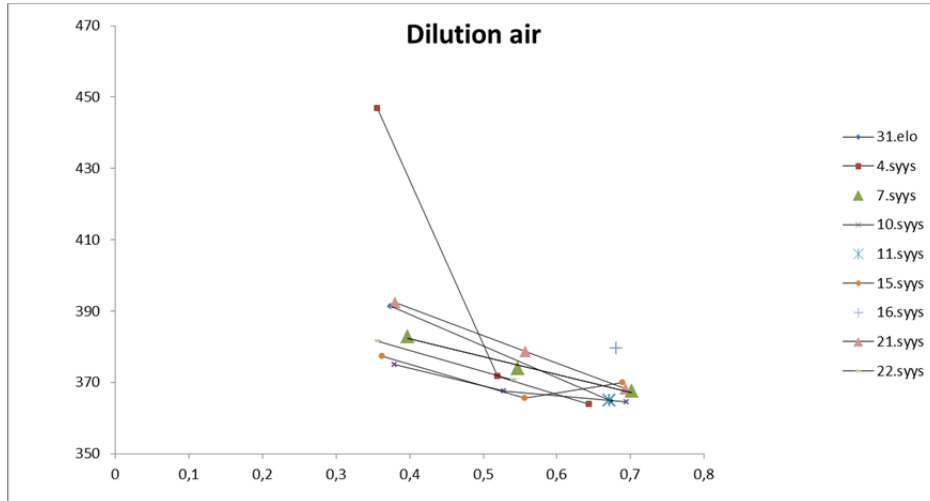


Figure 3.8. CO<sub>2</sub> concentrations measured from dilution air.

When DR was below 200, uncertainty in DR was approximately  $\pm 15\%$ . When using DR of 600 or higher, uncertainty of DR was very high due to the CO<sub>2</sub> concentrations of diluted exhaust close to those of dilution air (Figure 3.9). Thus ultra-pure dilution air is recommended for the BC measurements when high DRs are applied.

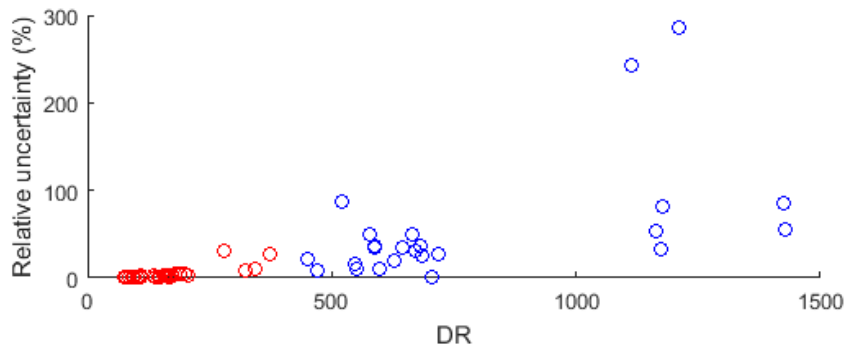


Figure 3.9. Uncertainties in DR. Red circles illustrate uncertainties of lower DRs (PTD system) and blue ones that of higher DRs (ejector system).

### 3.6.6 Summary of sampling, flows, residence times and sample temperatures

Summary of sampling details are shown in Table 3.7.

Table 3.7. Summary of the sampling and dilution conditions.

	Line	Flow 75%/25% load	Residence time 75%/25% load (s)	Sample temp. 75%/25% load (°C)	DR	Range	Note
<b>Exhaust duct (engine-M3)</b>	590cm, id 44.8 cm	116/54 Sm <sup>3</sup> /min	0.5 / 1.5	360 / 310			Sampling probes for dilutions (M3) i.d. 8 mm
<b>In-stack sampling</b>	Exh duct 1785 cm, id 44.8 cm	Isokinetic sampling, 23-31 lpm	1.5 / 3.0	360 / 310	No dilution		Munktell MK 360 (o.d. 47 mm) quartz filters. Pre-cleaned at 400 °C.
<b>EC/OC</b>	from ISO 8178 (below)					EC: 1-15 µgC/cm <sup>2</sup>	DL: 0.2 µgC/cm <sup>2</sup> Repeatability: ± 5%
<b>ISO 8178 Microtroll</b>	Heated line 3 m, 250 °C	Conc. controlled 6 kg/h tot		<52	~30		Filters: a) Munktell MK 360, o.d. 70 mm quartz. Pre-cleaned 850 °C, 2 h, stabilized. b) Pallflex TX40 o.d. 70 mm. Loaded ones in freezer.
<b>ISO 8178 Smart Sampler</b>	Heated line 1.0 m, 220 °C	Flow control. 5.4 kg/h tot		<52	8		
<b>AVL 415S (FSN)</b>	Heated line 2 m, 70 °C	10 lpm	~ 0.3	63	No dilution	0-32 000 mg/m <sup>3</sup>	Resolution: 0.01 mg/m <sup>3</sup> DL: 0.02 mg/m <sup>3</sup>
<b>AVL 415SE (FSN)</b>	Heated line 3 m, 70 °C	10 lpm	~ 0.5	63	No dilution	0-32 000 mg/m <sup>3</sup>	
<b>AVL MSS (PAS)</b>	Heated line 2 m, 52 °C	3.8 lpm	~ 1.5	52	7 (Spec 2-20)	0-1000 mg/m <sup>3</sup> (Range with dilution)	Time basis up to 10 Hz Rise time <1sec Sensitivity 5 µg/m <sup>3</sup>
<b>Pegasor PPS-M</b>	Heated line 1 m, 200 °C	<10 lpm	<0.3 s	<200 °C	5	PM 1 µg/m <sup>3</sup> –250 mg/m <sup>3</sup> .	Resolution: 0.2 s real-time
<b>After TUT diluters (porous tube, ejectors)</b>							
<b>Aethalometer AE42</b>	~ 3 m	2 lpm (spec 2-5 lpm)	~3.5		<200 >600	Time base 1 min (1 s option)	PM1 Inlet.
<b>Aethalometer AE33</b>	~ 3 m	2 lpm (spec 2-4 lpm)	~ 3.5		<200 >600	Range: <0.01 to >100 µg/m <sup>3</sup> Time basis 1 min (1s option)	7 wavelengths 370 – 950 nm. 880 nm BC. Resolution: 1 ng/ m <sup>3</sup> Sensitivity: ~0.03 µg/m <sup>3</sup> DL (1 h): <0.005 µg/m <sup>3</sup>
<b>MAAP</b>	~ 3 m	6 lpm (spec 16.7 lpm) PM1	~ 1.2		<200 >600	0-60, 0-180, µg/m <sup>3</sup> BC @ 30, 10, average, here 1 min av.	DL: 2min. av <100 ng/m <sup>3</sup> ; 10min. av <50 ng/m <sup>3</sup> ; 30min. av <100 ng/m <sup>3</sup> ; PM1 cyclone
<b>SP-AMS</b>	~ 8 m	0.1 lpm (spec 1.5 lpm)	~ 12.3		<200 >600	BC 0.04 µg/m <sup>3</sup> -2 mg/m <sup>3</sup> Time basis 1 min	DL (1min): <0.04 µg/ m <sup>3</sup> Measured Size: 30 nm to 800 nm
<b>PAM/CS</b>		4-10/<10			<200 >600		Sample treatment

DL = detection limit

## 4. Methods

### 4.1 Gaseous emissions and parameters

The regulated gaseous emissions were measured with the analyzers (Figure 4.1) meeting the ISO 8178 requirements:

- THC: Heated Flame Ionisation Detector (HFID). J.U.M Engineering
- NO<sub>x</sub>: Heated Chemiluminescence (HCLD). Eco Physics
- CO, CO<sub>2</sub>: Nondispersive Infrared (NDIR). Raw exhaust gas is dried by cooling it at approximately 3 °C. Maihak AG.
- O<sub>2</sub>: Paramagnetic cell. Maihak AG.



Figure 4.1. Analysers for measuring CO, HC, NO<sub>x</sub>, CO<sub>2</sub> and O<sub>2</sub> emissions.

The concentrations were recorded in one second time intervals and averaged over 10/15 minutes. Calculation of the results was according to the ISO 8178 standard.

More than 10 gaseous compounds were measured on-line at 20 seconds intervals using the Fourier transformation infrared (FTIR) equipment (Gasmeter DX-4000, purchased in 2012, Figure 4.2). The compounds measured with FTIR include for example sulfur dioxide (SO<sub>2</sub>).



Figure 4.2. The FTIR analyser for on-line multi-component analysis of gaseous emissions.

In addition to the regulated gaseous emissions, many parameters were recorded at one second time intervals and averaged over 10/15 minutes as presented below.

- *Engine*: Engine speed, alternator power, rack position, thrust bearing temperature, main bearing 1, 2, 3, 4, 5 temperatures
- *Gas exchange*: Atmospheric pressure, test cell temperature, test cell relative humidity, intake air temperature, pressure difference at measurement orifice, under pressure in measurement pipe, air temp. before turbo charger (TC), TC speed, air temp. after TC, air gauge pressure before CA cooler, air gauge pressure and air temperature in receiver, exhaust gas temp. cyl. 1, 2, 3, 4, exhaust gas gauge pressure bef. TC, exhaust gas temp. bef. TC, exhaust gas gauge pressure after TC, exhaust gas temperature after TC. The mass flow rate of the intake air was measured, but the exhaust gas flow rate used in the calculations of the final results was based on the carbon balance method.
- *Fuel system*: fuel mass flow rate in and out, fuel pressure after feed pump, fuel temp. after feed pump, fuel mass flow rate (booster), fuel pressure before engine (booster), fuel pressure after engine (booster), fuel volume flow rate in, fuel volume flow rate out, fuel temperature before engine, fuel temperature after engine, fuel viscosity before engine, fuel pressure on engine (in), fuel pressure on engine (out)
- *Cooling and lubrication*: HT-water temp. bef. engine, T-water temp. after engine, LT-water temp. bef. engine, LT-water temp. after CAC, LT-water temp. bef. LOC, LT-

water temp. after LOC, LT-water after engine, lube oil temp. bef. LOC, lub. oil temp. after LOC, lub. oil pressure, lub. oil temp. before engine.

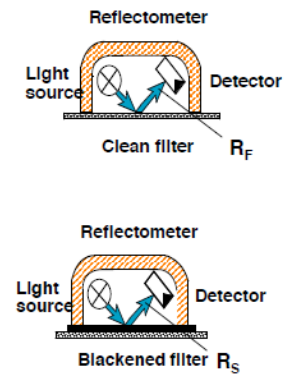
## 4.2 Filter Smoke Number, AVL 415S and AVL 415SE

<b>Filter Smoke Number (FSN) AVL 415S</b>	<b>Filter Smoke Number (FSN) AVL 415SE</b>
---	--

Owner: VTT	Owner: AVL
Operators: Sami Nyysönen, Jarno Martikainen, Matti Niinistö, VTT	Operator: Monica Tutuianu, AVL Timo Murtonen, VTT



FSN is a traditional method used to measure “soot” in the raw exhaust gas without the need for exhaust dilution. The FSN measurement principle implemented in the AVL Smoke Meter is based on light absorption. The change in optical reflectance of visible light from a loaded filter relative to clean filter is measured (blackening of filter tape). Absorbing eye response is according CIE 69.



Two different generations of Filter Smoke Meters were used: AVL 415S and AVL 415SE. Most significant difference between these instruments regards shop air option in AVL 415SE, which ensures improved cleaning efficiency and increased robustness against wet exhaust gas due to shop air purging from the inlet to the measurement block until back to the sample probe. On long term use this option enables high reproducibility of the measurements. Absolute pressure sensor is also provided. FSN can be converted to the BC concentration according to the equation provided by the manufacturer and correlations are available also by ISO 8178-1 (2006, eq. A. 16). FSN is a standardized method conforming to ISO 10054.

In these measurements, Smoke Meter AVL 415S was located below the sampling point, while AVL 415SE was installed above the sampling point. Heated line of 2 m was used for AVL 415S, while heated line of 3 m was used for AVL 415SE, both at 70 °C. Temperature of measuring chamber was 63 °C in both instruments. AVL 415S was remote-controlled and the results were manually recorded. The representative of manufacturer was in charge of the measurements with AVL 415SE, data acquisition and calculations of data. VTT was responsible for the measurements and results obtained with AVL 415S.

Range:	0 to 10 FSN or 20 µg/m <sup>3</sup> to 32 g/m <sup>3</sup>
Resolution:	0.001FSN or 0.01 mg/m <sup>3</sup>
Detection Limit:	0.002FSN or ~ 0.02 mg/m <sup>3</sup>
Exhaust temperature	max. 600 °C with 340 mm probe (800 °C with 780 mm probe)
Compressed air:	appr. 150 l/min during purge
Sample flow:	appr. 10 l/min
Sampling time:	from 2 seconds up to 2 minutes.
Repeatability:	Standard deviation 1 σ = ± (0.005 FSN + 3% of the measured value) at 10 seconds intake time

### Pros:

- Developed for exhaust gas measurements
- Robust, low maintenance, well known
- No dilution needed
- Standardized by ISO – 10054.
- Correlations from manufacturers or ISO 8178-1 (2006, eq. A. 16)

### Cons:

- Estimate of eBC mass concentration (mg/m<sup>3</sup>) by using an empirical relation (may be sensitive towards the exhaust properties)
- Possible sensitivity to ash.

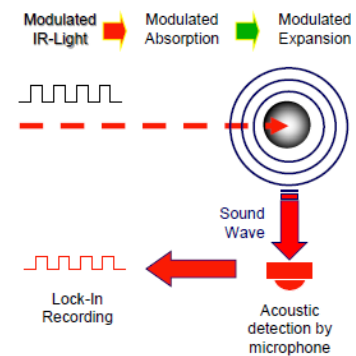
### 4.3 Photo acoustic method: AVL Micro Soot Sensor (MSS)

Owner: AVL List GmbH

Operators: Monica Tutuianu, AVL List GmbH, Timo Murtonen, VTT



The measurement principle of the MSS is based on the photo acoustic method, in which a modulated laser beam (heating) causes a sound pressure wave detected by a microphone. Diluted exhaust gas is directed through a measuring chamber and thermally animated by a modulated laser beam. The 808 nm light is absorbed by the particles. Modulated heating produces periodic pressure pulsation, which is detected by a microphone as an acoustic wave. The signal is amplified in a preamplifier and filtered in a “Lock-In”- amplifier. The MSS consists of a sensor unit and a conditioning unit for dilution, and provides a continuous on-line measurement of BC concentration.



- Time resolved signal: up to 10Hz
- Rise time below 1 second
- Sensitivity  $5 \mu\text{g}/\text{m}^3$
- Range with dilution  $\text{mg}/\text{m}^3$  to  $1 \text{g}/\text{m}^3$
- Dilution ratio 2-20, in these test 7

#### Pros:

- Continuous on-line measurement
- User-friendly interface
- Conditioning unit for dilution

#### Cons:

- Estimate of eBC by using calibration factors, achieved by calibration with artificial (surrogate) particles
- Sensitive towards exhaust properties (high humidity, high concentration of  $\text{NO}_2$ ).
- Dilution of raw exhaust is needed
- Not covered by standards

### 4.4 Multiangle Absorption Photometer, MAAP

Owner: FMI

Operators: Kimmo Teinilä, FMI

MAAP 5012 manufactured by Thermo Scientific was used in these measurements. MAAP is an improved Aethalometer method measuring the relative change in optical transmission as particles are collected on a filter

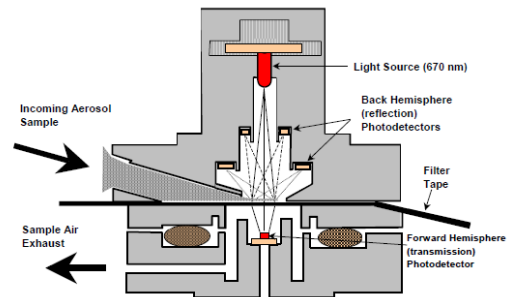


combined with measurement of reflectance of scattered light with multiple detectors simultaneously (Petzold et al. 2002). Reflection and scattering of light in multiple directions is due to variable particle size and shape. Calculation of BC is based on a specific absorption of BC at a certain wavelength (670nm). MAAP detects transmitted and backscattered light at two angles reducing instrumental artefacts and provides a more accurate measurement of BC than aethalometers. MAAP provides continuous on-line measurement, but requires high dilution ratio for high BC concentrations present in diesel exhaust.

In these measurements, sample flow rates of MAAP were calibrated, and the sample flow rate (6.0 lpm) of MAAP was corrected based on calibration. The results of MAAP were not corrected for spot

area, as this correction would have been marginal. Other calibrations of MAAP were not conducted. Hyvärinen et al. (Hyvärinen et al. 2013) developed a semi-empirical correction method for compensating the underestimation of BC by MAAP. In this study, MAAP data was processed with correction algorithm, but this did not affect the results. Therefore additional corrections were not applied. MAAP firmware 1.33 apparently takes into account necessary corrections.

- User-selectable sample averaging times. Automatic temperature and pressure correction.
- PM1 cyclone.
- Filter changes at 20% transmission (appr. 30µg) (Glass fiber, GF 10).
- Range: Measurement Range: 0-60, 0-180, µg/m<sup>3</sup> BC @ 30, 10, averaging, respectively.(95 % confidence level, 1000 l/h). In these measurements 1 min averaging
- Minimum Detection Limits:
  - 2 min. average <100ng/m<sup>3</sup>, <0.66M/m Babs;
  - 10 min. average is <50ng/m<sup>3</sup>, <0.33M/m Babs;
  - 30 min. average is <100ng/m<sup>3</sup>, <0.66M/m Babs



#### Pros:

- Calculation is based on a specific absorption of BC at a certain wavelength
- A combination of techniques provides a truer measurement of BC content compared to aethalometers.

#### Cons:

- High dilution ratio is needed for diesel engines
- Estimate of eBC by using conversion factors, achieved by calibration with artificial (surrogate) particles
- Sensitive towards exhaust properties (humidity, O<sub>3</sub>, NO<sub>2</sub> and SO<sub>x</sub>).
- Not covered by standards

## 4.5 Aethalometers

### MAGEE AE42

Owner: FMI  
Operators: Kimmo Teinilä, FMI



### MAGEE AE33



Owner: Metropolia  
Operators: Päivi Aakko-Saksa and Päivi Koponen, VTT, Aleksi Malinen, Metropolia

Aethalometers are based on the change in absorption of transmitted light due to collection of aerosol deposit on reinforced quartz fiber tape, which advances automatically when loading threshold is reached (Hansen et al. 1984). The attenuation of transmitted light is measured continuously. Traditional aethalometers tend to overestimate BC on a fresh filter and underestimate BC on loaded filter (Arnott et al. 2005). The values measured on lightly loaded filters are deemed to be the closest to the real concentration (Collaud Coen et al. 2010). In MAGEE AE42, absorption at 880

New MAGEE AE33 uses seven wavelengths. Measurement of absorption at 880 nm is interpreted as BC. AE33 has also a DUALSPOT™ technology, in which aerosol is collected on two spots in parallel using different loading rates and both spots are simultaneously analysed to avoid "spot loading effects" (Drinovec et al. 2015). Mathematical combination of data yields BC result independent of "spot loading effects". Simultaneous measurement at multiple wavelengths enables studies of aerosol light absorption, atmospheric optics, radiative transfer, emissions testing, and source

nm is interpreted as BC. Additional measurement at 370 nm designated as 'UVPM' is interpreted as an indicator of aromatic organic compounds such as are found in tobacco smoke, wood and biomass-burning smoke. Aethalometers can provide continuous on-line BC measurements, but correction of aethalometer data is challenging as corrections should take into account many artefacts and should be applicable to all kind of matrices. Aethalometers require high DR when BC concentrations are high. AE42:

- Tape advances 1 cm automatically when user selectable loading threshold is reached, time interval depends on BC concentration and flow rate.
- Sensitivity: Proportional to flow rate, inversely proportional to time resolution; approximately  $0.1 \mu\text{g}/\text{m}^3$  (1 minute resolution 3 lpm flow rate).

apportionment. AE33:

- Time-base from 1 second or 1 minute. Flow rate from 2 to 5 lpm. Teflon-coated glass fiber filter tape. Tape advances automatically when user selectable loading threshold is reached. PM1 Inlet in use.
- LED Optical Source Range: 370 – 950 nm: (UV), 470 (blue), 520 (green), 590 (yellow), 660 (red), 880 (IR-1) and 950 nm (IR-2). Absorption at 880 nm interpreted as BC and at 370 as UV.
- Resolution:  $1 \text{ ng}/\text{m}^3$
- Sensitivity: appr.  $0.03 \mu\text{g}/\text{m}^3$  (1 min, 5 lpm).
- Detection Limit (1 hour):  $<0.005 \mu\text{g}/\text{m}^3$
- Range:  $<0.01$  to  $>100 \mu\text{g}/\text{m}^3$  BC

*Procedure:* MAGEE AE42 and a new model MAGEE AE33 described by Drinovec et al. (2015) were used in these tests. Sample flow rates of AE42 were calibrated. No corrections were needed for the sample flow rate of AE42. The results of aethalometers were not corrected for spot area, as this correction would have been marginal. Other calibrations of aethalometers were not conducted. The BC concentrations for the AE42 were manually selected (representing lightly loaded filters), while the new AE33 defined the BC concentrations automatically. AE-33 used 1 min, 2 lpm settings.

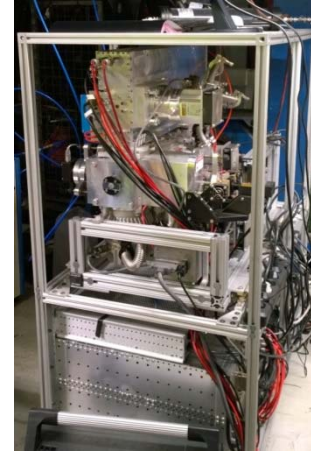
## 4.6 The Soot Particle Aerosol Mass Spectrometer, SP-AMS

Owner: FMI  
Operators: Hilkka Timonen, Jesse Jokela, FMI

SP-AMS is a high resolution time-of-flight aerosol mass spectrometer (HR-ToF-AMS) with added laser (intracavity Nd:YAG, 1064 nm) vaporizer (Onasch et al. 2012). Dual vaporizer system enables the real-time measurements of PM mass and size-resolved chemical composition of submicron non-refractory particulate matter, refractory BC and some metals and elements. In the HR-ToF-AMS an aerodynamic lens is used to form a narrow beam of particles that is transmitted into the detection chamber, where the non-refractory species are flash-vaporized upon impact on a hot surface ( $600^\circ\text{C}$ ) under high vacuum. Only non-refractory species are vaporized at this temperature. Crustal material, sea salt, metals and BC cannot be vaporized and thus are not detected using this technique. In the SP-AMS, particles are vaporized either by normal tungsten vaporizer in (600) to analyze inorganic ion and OC concentrations and with SP laser (intracavity Nd:YAG, 1064 nm) in order to analyze light absorbing refractory species such as BC and metals. The vaporized compounds are ionized using electron impact ionization (70 eV). Ions formed are guided to the time-of flight chamber. A multi-channel plate (MCP) is used as a detector.

The time resolution of AMS measurements was 60 seconds (30 s for composition and 30 s for size distribution). SP-AMS provides on-line analysis of refractory BC (rBC), composition of PM (organics, sulfates, nitrates, etc.), and chemically resolved particle size distribution. However, high dilution ratio is needed for diesel exhaust. In addition, particles smaller than 30 nm are not detected due to limitations of aerodynamic lens.

- |                            |                                 |
|----------------------------|---------------------------------|
| • Compounds:               | Main ions, organics, BC, metals |
| • Mass resolution:         | 2000                            |
| • Detection Limit (1 min): | <0.04 $\mu\text{g}/\text{m}^3$  |
| • Measured Size Range:     | 30 nm to 800 nm                 |
| • Measurement Time Base:   | 1 min                           |



#### Pros

- An efficient method for on-line analysis of chemical composition of PM (rBC, organics, sulfates, nitrates, etc.), and particle size distribution.

#### Cons

- Estimate of rBC (refractory). Accuracy not validated for medium-speed diesel engines.
- Dilution of raw exhaust is needed.
- Measured size range is limited.
- Developed for research purposes. Expensive and demanding for users.
- Not covered by standards.

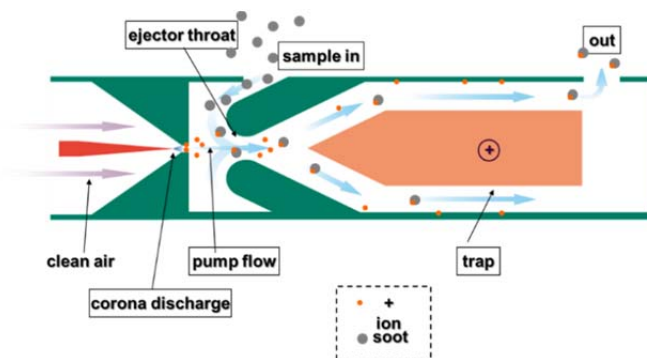
## 4.7 Pegasor Particle Sensor (PPS-M)

Owner: Pegasor

Operators: Panu Karjalainen, Niina Kuittinen, Pauli Simonen, Hugo Wihersaari, TUT



The PPS-M measurement principle is based on the measurement of electrical charge carried by particles. PPS-M comprises an ejector where the motive fluid flow is generated by pure, particle free gas. The ionized air is used to charge the particles in the sensor. Particle charging is relative to the particle size (Rostedt et al. 2014). Ions that are not attached to the particles are removed from the gas flow by an ion trap, which is basically an electrostatic precipitator with a small electrical field.



When the free ions are removed, the electrical current is carried only by the flow of charged particles. The electrical current escaping from the sensor with the charged particles can be measured and this gives a direct, fast, real-time measurement of the particle concentration expressed as mass or number concentration. The non-collective feature ensures long maintenance and cleaning interval and thus providing service-free operation. PPS-M provides an on-line measurement with low need of service and no consumables. Time response is fast and dynamic range wide. However, on-site calibration is needed at installation site, and sensitivity is limited for particle mass with large particles ( $D_p > 1$ ).

- Resolution: 0.2 s real-time
- Range: 1  $\mu\text{g}/\text{m}^3$ – 250  $\text{mg}/\text{m}^3$



**Pros:**

- On-line measurement
- Low need of service, no consumables
- Fast time response
- Wide dynamic range

**Cons:**

- On-site calibration needed at installation site
- Limited sensitivity for particle mass with large particles
- With high particle concentrations the ejector throat may partly clog over the time

## 4.8 SMPS, CPC, ELPI+ and HDTMA.

Owner: TUT

Operators: Panu Karjalainen, Niina Kuittinen, Pauli Simonen, Fanni Mylläri, Hugo Wihersaari

### Scanning mobility particle sizer (SMPS)

*Principle:* Scanning mobility particle sizer (SMPS) measures mobility particle size distribution at the time resolution of few minutes. Size distribution is separated in over 100 size classes.

*Procedure:* Nano-SMPS (DMA 3085 + CPC 3776) used flows 15+1.5 lpm and operated in the size range of 3-65 nm. Long-SMPS (DMA 3071 + CPC 3775) used flows 6+0.6 lpm and operated in the size range of 10-420 nm. Both SMPSs used 120 s upscan time, and recorded size distributions every 3 minutes during the whole measurement day.



*Nano-SMPS in front and Long-SMPS in the back.*

### Condensation particle counter (CPC)

*Principle:* Condensation particle counter measures particle number concentration. Airmodus A20 CPC was used here with a cut size of 7 nm.

*Procedure:* CPC (Airmodus A20) was used after two additional passive diluters (dilution ratios 41 and 10).



*CPC A20.*

### Engine Exhaust Particle Sizer (EEPS)

*Principle:* Engine Exhaust Particle Sizer measures mobility particle size distribution with one second time range.

*Procedure:* EEPS (TSI Engine Exhaust Particle Sizer Spectrometer 3090) measured the mobility particle size distribution in the size range from 5.6 to 560 nm. Size distribution is separated in 32 channels. EEPS measurement point could be chosen either before or after PAM chamber.



*EEPS*

### Electrical Low Pressure Impactor (ELPI+)

*Principle:* Electrical Low Pressure Impactor measures the particle size distribution according to their aerodynamic diameter.

*Procedure:* Electrical Low Pressure Impactor (Dekati ELPI+) measured particles in 14 size fractions in the size range from 6 nm to 10  $\mu\text{m}$ . The particles are first charged unipolarly and then classified in a low-pressure cascade impactor. ELPI+ was used to record and monitor the particle size distribution in real time.



ELPI+

### Hygroscopic Tandem Differential Mobility Analyzer (HTDMA)

*Principle:* Hygroscopic Tandem Differential Mobility Analyzer (HTDMA) measures the change in particle mobility size distribution after the sample is subjected to chosen relative humidity

*Procedure:* The first DMA used flows 6+0.6 lpm and was used to select a single particle size. The chosen particle size was then subjected to a selected relative humidity. The second, Vienna type, DMA used flows 10 + 1 lpm and was combined with Condensation Particle Counter (CPC 3025) to work as a DMPS. The DMPS was used to measure the particle size distribution in the humidified sample. With small modifications the instrument was used as a iDMPS (ion differential mobility particle sizer), to measure the probability of 0,  $\pm 1 e$ ,  $\pm 2 e$  and  $\pm 3 e$  charged particles.



HTDMA: the first DMA on top, the 2nd DMA and CPC below.

## 4.9 Catalytic strippers and thermodenuder

The effect of sample treatment on measured BC concentration was studied by using catalytic strippers (Amanatidis et al. 2013) and thermodenuder (Rönkkö et al. 2011) in front of aethalometers, MAAP, SP-AMS, Scanning Mobility Particle Sizers (Nano-SMPS and Long-SMPS) and Condensation Particle Counter (CPC) according to a pre-defined program. Thermal treatment of the exhaust aerosol removes semivolatile compounds from particles and leaves more solid (or non-volatile) part of particles to be measured, which, in principle, could improve accuracy of BC determination from different exhaust matrices. The CS removes the volatile and semi-volatile organic carbon, and also traps sulphur containing compounds over a catalyst heated to 300  $^{\circ}\text{C}$ . TD removes semivolatile material by adsorption of gaseous compounds. In the TD, the aerosol is first heated to 265  $^{\circ}\text{C}$ , and then the evaporated material is adsorbed by activated carbon. CS1 and TD were periodically on/off before MAGEE AE33. CS2 was periodically on/off before MAAP, and CS3 before PPS-M. For TD, measured solid particle losses were 24.5%, which is in the same range as the losses reported for a CS by Amanitidis et al. (2013).

- CS1, owner TUT: ON/OFF before MAGEE AE33
- CS2, owner Pegasor: ON/OFF before MAAP
- CS3, owner Pegasor: ON/OFF before PPS-M
- TD, owner TUT: ON/OFF before MAGEE AE33



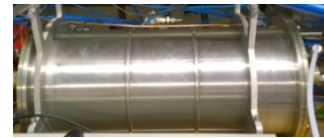
#### 4.10 Potential Aerosol Mass (PAM) chamber

Owner: FMI

Operators: Hilikka Timonen, Jesse Jokela, FMI

The effect of secondary aerosol formation on the BC emission measurements was studied using a potential aerosol mass (PAM) chamber. PAM is defined as the maximum aerosol mass that is produced in the chamber as the precursor gases are oxidized. PAM chamber used in these measurements is a small, simple, flow-through chamber that is flushed with ozone ( $O_3$ ), hydroxyl (OH), and hydroperoxyl ( $HO_2$ ) and irradiated with ultraviolet light (Kang et al. 2011, (Ortega 2013).

PAM chamber was used in pre-defined time periods with each fuel. The flow through the PAM chamber was set to 6–7 lpm and the voltage of the lamps was at the maximum value (230 V). Typical value for RH was 20–30%, for temperature 25 °C and for ozone concentration 13–20 ppm. The aging as the sample flows through the chamber in these measurements represents at least two day aging in the atmosphere. PM losses in the PAM chamber were estimated to be approximately 30%.



PAM chamber.



$CO$ ,  $SO_2$ , ozone  
analysers and  
humidifier.

#### 4.11 PM sampling

##### In-stack PM sampling, EN 13284-1

Owner: VTT

Operator: Harri Puustinen, VTT

In-stack sampling was conducted according to standard EN 13284-1. The filter, filter holder and nozzle arrangement was pre-heated at 430 °C, stabilized overnight in exsiccator and weighted. Pre-heating temperature at least 20 °C higher than that in the exhaust duct is required. Filter was located inside of the exhaust duct under the prevailing conditions. Flow through filter was approximately 13 lpm (STP, wet). After sampling, filter arrangement was after-heated at 160 °C, stabilized overnight in exsiccator and weighted. No cyclone for removing large particles was used. Munktell MK 360 (47 mm)



quartz filters were used.

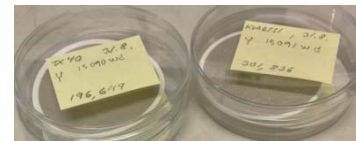
- Uncertainty of the in-stack results at 95% confidence:  $\pm 5\%$ .
- Standard: EN 13284-1

### ISO 8178 sampling

AVL Smart Sampler 472 (SPC), Owner: VTT  
 Operator: Hannu Vesala, VTT  
 Standard: ISO 8178

Microtroll (MT), Nova Messtechnik GmbH, Owner: VTT  
 Operators: Sami Nyyssönen and Jarno Martikainen, VTT  
 Standard: ISO 8178

Partial flow dilution system combined with gravimetric sampling of exhaust particulates is a standardised procedure (ISO 8178). Two ISO 8178 partial flow dilution systems were used to collect PM (AVL Smart Sampler SPC and Microtroll MT). A partial flow from the raw exhaust was taken for dilution with filtered and dried air, and then the flow was conducted through a filter to collect the particles. Microtroll uses CO<sub>2</sub> tracer for verification of dilution ratio, whereas SPC uses calibrated mass flow meters. No cyclone or hat for removing large particles was used. For SPC, DR was 8 and for MT DR was ~30. ISO 8178 requires DR not to be less than 4, temperature on filter lower than 52 °C and face velocity on filter 35–100 cm/s. Minimum temperature requirement of 42 °C on filter does not apply to older mini dilution tunnels. Transfer line heating was set to 200–250 °C. The ISO 8178 minimum loading requirement is 0.25 mg and recommended loading is 1.3 mg for 70 mm (o.d.) filter size.



Parameters for the AVL Smart Sampler 472:

- PM loading 0.7-27 mg on 70 mm (o.d.) filter (63 mm effective diameter).
- DR 8.
- Temperature on filter 35-44 °C.
- Face velocity was 37 cm/s.
- Transfer line heating 220 °C.

Parameters for Microtroll:

- PM loading 0.34-4.2 mg on 70 mm (o.d.) filter (63 mm effective diameter).
- DR 26-36
- Temperature on filter was 46-54 °C.
- Filter face velocity 42 cm/s.
- Transfer line heating 250 °C (failed until 9.9.2016).

**Pored tube dilution system:** Juha Heikkilä, Wärtsilä

### Filters

Pallflex TX40HI20-WW filters (o.d. 70 mm) were used for PM, SOF, anion and PAH analyses. For the EC/OC and elemental analyses, quartz microfiber filters (Munktell MK360) were used. Quartz filter size in in-stack sampling was smaller (o.d. 47 mm) than in the ISO 8178 PM sampling (o.d. 70 mm). Quartz filters were pre-cleaned at 400 °C for in-stack sampling. For ISO 8178 sampling, quartz filters were pre-cleaned for two hours at 850 °C followed with almost three weeks stabilisation. Loaded filters were stored in freezer.

4-7 replicate filters per fuel and load combination were obtained for each filter quality and sampling system. Number of TX40 filters was 78 with SPC and 39 with MT. On quartz filters, 41 samples were collected with SPC, 39 with MT and 61 with in-stack sampling.

Collections with back-up filters located after the primary filter showed that in most cases share of mass on the back-up filter was less than 5% of the total PM mass (Figure 4.3). Higher mass on back-up filter was observed at lower DR (SPC sampling) than at higher DR (MT sampling). At low DRs, semivolatile compounds are prone to condensing (see Chapter 5.4.7).

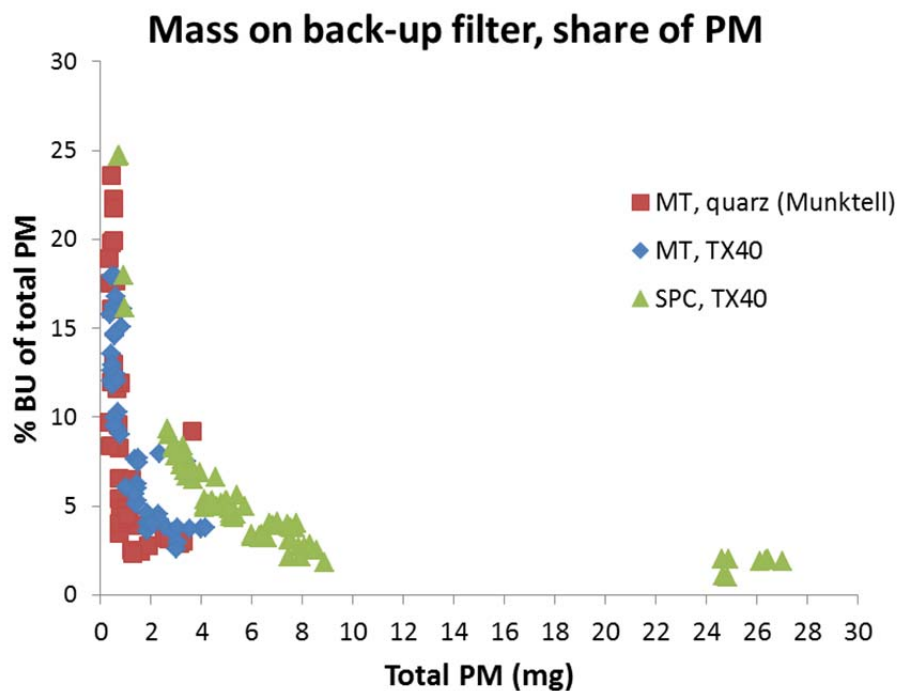


Figure 4.3. Share of mass on back-up filter of the total mass on filters.

High concentrations of trace elements in the Munktell MK360 reference filters were found, and this was also in accordance with manufacturer's information (Table 4.1).

Table 4.1. Trace elements in the Munktell MK360 filters (information from manufacturer).

Typical Levels of Trace Elements in MK 360 and T 293 – ppm																
Al	Ba	Ca	Cd	Co	Cr	Cu	Fe	Mg	Mn	Na	Ni	Pb	Sr	Ti	V	Zn
300	10	250	0.002	<0.5	2	2	50	25	2	100	2	<1	3	<1	<5	6

Due to high amount of trace elements present in the Munktell MK360 filters, another filter material was explored. Pallflex Tissuquartz 2500QAT-UP filters are ultra-pure and heat-treated for reduction of trace organics. Tissuquartz filters are designed for temperatures up to 1093°C and for aggressive atmospheres. As quartz filters are stabilized at elevated temperatures for the EC/OC analyses, a pre-analysis of the behaviour of Pallflex Tissuquartz filters was conducted (Table 4.2). Mass of Pallflex Tissuquartz filters reduced more than mass of Munktell filters in ovening. However, mass of Pallflex Tissuquartz filters was more stable than mass of Munktell filters after ovening. Pallflex filters were selected for the ship measurements in the WP2 of this project.

Table 4.2. Behavior of quartz filters in ovening.

	16.8.2016	25.8.2016	31.8.2016
	mg	mg	mg
<b>Difference compared with original mass</b>			
Munktell	-0.572	-0.517	-0.536
Tissuquartz	-3.145	-2.972	-3.112
<b>Difference compared with mass after ovening</b>			
Munktell	0.109	0.126	0.115
Tissuquartz	0.065	0.096	0.052

## 4.12 EC analysis

Owner: VTT  
 Operator: Päivi Koponen  
 Parallel analyses by VTT, FMI and UEF from  
 Munktell MK360 quartz filters



*Principle* – EC/OC method is based on a thermal-optical analysis technique (Bauer et al. 2009). Temperature and gas atmosphere is adjusted while continuously measuring the transmission of a laser through the sample matrix. In the first phase, sample is heated in steps up to 650–900 °C in Helium (He) atmosphere to remove OC (Figure 4.4). The organics may be pyrolytically converted to EC in this phase, which is monitored by measuring continuously the transmission of a laser. Any charring of the OC results in a decrease in transmittance of the laser. In the second phase, sample is cooled to for example 550 °C, 2% O<sub>2</sub>/He is introduced and temperature is raised again. Both the original EC and that produced by the pyrolysis are oxidized to CO<sub>2</sub>, which is then converted to methane and detected by the FID. The organic compounds pyrolytically converted to EC are compensated by continuous measurement of the transmission of a laser. Based on the FID response and laser transmission data, the quantities of OC and EC in the sample are calculated. Methane is injected into the sample oven providing the calibration of each sample analyzed to a known quantity of carbon. Saccharose is used as an external standard.

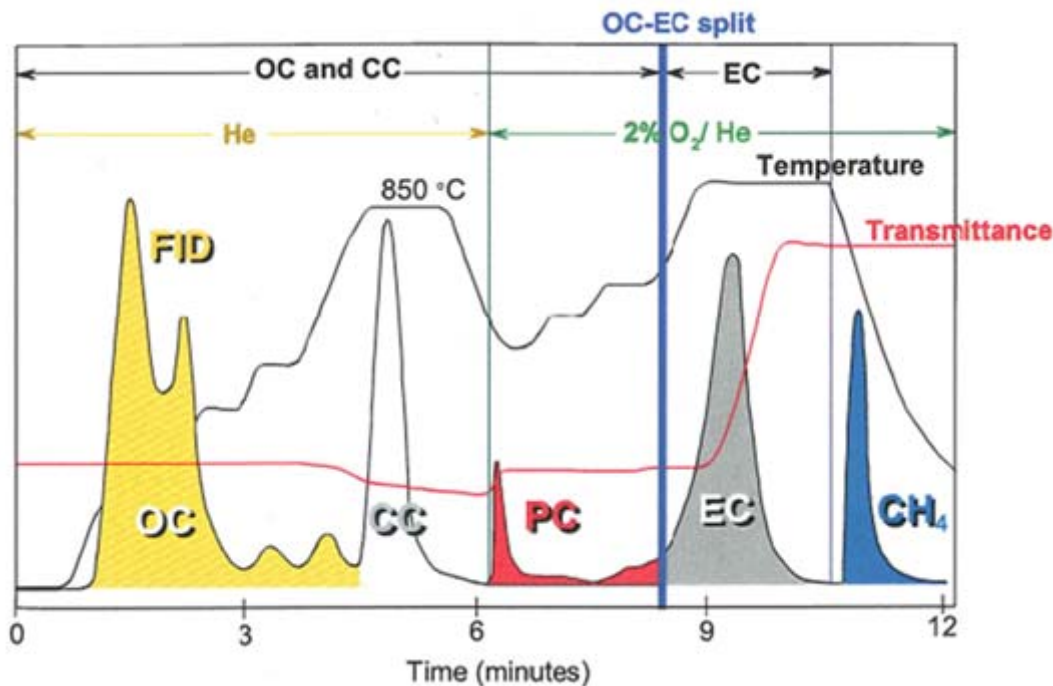


Figure 4.4. Thermogram for filter sample containing OC, carbonate (CC) and EC. PC is pyrolytically generated “char”. Final peak is methane calibration peak. (Birch & Cary 1996).

EC/OC analysis is a well-known procedure. However, it is sensitive towards PM constituents, and temperature offsets. Significant contribution of sulphates, metals and OC increases uncertainty of the thermal-optical EC analysis through challenges in determination of the EC/OC split. Premature evolving EC may be catalyzed by mineral oxides prone to catalytically enhance combustion of EC at high inert-mode temperatures. (Panteliadis et al. 2015; Jung et al. 2011; Karanasiou et al. 2011). Ambient aerosol samples may contain carbonate carbon (CC), which can be removed e.g. by HCl treatment prior to analysis. However, CC is not common for PM<sub>2.5</sub> aerosols (Maenhaut 2009).<sup>3</sup>

*Procedure* – Sunset Laboratories Inc’s EC/OC analyser model 4L was used at VTT. Sunset Laboratories Inc’s analyser model 5L (software ECOC1029, calculation Cal359) was used at FMI. UEF used Sunset analyser model from year 2005 (software Inst231, Calc150). From instrument manufacturers, Sunset Laboratory uses a thermal-optical transmission (TOT) method and DRI uses a thermal-optical reflectance (TOR) (Maenhaut 2009).

In this study, metals and oxygen present in fuels were suspected to promote premature evolving EC. The 2.5%S fuel had high ash content, and it also contained oxygen. The 0.5%S fuel contained relatively high ash content, but its oxygen content was low. The Bio30 fuel had substantially high oxygen content, however, its ash content was very low. To select temperature program for round-robin samples, behaviour of three temperature programs with these samples were studied:

- “NIOSH870” = NIOSH 5040 with 870 °C peak in He phase, duration 780 s
- “NIOSH750” = NIOSH 5040 with 750 °C peak in He phase, duration 780 s
- “EUSAAR2” = 650 °C peak in He phase, duration 1170 s

In the NIOSH 5040 program, the sample is heated in steps up to 850–900 °C in He atmosphere to remove OC, or lower peak temperature, for example 750 °C, if EC loss is evident. EUSAAR2 protocol proposed for the the ambient air samples (prEN 16909) uses a

<sup>3</sup> Information also from VTT’s internal method and <http://www.elementalanalysis.com/services/thermal-optical-analysis-ocec/>

peak temperature of 650 °C in He phase to decrease a risk for premature evolution of EC and to minimize pyrolysis. Prolonged temperature steps also support these aims. (Cavalli et al. 2010). Duration of EUSAAR2 is 1170 s, while duration of the NIOSH program is only 780 s. For the 0.1%S fuel, the last FID peak proved to occur close to the methane calibration peak. If true baseline level is not achieved in between of the EC and methane peaks, background is overestimated and methane calibration area is reduced leading to the overestimated TC result. This was taken into account for the round-robin samples by prolonging the last step of the EUSAAR2 program by 60 seconds. Also Maenhout (2009) recommended prolongation of the EUSAAR2. Temperature programs studied are shown in Table 4.3.

Table 4.3. Temperature programs used in this study: modified NIOSH 5040 (left-hand side) and EUSAAR2 (prEN 16909) (right-hand side).

NIOSH 5040 modified				EUSAAR 2*			
	Dura- tion s	Time s	Temp. °C		Dura- tion s	Time s	Temp. °C
Purge	10	10	Room temp.	Room temp.	10	0-10	
OC1 – He	80	10-90	310	OC1 – He	120	10-130	200
OC2 – He	60	90-150	475	OC2 – He	150	130-280	300
OC3 – He	60	150-210	615	OC3 – He	180	280-460	450
OC4/CC – He	90	210-300	870/750	OC4 – He	180	460-640	650
He	55	300-355	cooling	He	30	640-670	no heat
He/O <sub>2</sub>	45	355-400	550				
EC1/PC – He/O <sub>2</sub>	45	400-445	625	EC1/PC – He/O <sub>2</sub>	120	670-790	500
EC2 – He/O <sub>2</sub>	45	445-490	700	EC2 – He/O <sub>2</sub>	120	790-910	550
EC3 – He/O <sub>2</sub>	45	490-535	775	EC3 – He/O <sub>2</sub>	70	910-980	700
EC4 – He/O <sub>2</sub>	45	535-580	850	EC4 – He/O <sub>2</sub>	80	980-1060	850
EC5 – He/O <sub>2</sub>	90	580-670	870				
Cal & cooling	110	670-780				1060- 1170	

\* Prolongation of 60 s of the last step of EUSAAR2 program was used for the round-robin samples.

The EC results were calculated according to Eq. 1.

$$EC = \frac{ECw \cdot A \cdot PM}{PM_{mass}} \quad (1)$$

EC = EC result (mg/m<sup>3</sup>)

ECw = EC analysed from punch (mg/cm<sup>2</sup>)

A = Effective loaded filter area (cm<sup>2</sup>)

PM<sub>mass</sub> = PM loading on filter (mg)

PM = PM result (mg/m<sup>3</sup>)

Particular challenge was the EC analysis from the in-stack samples (raw exhaust sampling) due to the difficulties in obtaining sufficiently light samples for reliable determination of the EC/OC split time and simultaneously sufficient PM mass for weighing (filter holder is weighed together with filter). PM analysed separately by collecting “dark” samples combined with collection time of “light” samples were used to calculate very low PM masses of the “light” samples (Table 4.4). For most light samples, collection times were very short, in minimum five seconds.

Table 4.4. Collection times, PM and TC loadings for “dark” and “light” in-stack samples.



	Collection time	PM mass (mg)		TC ( $\mu\text{g}/\text{cm}^2$ )	
		min	max	min	max
Dark samples for PM and TC/PM determination					
0.1%S	20-30 min	2.5	7.6	68	414
0.5%S	15-30 min	4.2	9.0	163	613
2.5%S	10 min	11.0	14.5	108	568
Bio30	30 min	2.5	4.9	69	312
Light samples for EC/TC determination					
0.1%S	10-1200 s	0.04	3.5	2.6	14.7
0.5%S	10-90 s	0.10	0.31	6.5	14.6
2.5%S	5-60 s	0.12	1.10	4.2	17.2
Bio30	13-60 s	0.04	0.07	2.6	3.8

Differences were observed in the in-stack TC results analysed from same filters using the NIOSH750 program (79 to 492  $\mu\text{g}/\text{cm}^2$ ) and the EUSAAR2 program (108 to 622  $\mu\text{g}/\text{cm}^2$ ). TC of “dark” samples appeared to exceed the highest feasible saccharose standard within the FID measurement range. Higher saccharose concentrations were in the measurable range using the EUSAAR2 program (504  $\mu\text{g}/\text{cm}^2$ ) than using the NIOSH 5040 program (336  $\mu\text{g}/\text{cm}^2$ ) (Table 4.5). This due to evaporation of carbon in a wider time range in the EUSAAR2 than in the NIOSH 5040 leading to lower FID peaks. The inconsistencies in the TC results were highest for the samples with the high TC loadings outside of the calibration range.

Table 4.5. Saccharose standards at 336  $\mu\text{g}/\text{cm}^2$  and 504  $\mu\text{g}/\text{cm}^2$  loadings analysed with “NIOSH 750” and EUSAAR2 programs.

Standard ( $\mu\text{g}/\text{cm}^2$ )	Program	TC ( $\mu\text{g}/\text{cm}^2$ )	Punch area ( $\text{cm}^2$ )	FID1/FID2
336	EUSAAR2	373.7	0.78	ok/ok
504	EUSAAR2	601.7	1	ok/ok
336	NIOSH 750	367.2	1	offscale/ok
504	NIOSH 750	556.6	1	offscale/offscale

The TC/PM ratios for “dark” samples and the EC/TC ratios for the “light” samples could be used for calculation of the EC concentrations (Eq. 2). However, the in-stack EC results were calculated using Eq. 1 based and PM masses on light filters. These PM masses were calculated using the collection time and the known PM concentrations.

$$EC = PM \cdot RL_{EC/TC} \cdot RD_{TC/PM} \quad (2)$$

EC = EC result ( $\text{mg}/\text{m}^3$ )

PM = PM emission result ( $\text{mg}/\text{m}^3$ )

$RL_{EC/TC}$  = Ratio of EC and TC based on light samples

$RD_{TC/PM}$  = Ratio of TC and PM based on dark samples

Based on the results in Chapter 5, no pre-treatment of loaded filters was applied and EUSAAR2 was selected for the final analyses, and for round-robin between three laboratories (VTT, FMI and UEF). Summary of the procedure used in the EC analyses of the round-robin samples is as follows:

- No drying or extractions of loaded filters
- EUSAAR2 temperature program, last temperature step prolonged by 60 s
- Additional calculation using a constant split time of 750 s

EC range:	1-15 $\mu\text{gC}/\text{cm}^2$ .
OC range:	5-400 $\mu\text{gC}/\text{cm}^2$
Detection limit:	0.2 $\mu\text{gC}/\text{cm}^2$
Repeatability:	$\pm 5\%$

Pros	Cons
<ul style="list-style-type: none"> <li>Well-known and documented</li> <li>Calibration procedures are available</li> <li>Standardised procedures, such as NIOSH 5040 and proposal prEN 16909.</li> </ul>	<ul style="list-style-type: none"> <li>Sensitive towards PM constituents, e.g. mineral oxides, sulfuric acid, oxygen.</li> <li>PM sampling is required.</li> <li>OC/EC split determination is uncertain.</li> <li>Temperature program affects the results.</li> <li>Restricted to use in laboratory.</li> <li>Saccharose standard for OC.</li> </ul>

### 4.13 Metal analysis

Elemental and metal analysis of ISO 8178 PM samples collected on Munktell 360 quartz filters was conducted by Labtium (Report 123630, Marjo Lauren). Samples were extracted in micro oven by using nitric acid ( $\text{HNO}_3$ ) and hydrofluoric acid (HF) (EN 14385) and analysed by using inductively coupled plasma mass spectrometry (ICP-MS).

Elements analysed included Ag, Al, As, B, Ba, Be, Bi, Ca, Cd, Co, Cr, Cu, Fe, K, Li, Mg, Mn, Mo, Na, Ni, Pb, Rb, Sb, Se, Sr, Th, Tl, U, V ja Zn, Br, Cl, P, S, Si and Sn. Reference filters contained relatively high concentrations of some elements, such as Al, Ca, Na and Fe.

Metals from exhaust aerosol were analysed also by the FMI using SP-AMS instrument (Chapter 4.6). This method is described for example by (Carbone et al. 2015), who reported concentrations of 13 metals: Na, Al, Ca, V, Cr, Mn, Fe, Ni, Cu, Zn, Rb, Sr and Ba. SP-AMS instrument detects metals associated in particles larger than 30 nm.

### 4.14 Anions in PM

Anions are analysed from exhaust particles at VTT using using capillary electrophoresis (CE) based on the SAEJ1936 and IP 416 guidelines (internal method 23.01). ISO 8178 PM samples collected with SPC on the Pallflex TX40 filters were extracted using 10% isopropanol (IPA) in water pipetted on filters in Erlenmeyer, shaken carefully and treated in the ultrasonic bath for 60 min. Samples were left at room temperature for overnight. Reference filters were included in all test series and treated similarly to samples. CE used for analysis was Waters Capillary Ion Analyzer CIA 4100, IonSelect High Mobility Anion electrolyte,  $75\mu\text{m} \times 375\mu\text{m} \times 60\text{ cm}$  capillary column (internal method RO22/MK/130).

In addition to sulphates, other anions are also analysed (nitrates, phosphates, fluorides, oxalates, acetates, bromides, and chlorides). Uncertainty of the anion analysis by CE at VTT based on repeatability and accuracy of the instruments is estimated to be around  $\pm 5\%$  of the result for high concentrations of anions, and  $\pm 20\%$  for low concentrations of anions. Higher uncertainty is related to anions, which are hardly soluble with IPA, water, or acids.

#### Water combined with sulphates

“Sulphates” analysed from PM can be in a form of sulphuric acid, organic sulphates, ammonium sulphate or inorganic sulphates. All of these have different capability to combine water. The amount of combined water depends on the humidity of weighting chamber. For sulphuric acid at 50% relative humidity, the amount of “combined water” is assumed as  $1.32 \times$  sulphuric acid according to SAEJ1936. For ammonium sulphate the respective factor is only 0.19, and, for example, for dihydrate  $\text{CaSO}_4(\text{H}_2\text{O})_2$ , the factor is 0.38, for tetrahydrate

0.75 and for pentahydrate 0.94. When minerals, metals or ammonia is present in the exhaust gas, the factor for “combined water” is different than that defined for sulphuric acid. Particularly for marine engine PM, assumed amount of water in PM is inaccurate, if sulphuric acid and other sulphates have not been determined separately. Water content of PM can also be analysed by weighting the particulate filters after stabilization in an exsiccator.

In this project, sulphate results obtained with the ISO 8178 and in-stack sampling were used to estimate concentration of sulphuric acid and other sulphates in PM separately. Sulphuric acid was not present in the in-stack PM as the prevailing temperature (350–400 °C) was above the dew point of sulphuric acid.

#### 4.15 PAHs and SOF associated with PM

PAHs were analysed by a subcontractor, Metropolilab. A total of 24 individual PAH compounds (Table 4.6) were analysed according to ISO 16000 and EN 14662 analysis methods. ISO 8178 PM samples collected on Pallflex TX40 filters were extracted with toluene in ultrasound bath. Soluble organic fraction (SOF) of PM was determined by toluene extraction and weighing of filters.

Detection limits of the PAH analysis at Metropolilab are 10 – 30 ng compound per sample and measurement uncertainty is 30%.

Sum of 7 heavy PAHs in PM (benz[a]anthracene, chrysene, benzo[b]fluoranthene, benzo[k]fluoranthene, benzo[a]pyrene, indeno[1,2,3-cd]pyrene, dibenz(a,h)anthracene) are shown in the final results. VTT has an internal method M23.01 for the PAH analyses.

Table 4.6. The PAH compounds analysed by Metropolilab.

<b>naphthalene</b> 2-methylnaphthalene 1- methylnaphthalene 1,1-biphenyl <b>acenaphthylene</b> <b>acenaphthene</b> <b>fluorene</b> <b>phenanthrene</b>	<b>anthracene</b> <b>fluoranthene</b> <b>pyrene</b> <b>benz[a]anthracene*</b> <b>chrysene*</b> <b>benzo[b]fluoranthene*</b> <b>benzo[k]fluoranthene*</b> benzo[e]pyrene	<b>benzo[a]pyrene*</b> perylene <b>indeno[1,2,3-cd]pyrene*</b> <b>dibenzo[a,h]anthracene*</b> <b>benzo[g,h,i ]perylene</b> 2,6-dimethylnaphthalene 2,3,5-trimethylnaphthalene 1-methylphenanthrene
---	--	---

PAH16 marked with boldface. PAH7 marked with an asterix

#### 4.16 Fuel/lube originating constituents in PM

Role of fuel/lube oil in the PM was evaluated by using fingerprint elements. Calcium proved to be the best fingerprint element for lube and vanadium for the high-sulphur fuel.

#### 4.17 Units of the results

The results in this report are shown as mass/Sm<sup>3</sup>, mass/kWh, and kilograms of oil equivalent (kg<sub>oe</sub>). The latter one is a unit equivalent to the approximate amount of energy of one kilogram of crude oil, equivalent to a net calorific value of 41 868 kJ/kg. Emission per oil equivalent mass is used when fuels with different energy contents are compared with each other as it is a commensurable unit, which compensates the differences in the energy contents of fuels. Energy contents of 2.5%S and Bio30 fuels were lower than those of the 0.1%S and 0.5%S fuels mainly due to their low hydrogen to carbon ratios.

The concentrations ( $c$ ) at the prevailing pressure and temperature ( $T, p$ ) are converted in the concentrations ( $c_0$ ) at standard pressure ( $p_0$ ) and temperature ( $T_0$ ) by using equation (6). This formula is based on the gas law, which combines Charles's law, Boyle's law, and Gay-Lussac's law: "The ratio between the pressure-volume product and the temperature of a system remains constant". In this report, standard temperature  $T_0$  is 273.15 K (0 °C) and standard pressure  $p_0$  is 101325 Pa<sup>4</sup>. The unit is mass/Sm<sup>3</sup>.

$$c_0 = c * \frac{T * p_0}{T_0 * p} \quad (6)$$

---

<sup>4</sup> See "Abbreviations" section: IUPAC definitions for conditions

## 5 Results

### 5.1 Stability of the test engine

Stability of engine was monitored by measuring emissions with the 0.1%S fuel before and after the test campaign (Table 5.1).

For gaseous emissions, only small changes were seen over the measurement campaign. Also the PM emissions remained at the same level when the in-stack sampling or the ISO 8178 sampling with SPC was used, while those obtained with the Microtroll sampling decreased substantially over the measurement campaign: at low load from 34 mg/Sm<sup>3</sup> (on 31.8 and 2.9) to 18.5 mg/ Sm<sup>3</sup> (on 21.9 and 22.9). Inspection revealed that the MT transfer line was cold until 10 September 2015 due to failure in the heating system. This may affect the PM results, and thus the priority was given to the results obtained with the SPC collection system.

*Table 5.1. Comparison of the results with the 0.1%S fuel tested before and after the measurement campaign.*

	0.1%S fuel, 75%load			0.1%S fuel,, 25%load		
	Start of campaign mass/kWh	End of campaign mass/kWh	Change-%	Start of campaign mass/kWh	End of campaign mass/kWh	Change-%
<b>NO<sub>x</sub></b>	10.8	11.2	3.5 %	9.2	9.6	4.4 %
<b>HC</b>	0.52	0.48	-8.7 %	1.37	1.22	-10.9 %
<b>CO</b>	0.33	0.31	-6.5 %	1.01	1.02	1.5 %
<b>CO<sub>2</sub></b>	642.6	641.4	-0.2 %	750.0	739.3	-1.4 %
<b>PM ISO 8178 (SPC)</b>	0.11	0.11	3.6 %	0.47	0.50	5.6 %
<b>PM ISO 8178 (MT)</b>	0.05	0.04	-14.7 %	0.28	0.14	-49.0 %
<b>PM in-stack</b>	0.1	0.1	-1.6 %	0.20	0.19	-2.6 %
<b>BC (based on FSN)</b>	0.012	0.010	-10.8%	0.098	0.089	-8.8 %

Engine stability was also monitored on daily basis using continuous measurements with the Gasetm FTIR instrument. The NO concentrations were particularly useful for this purpose (Figure 5.1 and Figure 5.2). Some changes were observed in the NO concentrations, and consequent inspection revealed small differences in fuel temperatures for the 2.5%S fuel on replicate testing days (10.9. and 11.9.2015). In addition, the fuel system pressure was not in the adjustment of the normal operating range for the 0.1%S fuel on 21.9.2015. Otherwise, engine was running smoothly and emissions stayed at constant level over the measurement campaign.

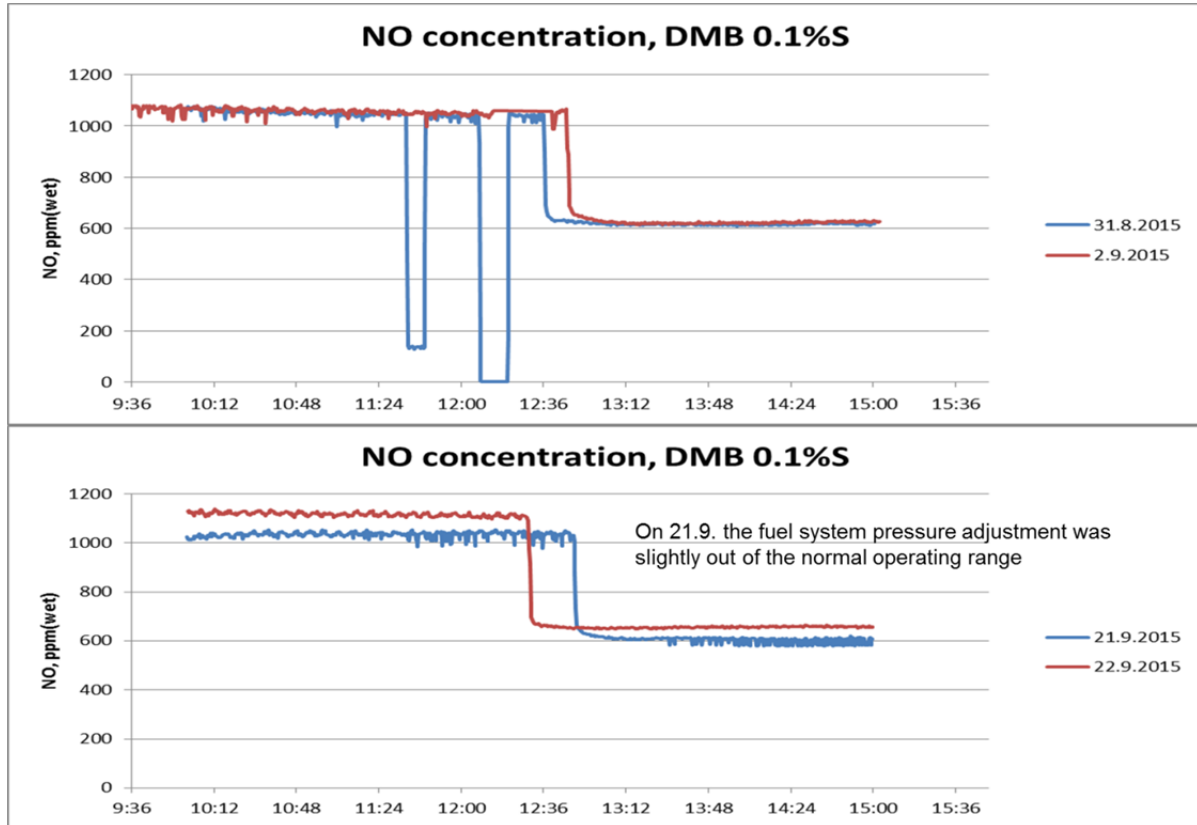


Figure 5.1. The engine stability was followed continuously using measurements of the NO concentrations (Gaset FTIR). Here the NO results with the 0.1%S fuel are shown in the beginning and in the end of the measurement campaign.

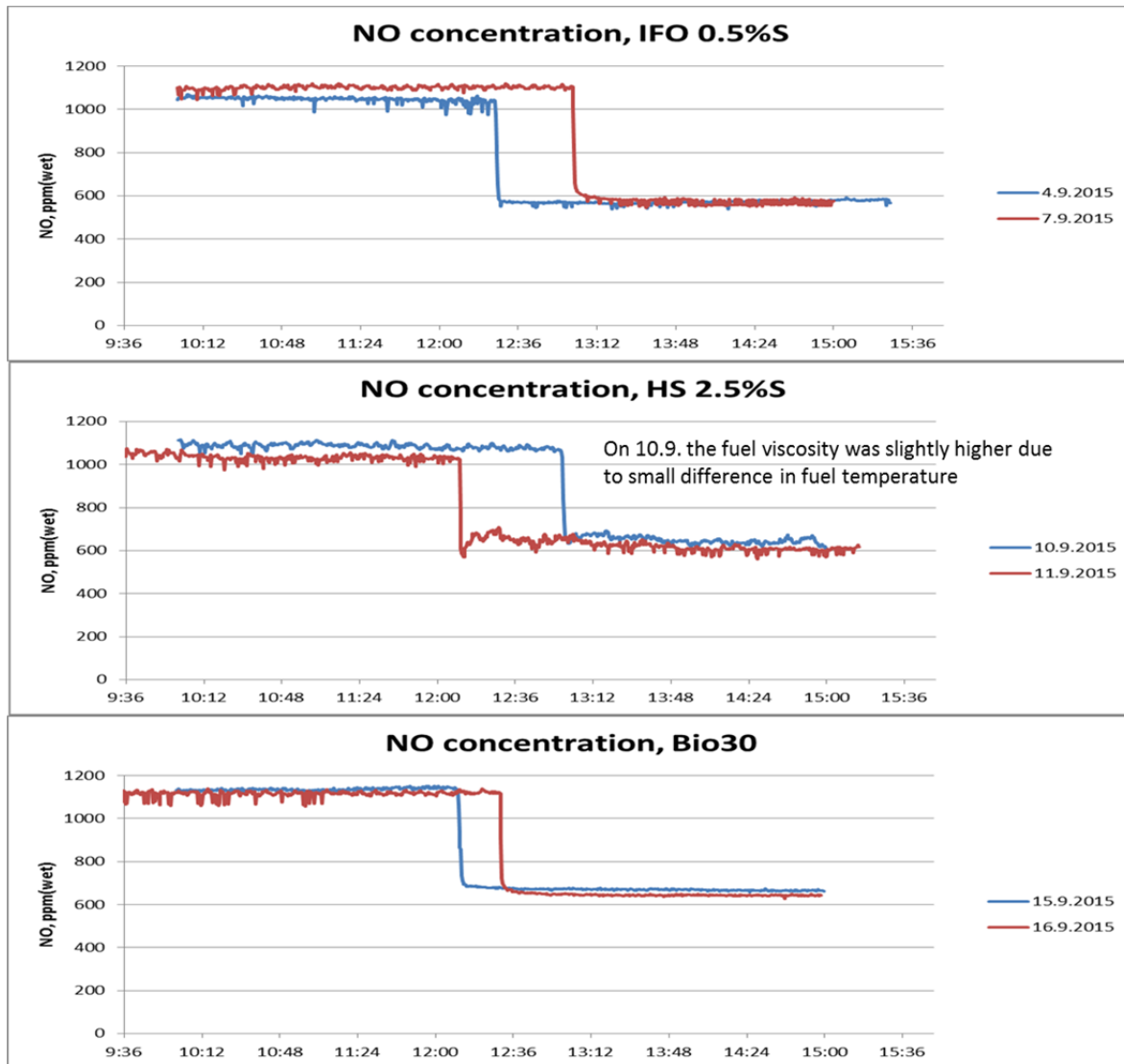


Figure 5.2. Follow-up of the engine stability by using measurements of the NO concentrations (Gaset FTIR) for the 0.5%S, 2.5%S and Bio30 fuels.

## 5.2 Engine parameters with different fuels

Four fuels tested were substantially different from each other. Sulphur contents of fuels were designed to vary, and one of the fuels, biofuel Bio30, contained oxygen. In addition, many of the main fuel properties, such as density and viscosity, varied between the test fuels.

Wärtsilä Vasa 4R32 LN engine is specified for certain viscosity range of the injected fuel. Proper viscosity of fuel was achieved by adjusting the fuel temperature. Table 5.2 shows the differences in fuel temperature: temperatures for the 0.1%S and Bio30 fuels were 28-34 °C, while temperatures for the 0.5%S and 2.5%S fuels were 100 °C and 134 °C. Fuel pressure before engine varied from 9.6 bar to 12 bar. Test cell temperature and humidity were relatively constant over the measurement campaign.

Different characteristics of fuel, both physical and chemical, affect injection, duration of injection, injection delay, the spray characteristics, speed of combustion, flame temperature and emissions. For example, early injection increases fuel efficiency and NO<sub>x</sub>, but decreases PM emission. Lower viscosity retards the start of injection leading to lower NO<sub>x</sub>, but higher

PM emissions, if aromatics and oxygen contents of fuels are at the same range (Nylund et al. 1997). Test engine used in this study is equipped with a mechanical injection system. Consequently it is more sensitive towards fuel properties than the modern engines equipped with advanced injection systems.

Table 5.2. Test parameters using different fuels at 75% and 25% engine loads.

	Unit	75% load				25% load			
		0.1 %S*	0.5%S	2.5%S	Bio30	0.1 %S*	0.5%S	2.5%S	Bio30
Test cell temperature	°C	29.1/26.9	28.8	30.0	29.9	29.2/26.4	28.0	29.7	29.7
Test cell rel. Humidity	%	34.7/39.4	36.4	32.3	32.6	37.7/38.5	39.6	32.8	25.1
Sampling point temperature	°C	367/360	364	356	345	310/309	316	308	295
Exhaust gas temp after TC	°C	361/359	362	364	360	321/317	324	325	319
Atmospheric pressure	mbar	1013/1010	1009	1033	1015	1015/1010	1009	1034	1016
Pressure diff at meas orifice	mbar	22	22	23	21	5	5	5	5
Under pressure in meas pipe	mbar	16	16	17	15	3	3	3	3
Exhaust gas pressure after TC	°C	71/58	75	55	70	65/48	65	47	62
Exhaust gas mass flow, wet	kg/h	8656/8659	8733	8873	8555	4128/4092	4213	4109	4044
Fuel mass flow rate	kg/h	246.8/246.2	250.1	265.9	255.1	97.4/95.7	99.4	104.6	99.4
Fuel viscosity before engine	mm <sup>2</sup> /s	4.7/5.5	15.8	24.8	6.8	4.8/5.1	15.8	23.9	6.6
Fuel temperature before engine	°C	33.7/28.4	99.1	132.9	31.2	33.2/30.6	98.8	133.7	31.7
Fuel pressure before engine	bar	9.6/11.3	11.1	11.4	10.6	10.4/11.3	11.3	12.0	10.8
Engine brake power	kW	1229.9/1229.3	1229.7	1230.6	1230.6	415.2/414.2	414.7	415.6	415.5
Torque	kNm	15.6	15,6	15,6	15,6	5.3	5.3	5.3	5.3
Engine speed	rpm	753.0	753.0	753.2	753.1	753.1/753	753.1	753.2	753.1
BMEP	bar	17.4	17.4	17.4	17.4	5.9	5.9	5.9	5.9

\*) Tested in the beginning and in the end of measurement campaign.

## 5.3 Gaseous emissions

### 5.3.1 CO, HC, NO<sub>x</sub> and CO<sub>2</sub>

The HC and CO emissions were lower at 75% load than at 25% load, whereas opposite was seen for the NO<sub>x</sub> emission (Figure 5.3). Higher combustion temperature at higher load leads to improved combustion, and consequently, increased NO<sub>x</sub> emissions. Also oxygen in biofuel tends to increase NO<sub>x</sub> emissions when compared to the non-oxygenated fuel (Murtonen et al. 2010).

The CO<sub>2</sub> emission depends primarily on the carbon content per energy content of fuel. The CO<sub>2</sub> emissions were the highest for the 2.5%S fuel, followed by the 0.5 %S, 0.1%S and Bio30 fuels.



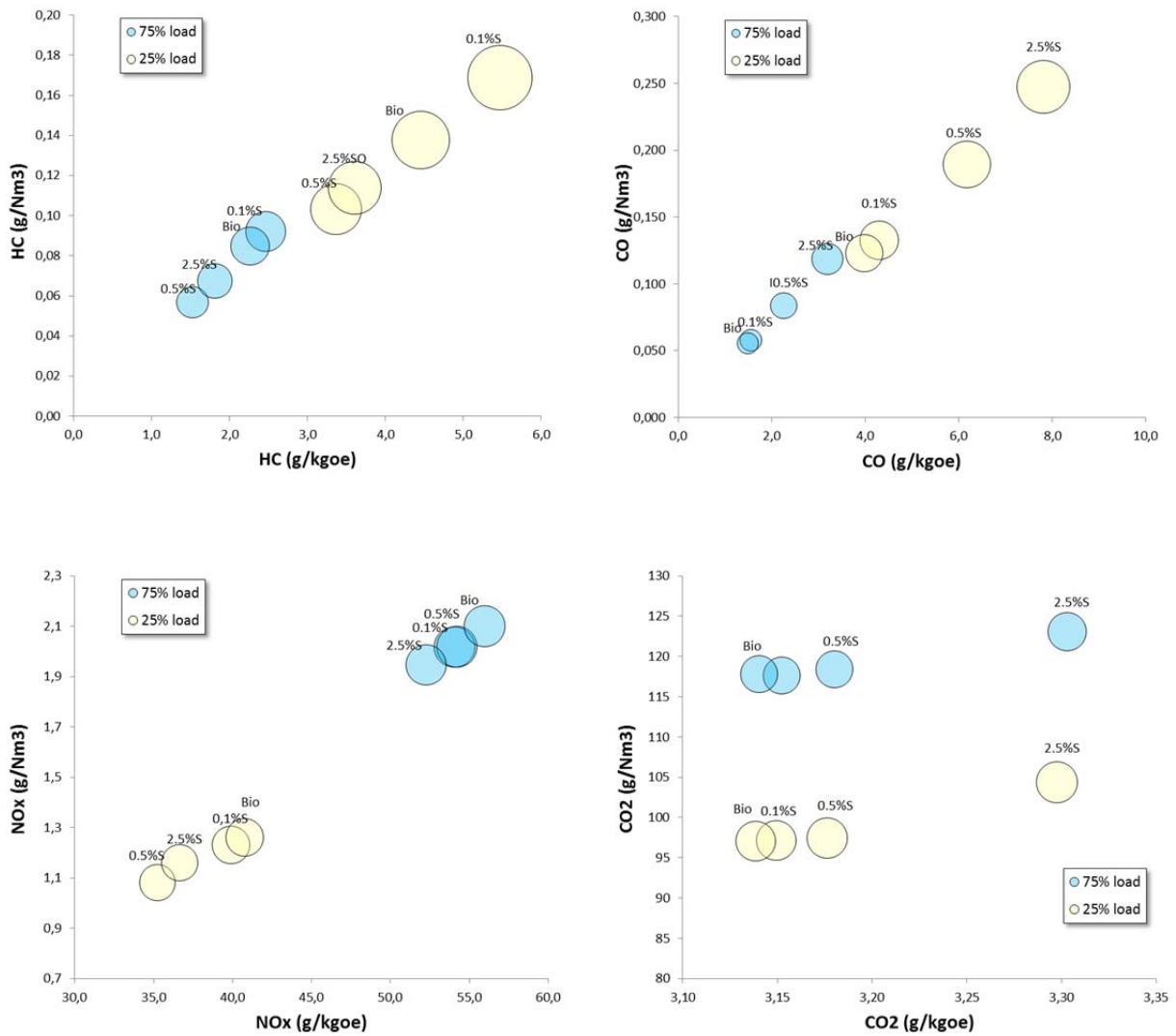


Figure 5.3. The CO, HC, NO<sub>x</sub> and CO<sub>2</sub> emissions in different units.

Figure 5.4 shows relationship between mass-based fuel consumption and the CO<sub>2</sub> emissions for different fuels and engine loads. In energy-basis (per kWh), fuel consumption and CO<sub>2</sub> emissions were lower at 75% load than at 25% load. This is due to the higher engine efficiency at higher engine loads. At the same time, the NO<sub>x</sub> emission increases when moving from 25% load to 75% load.

Fuel consumption and CO<sub>2</sub> emissions were higher for 2.5%S than for the other fuels due to its lower H/C-ratio and presence of low (or no)-energy containing constituents, such as sulphur, ash and oxygen. The Bio30 fuel contains 3.9 % (m/m) oxygen, and consequently its fuel consumption was slightly higher than that of the 0.1%S fuel. Energy contents of the 2.5%S and Bio30 fuels were lower than those of the 0.1%S and 0.5%S fuels.

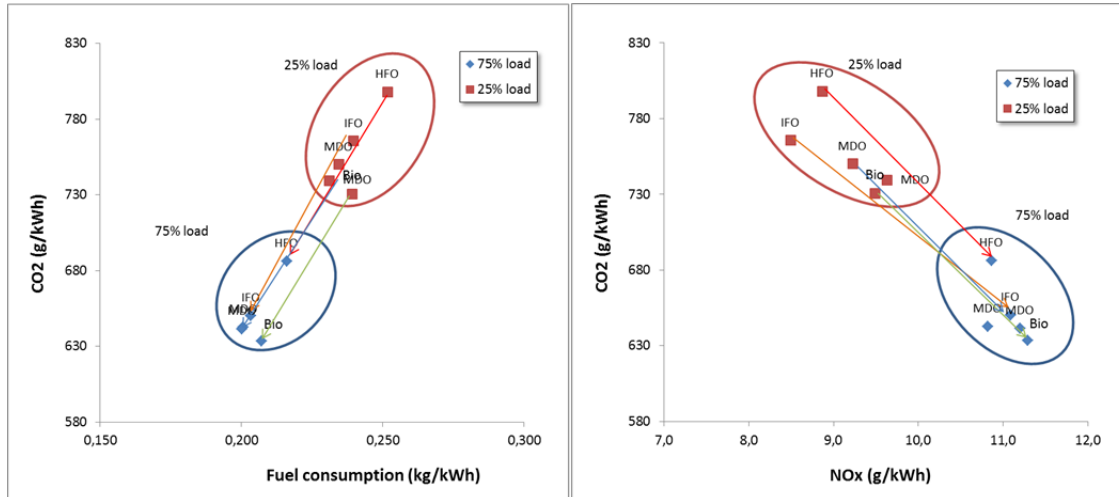


Figure 5.4. CO<sub>2</sub> compared with fuel consumption (left-hand side) and with the NO<sub>x</sub> emissions (right-hand side).

The HC and CO emissions decreased when moving from 25% load to 75% load (Figure 5.5). Differences between fuels were substantial particularly at 25% load. The HC and CO emissions typically decrease when combustion improves.

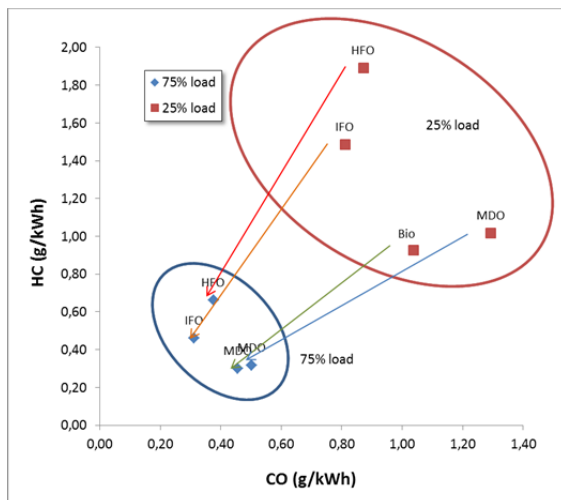


Figure 5.5. Comparison of the HC and CO emissions.

### 5.3.2 SO<sub>2</sub> and other gases measured with FTIR

SO<sub>2</sub> in the exhaust gas originate from fuel sulphur, which was clearly seen as higher SO<sub>2</sub> concentrations with high sulphur fuels (Figure 5.6) (see also sulphates in Chapter 5.4). SO<sub>2</sub> concentrations calculated from fuel sulphur content were close to those measured by the FTIR and with those measured by impinger method. The SO<sub>2</sub> results were close to each other particularly at low SO<sub>2</sub> concentrations, while discrepancy between the methods increased at high SO<sub>2</sub> concentrations.

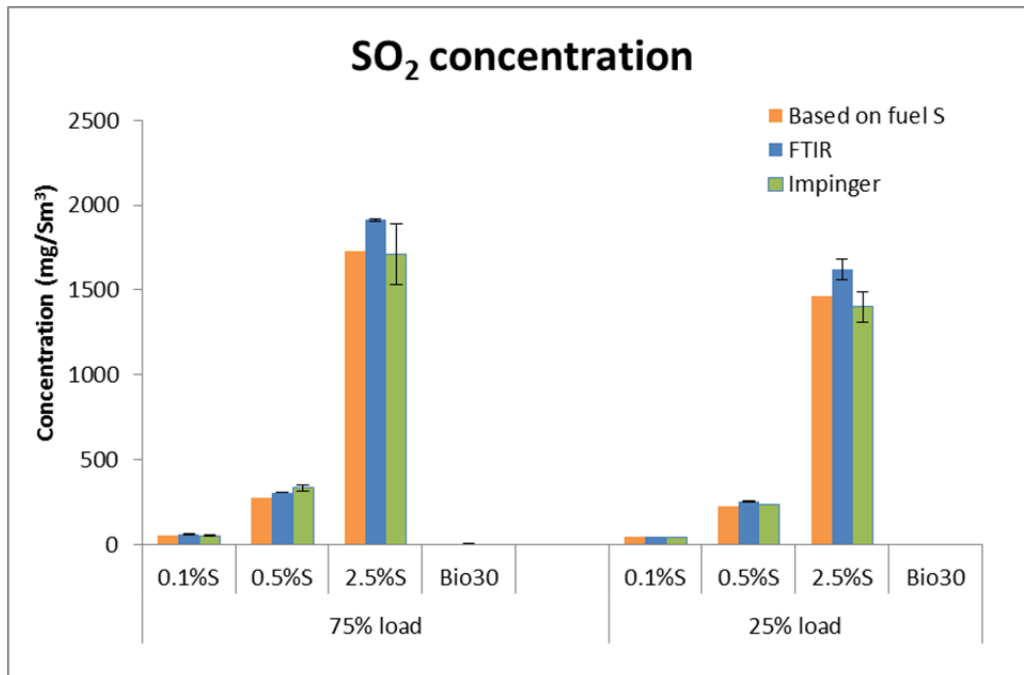


Figure 5.6. The SO<sub>2</sub> concentrations in the exhaust gas based on a) fuel sulphur content (calculated) b) FTIR measurements and c) the impinger collection method.

Water content of the exhaust was the lowest for the 2.5%S fuel and the highest for the Bio30 fuel (Table 5.3). Measured water concentrations of the exhaust gas were used in the calculation of the dilution ratios (dry/wet conversions of CO<sub>2</sub>).

The lowest NO<sub>2</sub> concentrations measured were 4-13 ppm for the 0.5%S and 2.5%S fuels, while the NO<sub>2</sub> concentrations varied from 15 to 28 ppm for the 0.1%S and Bio30 fuels. Detection limit for NO<sub>2</sub> is approximately 2 ppm.

The N<sub>2</sub>O and NH<sub>3</sub> concentrations were below the detection limits with all fuels at both engine loads (the detection limits 2 and 4 ppm).

The methane concentrations were below the detection limit (<2 ppm) at high engine load and in the range of 2 to 8 ppm at 25% engine load.

The formaldehyde and acetaldehyde concentrations were below the detection limit of 5 ppm at both engine loads.

Table 5.3. The selected concentrations measured with FTIR.

		H <sub>2</sub> O g/Sm <sup>3</sup>	NO <sub>2</sub> mg/Sm <sup>3</sup>	CH <sub>4</sub> mg/Sm <sup>3</sup>	N <sub>2</sub> O mg/Sm <sup>3</sup>	NH <sub>3</sub> mg/Sm <sup>3</sup>	SO <sub>2</sub> mg/Sm <sup>3</sup>	C <sub>2</sub> H <sub>4</sub> mg/Sm <sup>3</sup>	HCHO mg/Sm <sup>3</sup>	CH <sub>3</sub> CHO mg/Sm <sup>3</sup>
<b>Detect. limit</b>			2	2	2	4			5	5
<b>75% load</b>	0.1%S	49.5	58	1.4	bd	bd	62	3.1	0.1	bd
	0.5%S	49.5	26	0.5	2.4	bd	307	5.7	3.5	bd
	2.5%S	42.3	15	1.0	2.1	bd	1912	2.1	3.6	bd
	Bio30	51.9	49	1.1	bd	bd	5.2	3.3	2.0	bd
	0.1%S	49.8	45	1.3	bd	bd	64	2.7	1.6	bd
<b>25% load</b>	0.1%S	44.5	44	1.7	2.1	bd	49	4.2	2.6	bd
	0.5%S	42.6	9	6.0	2.2	bd	254	6.3	3.3	bd
	2.5%S	37.5	9	5.8	2.4	bd	1618	0.9	3.0	bd
	Bio30	43.9	35	2.2	bd	bd	1.7	4.7	4.4	bd
	0.1%S	41.8	30	3.1	bd	bd	52	4.1	3.0	bd

### 5.3.3 Hydrocarbon measurements – new options for on-line analyses

Spectral Engines calibrated and tested a multi-component hydrocarbon gas analyser as part of the project. The aim was to create a system capable of differentiating alkanes such as methane, ethane, and propane. Such a system could be used in multiple places, for example in gas engine operation. The core component of the analysis system was the M3.7 spectral sensor. The calibrations and subsequent laboratory testing with our co-operator proved that the analyser setup and the calibrations performed on the system were satisfactory. A limiting factor was the measurement speed of the setup. Spectral Engines is currently investigating improvements that could be applied to the setup in order to increase the performance on multiple levels, including measurement sensitivity, capability of differentiating more gas components including carbon monoxide and carbon dioxide, CO and CO<sub>2</sub> respectively, and decrease the measurement time per spectrum.

Spectral Engines also investigated NIR measurements from liquids together with the VTT team. We attempted to measure NIR spectra of four different marine fuels in order to determine whether NIR measurements could be used to detect differences in the fuels. Unfortunately only fuels that are transparent, and not completely black, could be measured without any sample preparation. As such the suitability of a simple measurement system for this case is quite limited, and more in-depth analysis of black fuels may only be possible if the fuels are dissolved in order to make them transparent in the NIR region. So in order to create an online system, heavy emphasis on the development of a dissolving and diluting sampling system would need to be done. For this, Spectral Engines would need more co-operators specialised in the sampling systems.

Furthermore, preliminary trial was conducted to monitor hydrocarbon emissions on-line using VTT's microhotplate sensor. This experience encourages to explore possibilities for continuation of this development.

## 5.4 Primary PM and its composition

### 5.4.1 PM emission

PM emissions were measured by in-stack sampling from raw exhaust without dilution and by the ISO 8178 sampling with dilution. In the ISO 8178 sampling, lower DR (8) was used with the SPC than with the MT (30). Examples of filters are shown in Figure 5.7 and Figure 5.8.

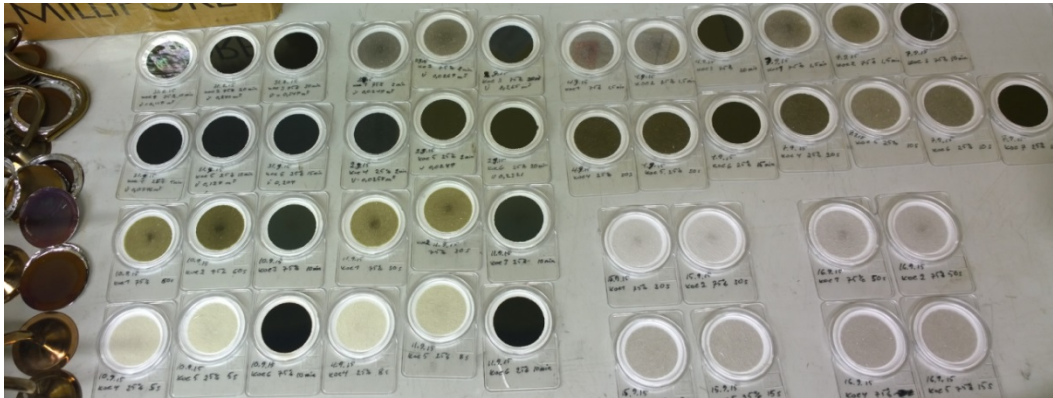


Figure 5.7. PM filters from the in-stack sampling.

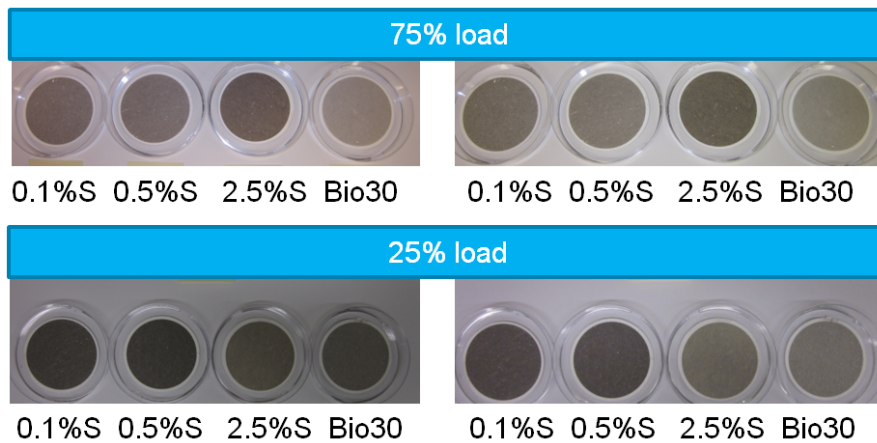


Figure 5.8. PM filters from the ISO 8178 (SPC) sampling.

The PM concentrations and emissions were strongly dependent on the fuel sulphur content (Figure 5.9). The highest PM concentrations and emissions were observed for the 2.5%S fuel: 153 mg/Sm<sup>3</sup> (850 mg/kWh) at 75% load, and 134 mg/Sm<sup>3</sup> (1040 mg/kWh) at 25% load. For the other fuels studied, PM varied from 18 to 44 mg/Sm<sup>3</sup> (100–240 mg/kWh) at 75% load, and from 52 to 103 mg/Sm<sup>3</sup> (390–810 mg/kWh) at 25% load. The second highest PM at both loads was observed for the 0.5%S fuel. Further reductions in PM were achieved with the 0.1%S and Bio30 fuels. The dependence of PM on the fuel sulphur content observed in this work is in line with the findings of Ristimäki et al. (Ristimäki et al. 2010) and Sippula et al. (Sippula et al. 2014).

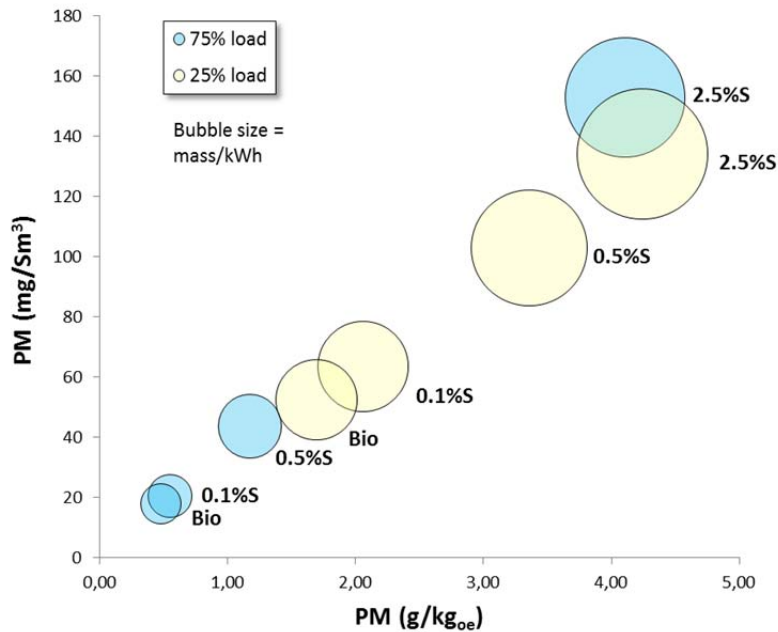


Figure 5.9. The PM concentrations as mass/Sm<sup>3</sup>, and the PM emissions as mass per kilograms of oil equivalent (kg<sub>oe</sub>) and mass/kWh, ISO 8178 PM sampling with SPC (DR=8).

The PM emissions using the hot in-stack sampling are typically lower than those using the ISO 8178 sampling with dilution, because low DR promotes condensation of the organic compounds and sulphuric acid on filter. Expectedly, the in-stack PM results were lower than those obtained with the ISO 8178 sampling with the SPC system using DR 8. However, in one case, viz. for the 2.5%S fuel at 25% load, the PM results using the in-stack and the ISO 8178 samplings were surprisingly close to each other (Figure 5.10). This Figure shows also the rejected PM results obtained with the MT sampling: the PM for the 2.5%S fuel was at the same level or even lower with MT than with the hot, in-stack sampling, which is not expected. For the 2.5%S fuel, substantial losses in the MT sampling (e.g. due to the wet spot) are suspected.

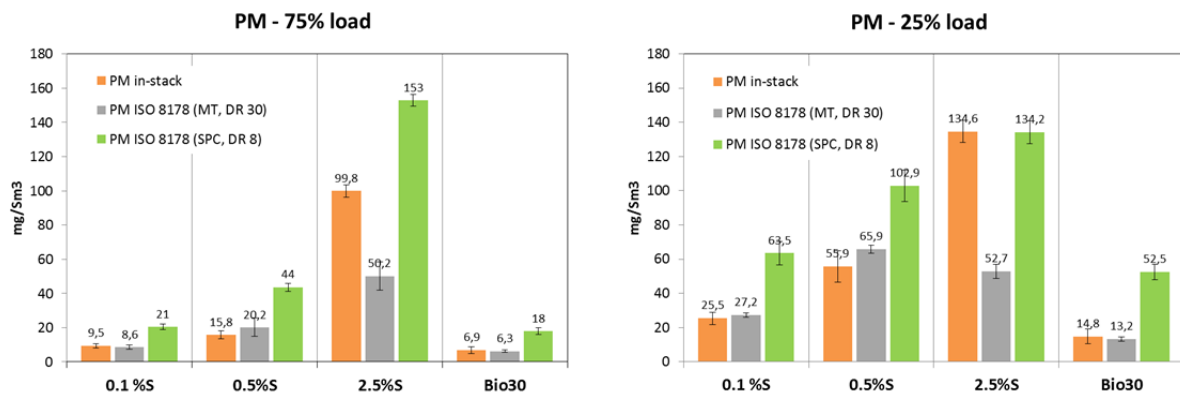


Figure 5.10. The PM concentrations using the in-stack and the ISO 8178 (SPC DR 8, MT DR 30) sampling. The MT results particularly with the 2.5%S fuel are suspected for losses.

The results from PPS-M were closest to the in-stack PM results (Figure 5.11). This is not surprising as in-stack PM does not contain much organic carbon and PPS-M measures the sample at elevated temperature above sulphuric acid dew point. PPS-M was capable for on-line monitoring of the PM mass concentrations resembling those obtained by the in-stack sampling.

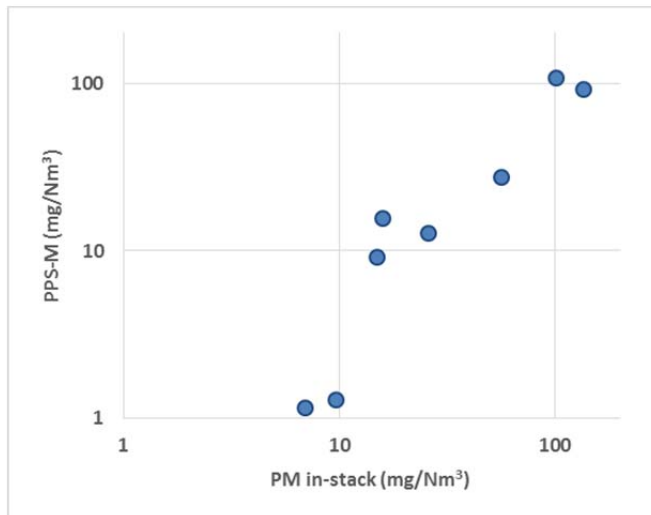


Figure 5.11. PPS-M signal comparison with the in-stack PM concentrations over all fuel and load conditions.

#### 5.4.2 Organic carbon

PM associated SOF results in Figure 5.12 represent the organic compounds that are soluble in toluene. The SOF results were surprisingly comparable with the OC results obtained by the EC/OC analyses (the EUSAAR2 program, see Chapter 5.5).

PM contained less SOF and OC at 75% engine load than at 25% engine load, which is an expected result as combustion is typically more complete at higher than at lower engine load.

For the 0.1%S, 0.5%S and Bio30 fuels, the OC represented 50-55% of PM at 75% load, and 60-70% of PM at 25% load (10–25 mg/Sm<sup>3</sup> at 75% load and 36–71 mg/Sm<sup>3</sup> at 25% load). The highest OC was observed for the 0.5%S fuel at both engine loads. The SOF and OC concentrations were the lowest for the 0.1%S fuel and for the Bio30 fuel. For the 2.5%S fuel, the share of OC in PM was lower than for the other fuels, only 12% and 38% of PM (18 and 53 mg/Sm<sup>3</sup>).

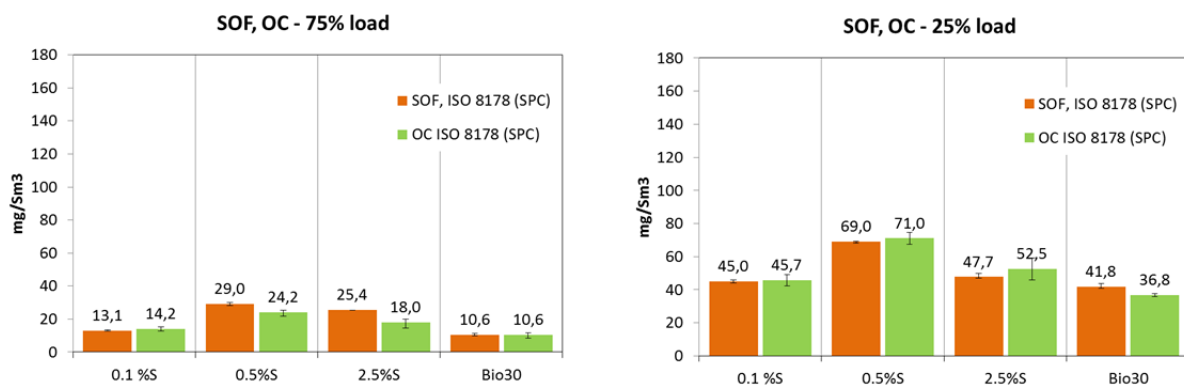


Figure 5.12. SOF and OC concentrations associated in PM (ISO 8178 SPC).

### 5.4.3 SO<sub>4</sub>, NO<sub>3</sub>, PO<sub>4</sub>, Br, Cl, F

Sulphates were the only anions substantially present in the PM samples. Concentrations of nitrates, phosphates, bromides, chlorides and fluorides in PM were at very low level (Figure 5.13).

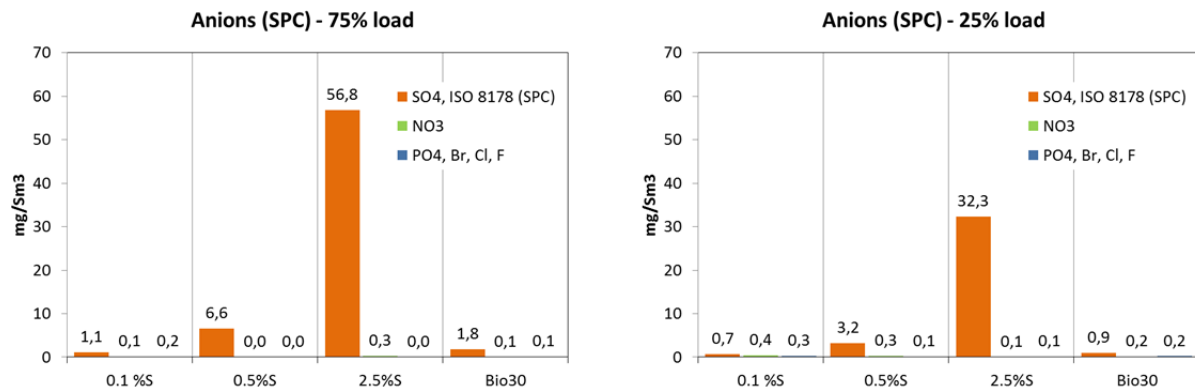


Figure 5.13. Anions in PM ISO 8178 (SPC).

Dew points of sulphuric acid were calculated for fuels used in this study (Figure 5.1). Temperature of the hot in-stack sampling (310–360 °C) was higher than the dew point of sulphuric acid. Consequently, in-stack PM did not contain sulphuric acid, while other sulphates (e.g. metal sulphates) could be present. In the ISO 8178 sampling at DR 8, the temperature of the diluted exhaust was low enough for condensation of sulphuric acid with all fuels, while at DR 30 only with the 2.5%S fuel. By using high DR of 100, sulphuric acid does not condense at normal temperature with the fuels studied.

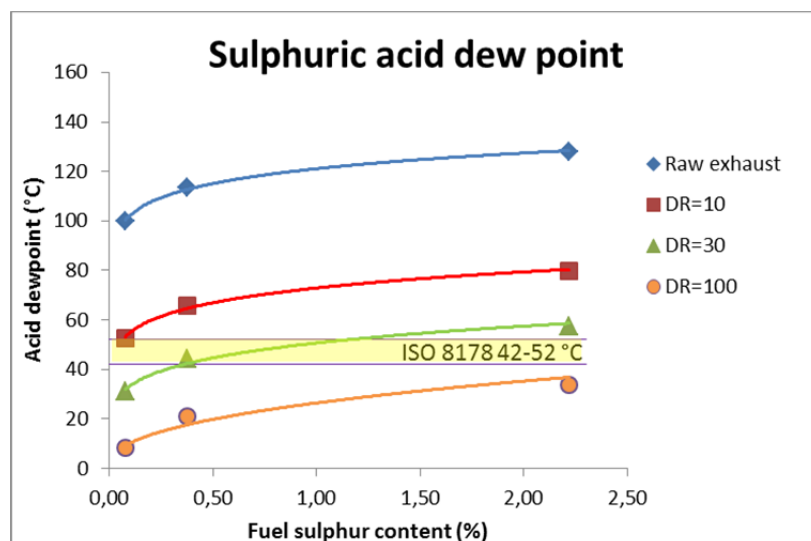


Figure 5.14. Dependence of the dew point of sulphuric acid on fuel sulphur content and dilution ratio (calculation based on the results of this study).

High sulphate concentrations in PM were observed for the ISO 8178 samples using DR 8 (SPC system) (Figure 5.15). Low sulphate concentrations in the PM collected with the in-stack and MT systems is in-line with theory of having only other sulphates than sulphuric acid



on filter. On the opposite, sulphates collected with the MT system using the 2.5%S fuel should contain sulphuric acid and concentration of sulphates should be far above that of the in-stack samples. Low concentration of sulphates in the MT samples indicates that sulphates are lost in sampling, for example due to the wet spots (note earlier failure in temperature control).

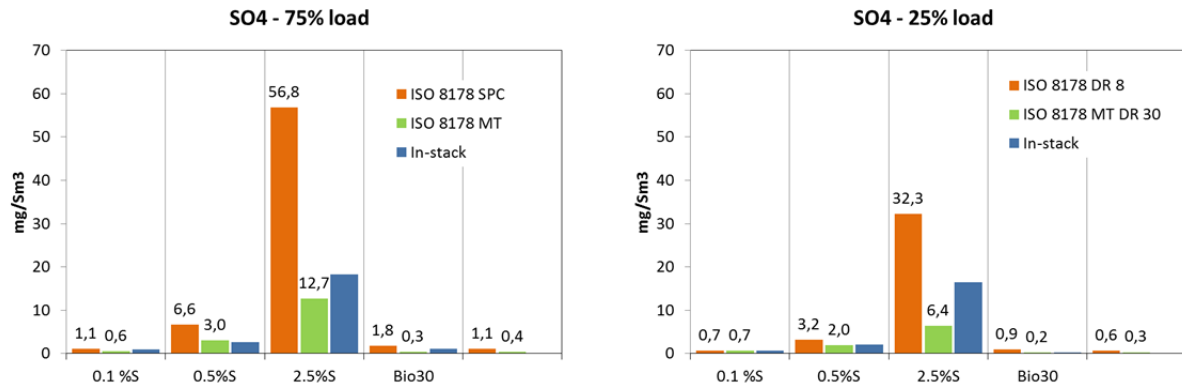


Figure 5.15.  $SO_4$  in ISO 8178 and in-stack sampling.

Conversions of  $SO_2$  to  $SO_4$  in PM obtained with ISO 8178 SPC sampling at DR 8 are shown in Figure 5.16. Conversions were slightly higher at 75% than at 25% engine load. For the 2.5%S fuel, conversion was 2.0% at 75% engine load, while 1.3% at 25% engine load. The respective conversions were 1.4% and 0.8% for the 0.5%S fuel, and 1.2% and 0.8% for the 0.1%S fuel. High combustion temperature at 75% engine load may enhance conversion of  $SO_2$  to  $SO_3$ . Conversions of  $SO_2$  to  $SO_4$  in in-stack PM were expectedly lower than those for the ISO 8178 sampling as sulphuric acid is not present in the in-stack PM. Engine load did not affect conversions in the in-stack case. Conversions of  $SO_2$  to  $SO_4$  were not calculated for the Bio30 fuel, because it contained only 4.3 mg/kg sulphur leading to high uncertainty in the calculations.

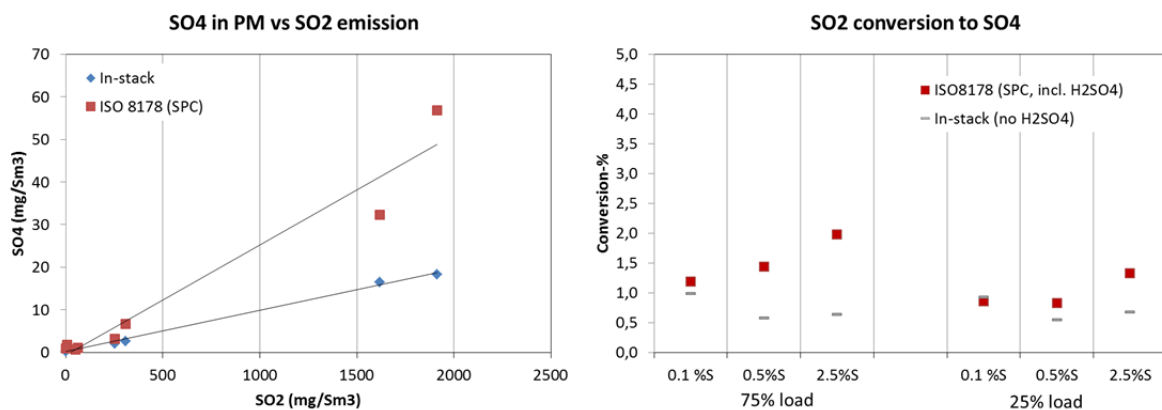


Figure 5.16.  $SO_2$  conversion to primary PM  $SO_4$ .

#### 5.4.4 Oxygen

Elemental analysis of PM samples was not conducted in this measurement campaign. However, during the on-board measurements in the WP2 of the SEA-EFFECTS BC project, oxygen content of some PM samples was analysed (ship used 0.7%S fuel) (Timonen et al. 2017). Oxygen content of 12 PM samples (ISO 8178) was on average 24%(m/m) $\pm$ 7%(m/m). This shows that substantial amount of oxygen can be present in marine engine PM

associated with sulphates, sulphuric acid, water, oxides of metals and non-metals, and with organic compounds.

#### 5.4.5 Metals in PM and fuel/lube

Figure 5.17 and Figure 5.18 show the concentrations of metals analysed from PM at 75% and 25% engine loads, and metals analysed from fuel and engine oil.

Lube oil contained substantial amounts of calcium (Ca), phosphorus (P) and zinc (Zn). Also PM samples contained substantial amounts of Ca, which was not significantly present in fuels other than in the 2.5%S fuel. The 2.5%S and 0.5%S fuels contained some phosphorus.

The 2.5%S and 0.5%S fuels contained vanadium (V), nickel (Ni), and also some Ca and P. Considerable V concentration was observed also in the PM samples obtained with the 2.5%S and 0.5%S fuels. V was not present in the lube oil. Metal contents of the 0.1%S and Bio30 fuels were generally low.

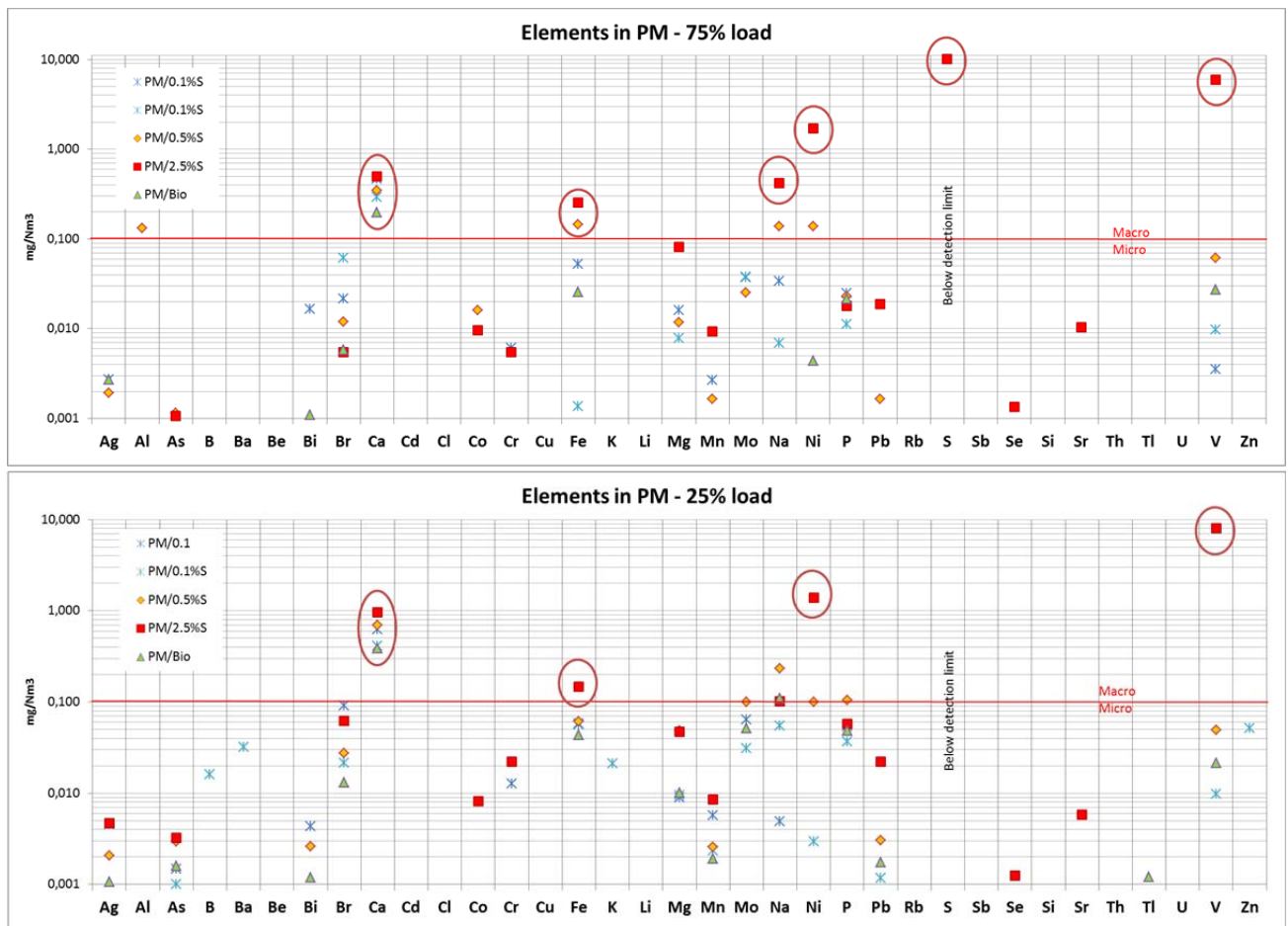


Figure 5.17. Elements analysed from PM (ISO 8178 SPC).

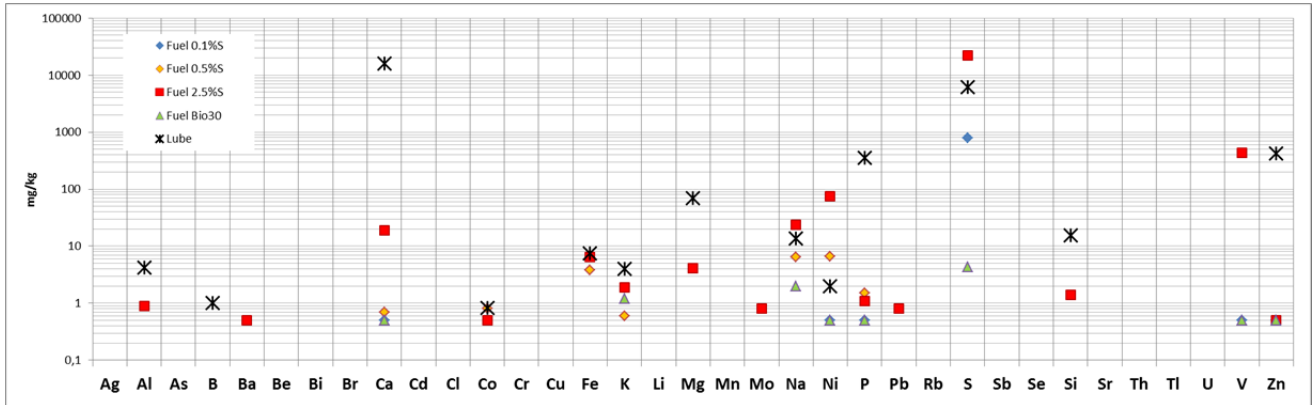


Figure 5.18. Elements analysed from fuel and engine oil samples.

Ca was used as a fingerprint compound for lube, and V for high-sulphur fuels to study the role of fuel and lube in PM (Figure 5.19). V and Ni contents of 2.5%S and 0.5%S fuels were sufficient to explain the V and Ni present in the respective PM samples.

Ca contents of the other fuels than the 2.5%S fuel were too low to explain the Ca content of the respective PM samples. Share of Ca of metals in PM was 30–70% for other samples, while below 10% for the 2.5%S sample.

For the 0.1%S, 0.5%S and Bio30 fuels, lube consumption of 18–29 mg/Sm<sup>3</sup> at 75% load, and 24–44 mg/Sm<sup>3</sup> at 25% load, were sufficient to explain Ca content of the respective PM samples. This would mean lube oil consumption less than 0.1% of fuel consumption at 75% load and below 0.2% at 25% load. With estimated lube consumption (18–44 mg/Sm<sup>3</sup>), it seems that engine oil can significantly contribute in the PM associated OC (13–71 mg/Sm<sup>3</sup>).

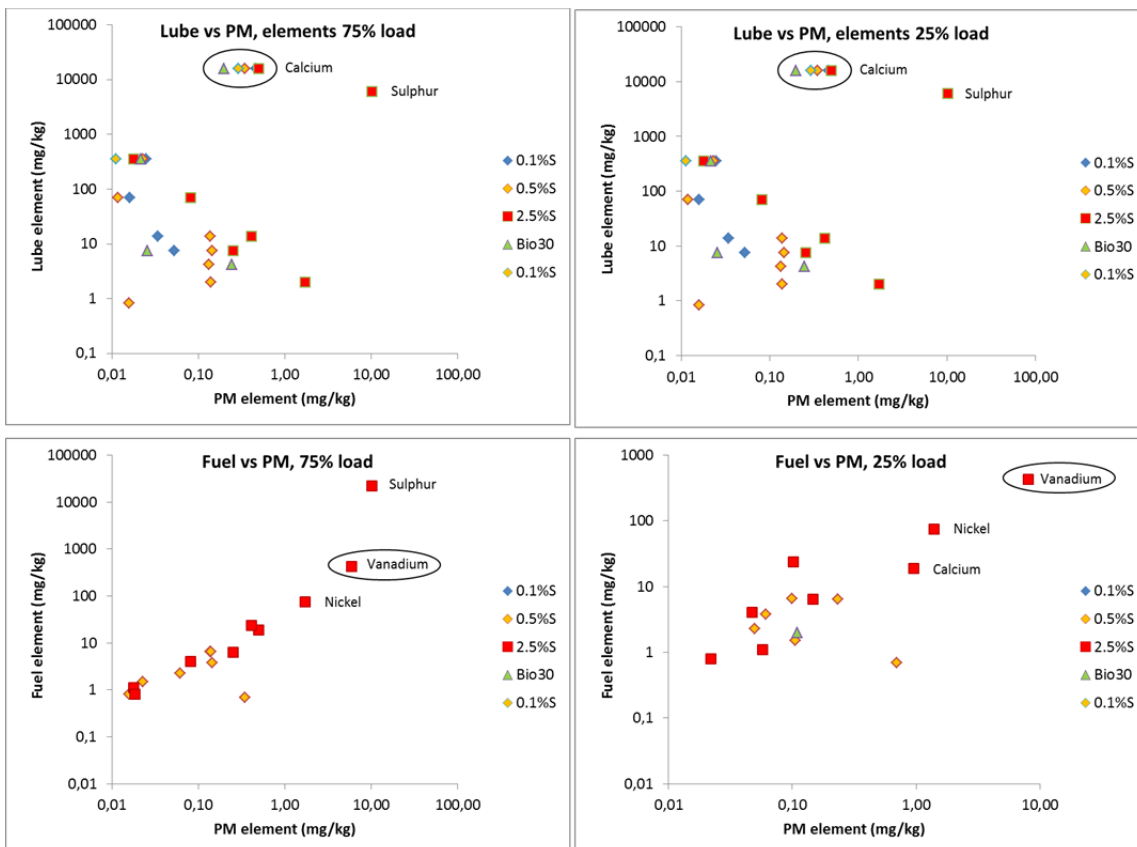


Figure 5.19. Metal content in fuel, engine oil and PM at the 75% load.

#### 5.4.6 PAHs in PM

Heavy PAHs were found at higher concentration in the PM for the 0.5%S fuel than for the other fuels, particularly at 25% engine load (Figure 5.20). The results indicate that even at 0.5%S level, residual fuel may contain substantial amount of PAH precursors, probably depending on crude oil and processing technology. The lowest PAH concentrations were found for the 0.1%S and Bio30 fuels. At 75% engine load, also 2.5%S fuel resulted in surprisingly low sum of 7 PAHs.

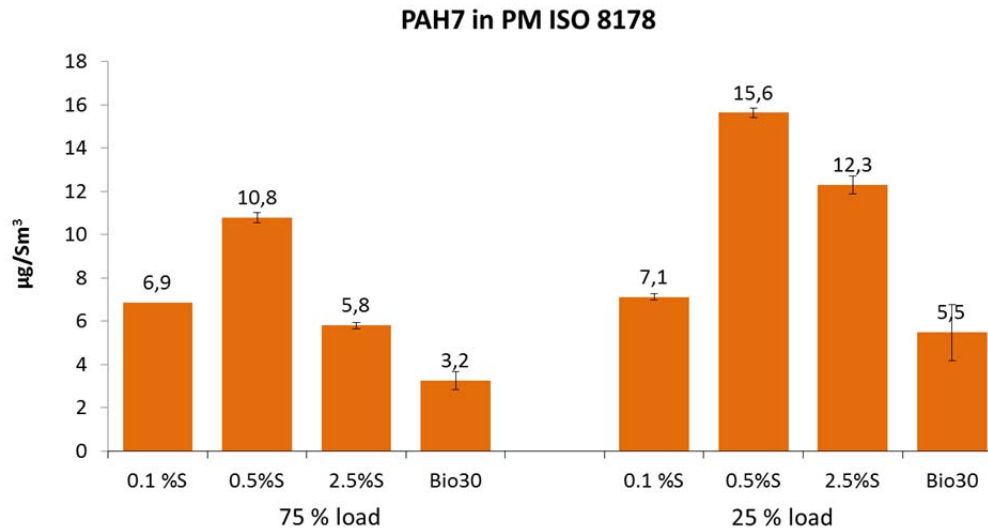


Figure 5.20. Sum of 7 heavy PAHs in PM (benz[a]anthracene, chrysene, benzo[b]fluoranthene, benzo[k]fluoranthene, benzo[a]pyrene, indeno[1,2,3-cd]pyrene, dibenz(a,h)anthracene).

Distributions of different PAH compounds associated with PM are shown in Figure 5.21. Concentrations of the heaviest PAHs were the highest for the 0.5%S fuel, while the lowest concentrations of individual PAHs were observed for the Bio30 fuel. High concentrations were found for example for phenanthrenes, pyrene, chrysene and benzo(e)pyrene.

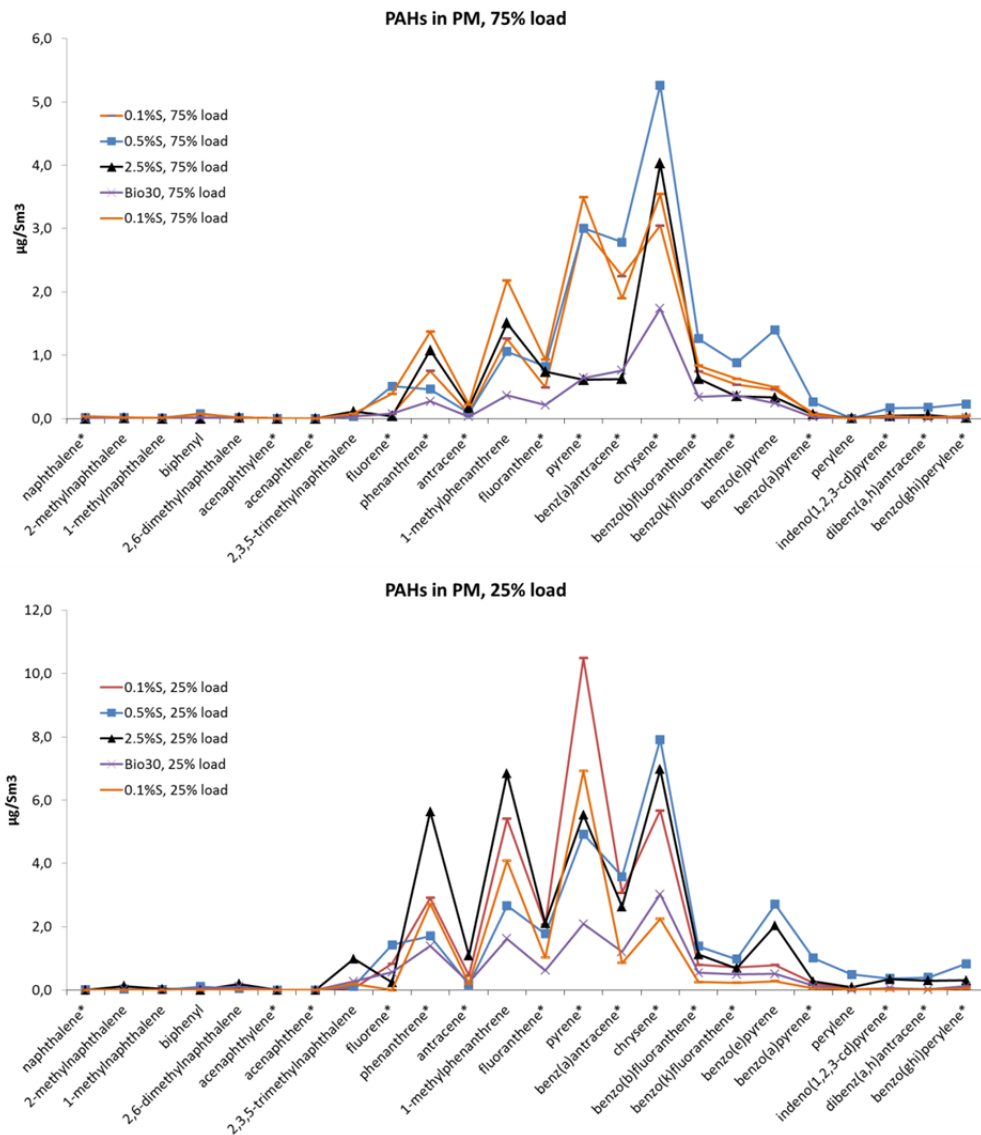


Figure 5.21. Distribution of PAH compounds in PM.

#### 5.4.7 Summary of the PM composition

Detailed composition of PM was achieved by combining compositional analyses results from the ISO 8178 SPC and in-stack samplings (Figure 5.22) and MT sampling (Figure 5.23). Analyses and dependences between the constituents from different PM samples are as follows:

- **EC** results obtained with the EUSAAR2 program (see Chapter 5.5).
- **“Heavy OC”** is associated in the in-stack samples (hot-sampling).
- **“Light OC”** is calculated by reducing “heavy OC” from total OC from the ISO 8178 samples (DR 8).
- **“mSO<sub>4</sub>”** means sulphates other than H<sub>2</sub>SO<sub>4</sub> viz. sulphates analysed from the in-stack samples (metal and non-metal sulphates).
- **H<sub>2</sub>SO<sub>4</sub>** is calculated by reducing the “mSO<sub>4</sub>” from the total sulphates analysed from the ISO 8178 samples (DR 8).

- **Metals** (and some other elements) were analysed from the ISO 8178 samples and the same concentrations are assumed in the in-stack samples.
- **“Rest”** is calculated by reducing the other constituents from total PM. “Rest” is mainly oxygen associated in water, sulphates, metal/non-metal oxides, and also in the incompletely burned fuel in the case of Bio30.

The share of EC in PM was generally low, although substantial differences were seen between fuels and engine loads (see Chapter 5.5). EC was below 5 mg/m<sup>3</sup> at 75% engine load with all fuels, whereas it was even as high as 22 mg/m<sup>3</sup> at 25% engine load. The highest EC concentration was observed for the 2.5%S fuel at 75% engine load and for the 0.5%S fuel at 25% engine load. The lowest EC concentrations were observed for the 0.1%S and Bio30 fuels.

There were differences in OC and sulphate concentrations between the sampling methods. A low portion of OC was observed in the in-stack samples due to the sampling of the hot exhaust. For the ISO 8178 PM collection, the OC concentrations depend on DR and on the filter face temperature. Phase partitioning of semivolatile organic compounds depends on their concentration and saturation pressure, and on the other constituents of PM. At low DR, OC is mainly present in the particulate phase, while increasing DR shifts OC to the gas phase along with decreasing concentration of semivolatile organic compounds. In addition to lower DR, cooling of the exhaust leads to a gas-to-particle conversion through decreased saturation pressures of the semivolatile organic compounds. The ISO 8178 sampling is relatively isothermal, while the maximum DR is not limited (Ristimäki et al. 2010; Lipsky & Robinson 2006). The OC concentrations were higher at 25% load than at 75% load for all fuels. The highest OC was observed for the 0.5%S fuel at both engine loads. For the 2.5%S fuel, the share of OC in PM was lower than for the other fuels. However, for the 2.5%S fuel PM contained “heavy OC” substantially.

Besides sulphuric acid, PM can contain metal/non-metal sulphates and organic sulphates. Sulphuric acid was not present in the in-stack samples due to the sampling temperature above the dew point of sulphuric acid. The ISO 8178 SPC samples contained higher shares of sulphates than the in-stack samples, as the DR 8 moderately promotes condensation of these species on the filter. The contribution of sulphates in PM followed the fuel sulphur content.

Metals were analysed from the ISO 8178 samples. The ash content of the 2.5%S fuel was substantially higher than that of the other fuels studied (Chapter 3), and so was the metal content of PM. Metals in PM originate mainly from fuel and engine oil.

The “rest” portion contains mainly oxygen associated with water, sulphates, oxides and organic compounds. PM may contain a substantial amount of water associated with sulphuric acid and sulphates, or as crystal water. Sulphuric acid and sulphates have different capabilities to combine water (see Chapter 4.14). For metal sulphates the factor for “bound water” is not the same as for the sulphuric acid. This explains low factor for maximum bound water based on compositional analyses (e.g. factor max. 0.86 at 25% load for the 2.5%S fuel). Composition of the in-stack samples for the 2.5%S fuel remains partly unexplained.

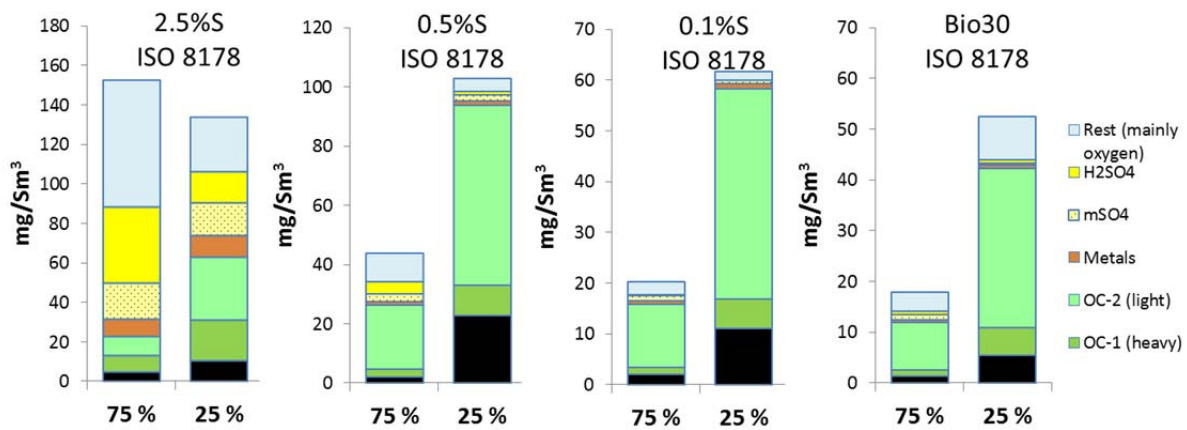


Figure 5.22. Composition of PM for samples collected with ISO 8178 SPC (DR 8) sampling.

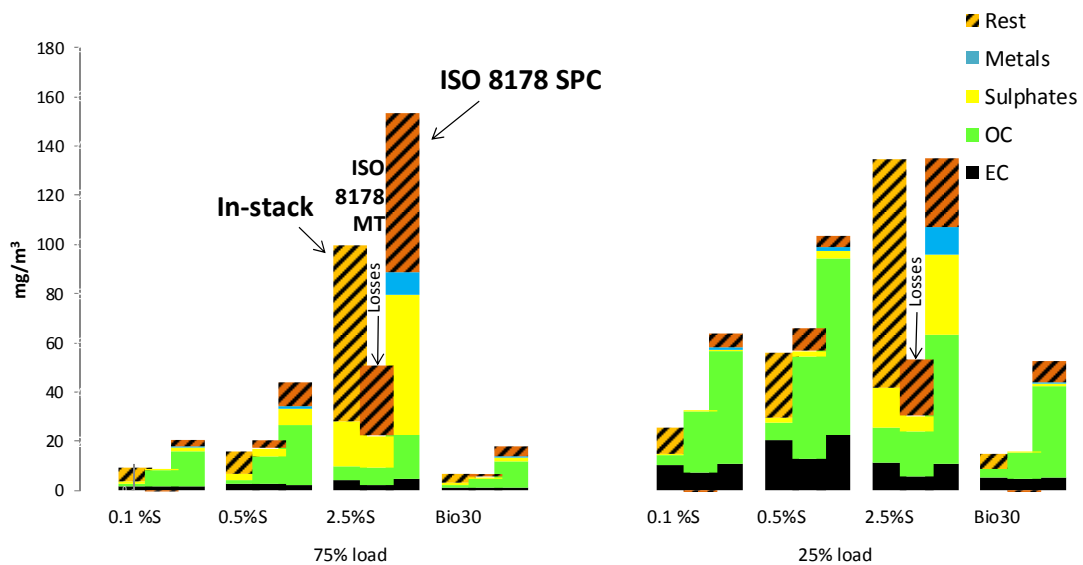


Figure 5.23. Composition of PM for samples collected with in-stack and ISO 8178 SPC (DR 8) and MT (DR30) samplings. The results for 2.5%S fuel with MT are not valid.

## 5.5 EC results

In this work, first the possible artefacts and interpretation of the thermograms are discussed. Then a pre-study to select the temperature program for the round-robin is presented, as well as the results of the limited study on the extractions of samples. Observations led to a study of using constant split as a quality control method. Finally, a round-robin between three laboratories was carried out with procedure defined in the pre-study at VTT.

### 5.5.1 Possible artefacts and interpretation of the thermograms

PM consists typically of carbonaceous compounds (organic, elemental and carbonate carbon), inorganic ions (sulphates, nitrates, ammonium), metals (V, Fe, Ca, Na) and oxygen

bound in water and metals. EC represents typically 5-25% of fine particle mass in ambient samples, for which EC/OC aerosol analysis is typically used (Viidanoja et al. 2002; Viana et al. 2007; Saarikoski et al. 2008). The distinction between OC and EC is generally simpler for ambient aerosol samples with relatively low PM concentration and expected composition, when compared with samples from the combustion processes with highly variable composition and concentrations. Lowest spread in the EC/OC results was observed for the rural samples, while the spread was the largest for the biomass burning impacted samples in a study by Maenhaut et al. (Maenhaut in (Kuhlbusch et al. 2009)). PM from high-speed diesel engines using distillate fuels contain only a low share of non-EC material (Murtonen et al. 2012; Karjalainen et al. 2016; Saarikoski et al. 2017). The composition of the ship PM resembles rather ambient PM from the biomass burning than that from the high-speed diesel engines (Long et al. 2013). The EC determination using thermal-optical principle is challenging, particularly for samples containing metals, organics, inorganic ions (sulphates, cations) and water substantially. (Panteliadis et al. 2015; Jung et al. 2011) (Maenhaut 2009 in (Kuhlbusch et al. 2009)). These constituents are typically present in the ship PM samples when using residual fuels (e.g. (Aakko-Saksa 2016; Ntziachristos et al. 2016)). Residual fuels also contain heavy organic compounds, such as asphaltenes. Distillation range of heavy part of residual fuel can be in a range of 350-850 °C. (Neste 1987). Barneto (Barneto et al. 2014) found in a study of oil refinery wastes by thermogravimetric analysis that the light fraction evaporated at below 300 °C, resins from 400–550 °C and asphaltenes from 550 to 600 °C.

There are many potential artefacts to be taken into account in the EC analysis of ship PM:

- Premature evolving EC. Metals in PM can catalytically enhance combustion of EC at high inert-mode temperatures. Also oxygen containing compounds (or instrument leak) can interfere with the same principle (Panteliadis et al. 2015; Jung et al. 2011; Karanasiou et al. 2011).
- Large amount of OC prone to pyrolysis may bias EC, although this is taken into account by recording the laser intensity over the analysis.
- Loading of filter (low or high) may bias the EC results.
- Drift of laser intensity reading during the temperature program. Sample colour may affect the laser correction factor.
- Misinterpretation of thermograms for wet filters.
- The optical correction principle. Larger EC/TC ratios have been observed for the TOR than for the TOT (Maenhaut in (Kuhlbusch et al. 2009)).
- Multiple overlapping reactions complicate interpretation of the results.

A recent review by Karanasiou et al. (Karanasiou et al. 2015) discusses widely the aspects of the EC/OC analysis. For example, samples can be extracted with organic solvents, alcohols and/or water to remove OC and other soluble constituent that may interfere with the EC/OC analysis.

### **Interpretation of the thermograms**

At VTT, EC/OC analysis from marine engine PM samples have been studied earlier (Lappi & Ristimäki 2017). Typically, analysis has been conducted using the modified NIOSH 5040 procedure. Challenges in the interpretation of thermograms have been noticed, and manual split point has been used when necessary.

The thermograms of PM samples for four fuels at 75% and 25% engine loads are shown in Figure 5.24. Thermograms of PM samples are influenced by compositional variation of PM (Chapter 5.4.7). The PM from the 2.5%S fuel was characterised by high amount of sulphates. The PM samples from the 2.5%S and 0.5%S fuels contain residual type “heavy



OC” and metals. The PM samples for the 0.1%S and Bio30 fuels have lower-boiling OC than samoles for the residual fuels, and only a minor amount of sulphates or metals.

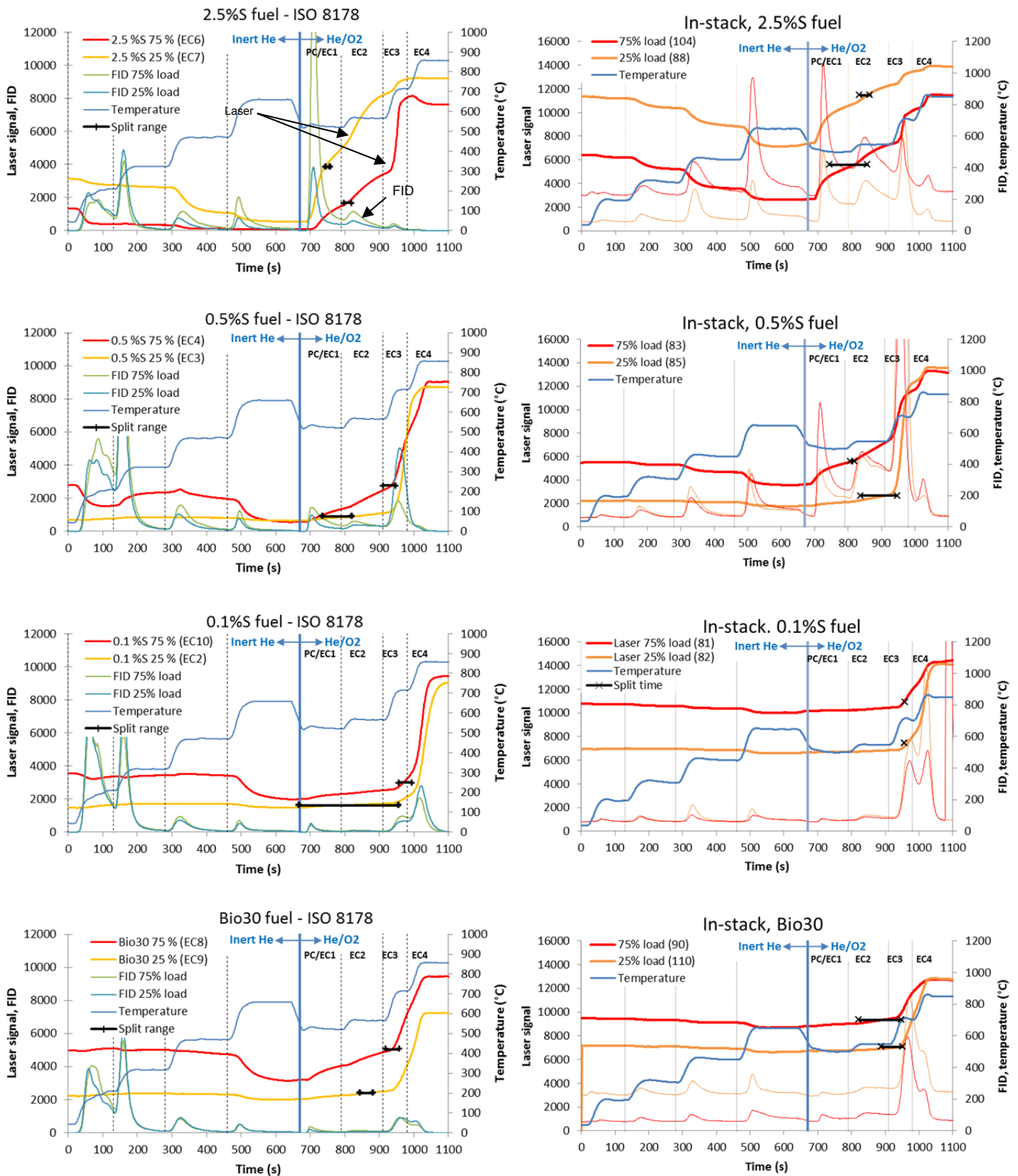


Figure 5.24. Thermograms of the EC/OC runs for the samples obtained by ISO 8178 SPC and in-stack sampling for four fuels at 75% and 25% engine loads (EUSAAR2 program).

### Drying of filters may cause an early drop in laser signal

Early drop in laser signal at temperatures below 200 °C during inert phase of EUSAAR2 was observed for the ISO 8178 diluted samples at 75% load, particularly for the samples obtained with high-sulphur fuels (2.5%S and 0.5%S) having also high concentrations of sulphuric acid and water. Early laser drop was observed for the Bio30 and 0.1%S fuels to lesser extent and not at all for the in-stack samples or samples obtained at 25% load. Sulphuric acid and water were in minor role for the 0.1%S and Bio30 samples, and in-stack samples do not contain sulphuric acid by default. Samples obtained at 25% engine load contained lower amount of sulphates than those obtained at 75% engine load probably due to the differences in the combustion temperature affecting the SO<sub>3</sub> formation tendency. For the 0.1%S and Bio30 fuels, PM may be slightly “wet” also due to the light organic compounds. PM can be hygroscopic when fuel contains oxygenates (Happonen et al. 2013).

The Sunset program deems the early laser drop as the start of pyrolysis, although it was due to drying of filters, phenomenon related to evaporation of water, sulphuric acid or light organic compounds, or due to other colour changes. Consequently, EC can be underestimated for the wet samples. Laser intensity reduces during drying of filters due to the changes in scattering. In some cases, colour of wet punches can be lighter than colour of dry punches. Pyrolysis is not expected below 200°C, at least if catalysts and compounds especially prone to pyrolysis are not present (e.g. oxygenates). Early drop in the laser signal induced by drying of filters can be compensated by using manual split or by drying filters before analysis.

To demonstrate the early drop in the laser signal, tests were conducted on white and yellow punches by adding a) water b) saccharose on the punches. Yellow punches were obtained by pre-running loaded punches (high sulphur fuel) with the EUSAAR2 program. Early drop in laser signal was observed for the yellow punch when water was added. Saccharose/water solution on the yellow punch also caused an early drop in the laser signal, while this was not observed for the white punch (Figure 5.25). The colour of the yellow punch changed to pale yellow in the contact with water, and colour can return to darker yellow during drying.

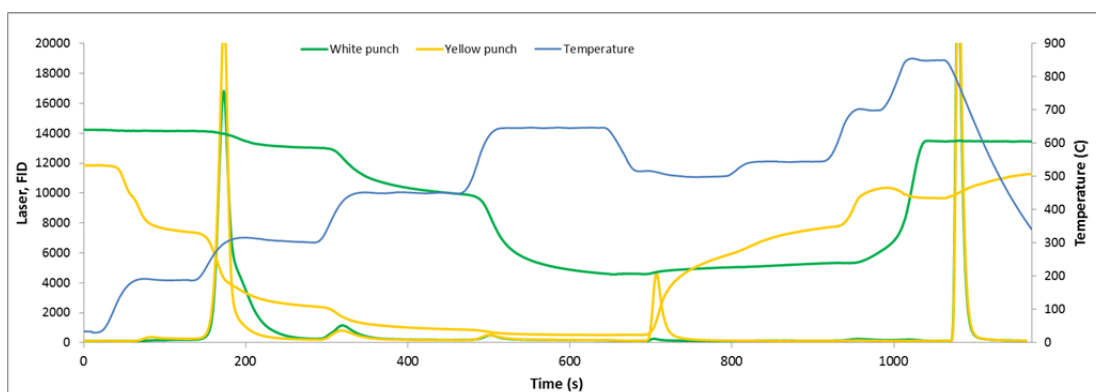


Figure 5.25. Early laser drop is observed when saccharose is added to yellow punch (yellow line), while not when added to white punch (green line). Yellow punch from test 17EC031, Q\_64, 25.4.2017.

### Transformations in the inert mode

Peculiar changes in laser intensity were observed around 150 °C and 350 °C for samples obtained with 0.5%S fuel at 75% engine load. Lightening of sample (increased laser signal) may be due to evolving coloured OC. Water typically evaporates during the first temperature

step of EUSAAR2, however, the crystal water bound in metal oxides may be evaporated in later phase. For example, the last step of dehydration of many metal sulphates takes place at temperatures above 300 °C (Földvári 2011). Other simultaneous transformations can occur when the PM sample is heated. In the temperature step of 450 °C, a small peak was seen in the laser signal.

### **Pyrolysis in the inert mode and premature evolving EC**

In the last temperature step of inert phase, a gradual darkening of sample started indicating pyrolysis of OC. With the 2.5%S fuel, step-wise transformations were started around 500 s in inert phase. Residual fuels contain asphaltenes, which have been observed as the greatest sources of char produced between 400 and 500 °C. (Barneto et al. 2014).

At high temperatures in the inert phase, premature evolving EC may occur when catalytic species and oxygen are present in samples leading to the underestimated EC. This is a potential threat for some samples in this study (e.g. 2.5%S and oxygenated Bio30). Also coloured constituents may evaporate leading to lightening of samples. Simultaneous transformations and colour changes due to the vanadium, calcium and nickel salts may occur. All these changes may interfere with the compensations procedure for pyrolysis and determination of split time. These artefacts could be alleviated by extractions of samples (see Chapter 5.5.3) or by using a temperature program designed to minimise these phenomena.

### **Oxidation of PC and EC**

PC rapidly oxidizes at ca. 400 °C in the presence of oxygen, while it slowly volatiles under inert atmosphere from 400 to 900 °C. Inorganic compounds cause gradual mass loss from 600 to 900 °C after char combustion, while in inert atmosphere they degrade together with char with higher mass loss rate. (Barneto et al. 2014). In EUSAAR2, oxidation of PC is expected in He/O<sub>2</sub> atmosphere from 670 to 790 seconds (500 °C). The laser intensity at the start of pyrolysis in the inert phase is projected to the same intensity when PC has combusted to determine the EC/OC split time.

In our study, for 2.5%S and 0.5%S, EC combusted at 550 °C (790-900 s) in the He/O<sub>2</sub> phase while for the 0.1%S and Bio30 fuels at 700 °C or higher (after 910 s). Thus EC seems more graphite-type in the latter case. For the 0.1%S and Bio30 fuels, the EC/OC split point determination could be easy as the EC evolves late, but the spread of the automatically determined split was high. This is due to the early drop in the laser signal at 75% load, and small changes in laser signal at 25% load (e.g. evolving light absorbing compounds).

For the 2.5%S and 0.5%S fuels, substantial carbon output was observed in oxygen phase almost continuously until approximately 1000 s (probably PC, asphaltenes and EC). When the split point is located in the region of substantial carbon output, small changes in the laser signals are reflected in the split times leading to substantial differences in the EC results, even if thermograms were similar in the EC part. For the 0.1%S and Bio30 fuels, large spread in the split points was sometimes seen regardless of seemingly simple thermograms. However, when EC combustion takes place during only a short period late in the He/O<sub>2</sub> phase, the high spread in the split times does not necessarily lead to the high spread in the EC results. All in all, reliable split time determination with the thermo-optical method was challenging for marine engine PM samples.

### **Summary of potential reactions in the EC analysis**

Possible relationships between constituents of PM and phenomena observed in the thermograms for different samples are summarised in Table 5.4. It is noticeable, that even distillate marine fuels may contain sulphur close to 1000 mg/kg and also relatively heavy organic compounds. Consequently, they are different from the distillate diesel fuels used in the high-speed diesel engines for ground-transport applications.

Table 5.4. Possible reactions in the EC analysis.

Temperature/laser behaviour	Residual fuels	Oxygenated oils and fats	Distillate fuel
<b>Major features of PM (ISO 8178)</b>	<ul style="list-style-type: none"> <li>- Heavy OC</li> <li>- H<sub>2</sub>SO<sub>4</sub> &amp; water</li> <li>- V, Ca etc. sulphates &amp; crystal water</li> <li>- V, Ca etc. oxides</li> <li>- Oxygen</li> </ul>	<ul style="list-style-type: none"> <li>- Light OC</li> <li>- Fatty acids</li> <li>- Oxygen</li> <li>- EC</li> <li>- Hygroscopic</li> <li>- Low sulphur</li> </ul>	<ul style="list-style-type: none"> <li>- Light OC</li> <li>- EC</li> </ul>
<b>Inert &lt;200 °C Drop in laser signal</b>	H <sub>2</sub> SO <sub>4</sub> & water evaporation (Catalysed pyrolysis)	OC and water evaporation (Catalysed polymerisation)	OC evaporation
<b>Inert &gt;200 °C Increase in laser signal</b>	OC (coloured) evaporation EC combustion (catalyst & oxygen in sample) Crystal water & salts	EC combustion (oxygen in sample)	
<b>Inert &gt;200 °C Drop in laser signal</b>	OC pyrolysis Crystal water & salts	OC pyrolysis	OC pyrolysis
<b>Oxygen phase</b>	PC combustion EC combustion	PC combustion EC combustion	PC combustion EC combustion

### 5.5.2 Validity of samples

Collection time of PM on quartz filters using the ISO 8178 sampling (diluted) and the in-stack sampling (EN 13284-1) without dilution was adjusted to reach the recommended EC loadings (Table 5.4). All except a few loadings were within the recommended range. Loadings were the highest for the 0.1%S fuel. For the 2.5%S fuel at 75% load, and for the 0.1%S fuel in the additional tests (DR 5 and 30), laser correction factors were only 0.90-0.96. The in-stack sampling from raw exhaust is challenging for the EC/OC analyses as the recommended loading of the filters tends to be exceeded in a very short time and sufficiently light samples are difficult to obtain. Here, the EC loadings of the light in-stack samples met in most cases the recommended loadings being in a range from 0.8 to 15.6 µg/cm<sup>2</sup> (one exception for 0.1%S at 25% load) (see Table 5.5). Separate in-stack samples with high loadings were collected for the PM (and TC) measurements.

The laser correction factor should be over 0.90 in the EC analysis by the Sunset instrument. For the 2.5%S fuel at 75% load, laser correction factors were close to 0.90 and the punches were yellow after the EUSAAR2 program. Low laser correction factor increases uncertainty of the split time determination.

Table 5.5. The OC/EC requirements and mass on loaded quartz filters.

Requirements	In-stack, light samples	ISO 8178 (SPC)	ISO 8178 (MT)
	no dilution	DR 8	DR = 20-33
EC 1-15 µgC/cm <sup>2</sup>	0.8-15.6*	1,7-14,2 (av. 5.7)	2,2-9,8 (av. 4.1)
OC 5-400 µgC/cm <sup>2</sup>		19,4-57,7 (av. 32.4)	6,2-31,7 (av. 14.2)
Laser corr. factor >0.9		>0.90	>0.90
Laser transmittance 200-16000			
Pressure 0.5-2.0 psig			

\* 75% and 25% engine loads: 0.1%S: 1.0-7.7/2.3-33.6 µg/cm<sup>2</sup>; 0.5%S: 4.1-5.8/3.6-15.6 µg/cm<sup>2</sup>; 2.5%S: 5.3-9.8/0.8-1.6 µg/cm<sup>2</sup>; Bio30: 1.6-1.7/2.1 µg/cm<sup>2</sup>.

### 5.5.3 Pre-studies on sample pre-treatment and temperature programs

#### Drying and extraction of filters

Many constituents, such as moisture, liquid OC (through pyrolysis) and inorganic cations ( $K^+$ ,  $Na^+$  etc.) disturb the distinction between EC and OC when using the thermal-optical method. (Maenhaut 2009 in (Kuhlbusch et al. 2009)). To avoid this, samples can be dried and extracted to remove water, light OC and cations prior to the analysis. In this project, the washing experiments were carried out for the ISO 8178 (MT) samples from the tests with the 2.5%S and 0.5%S fuels at 75% load. These samples contained only low amount of light organics and sulphates when compared to those obtained by the SPC or in-stack sampling (Chapter 5.4.7).

Drying of filters at 180 °C for one hour removed constituents that were responsible for the early laser drop, but did not prevent other changes that complicate interpretation of the laser signal, such as evaporation of coloured compounds or pyrolysis of OC (Figure 5.26). The EC results for dried samples for the 2.5%S fuel at 75% engine load was on average +0.8  $mg/m^3$  higher than that for the native samples (automatic split). For 0.5%S fuel at 75% engine load, respective change was -0.13  $mg/m^3$ .

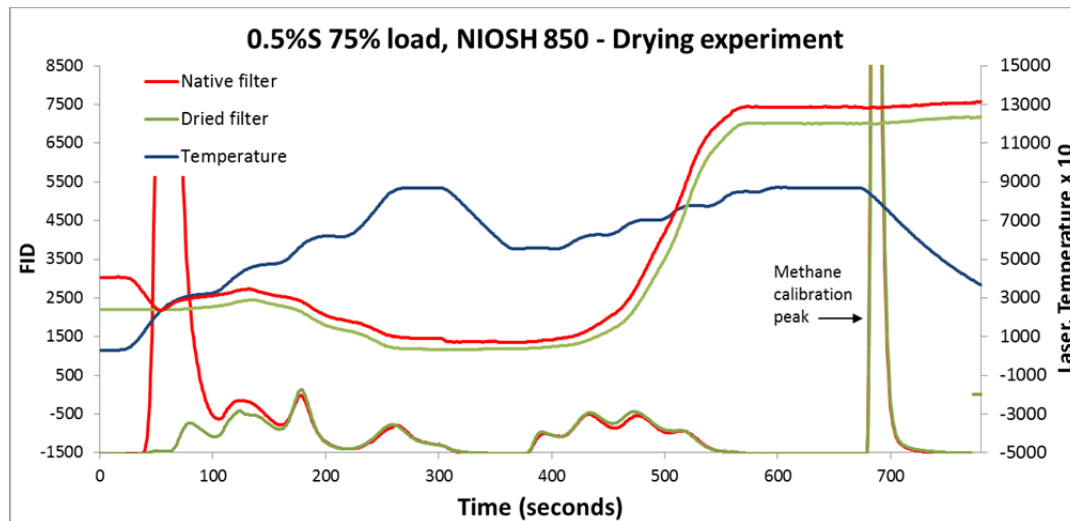


Figure 5.26. The EC results obtained from native and dried (180 °C, 1 hour) filters for 0.5%S fuel at 75% engine load.

The more severe extraction procedure included toluene extraction followed with the IPA/water extraction. In addition, extraction with water only was applied for two samples. The EC results varied between untreated and extracted filters (Figure 5.27). For the 0.5%S fuel, the EC results from the extracted filters were lower than those from the native filters. In the opposite, the EC results for the 2.5%S fuel from the washed filters were higher than those from the native filters. For 2.5%S using EUSAAR2, EC was 14% and 10% higher for extracted than for native sample, while 20% lower for the 0.5%S, respectively. In most cases, differences between native and washed filters were below 0.5  $mg/m^3$ .

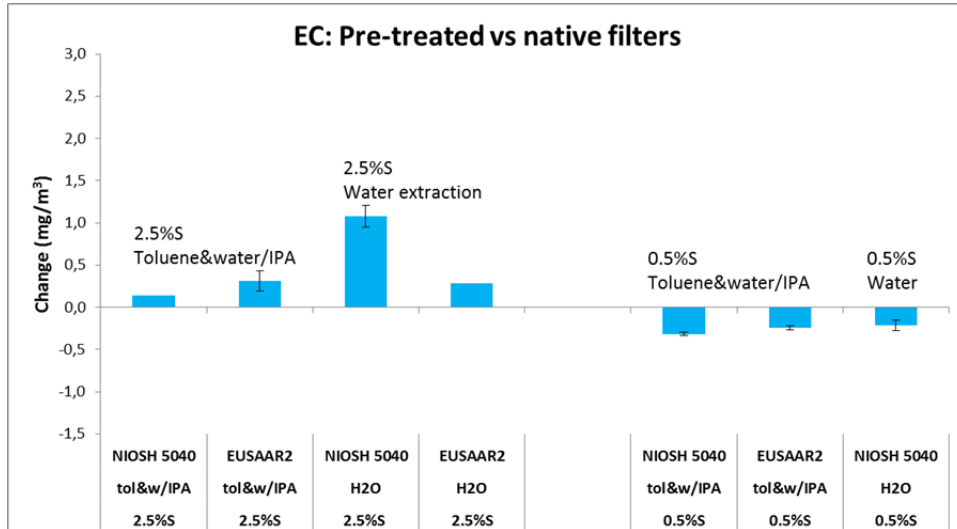


Figure 5.27. The EC results obtained from native filters and when pre-treatment procedures were applied for the 2.5%S and 0.5%S fuels at 75% engine load.

Figure 5.28 shows examples the thermograms before and after extraction with toluene followed by extraction with water/IPA. The differences are seen in the most refractive EC appearing after 900 s in the EUSAAR2 program: for the 0.5%S fuel, EC reduces in the refractory area, while for the 2.5%S EC increases. For the 2.5%S fuel the most refractory EC could be the most prone to the premature combustion in the inert phase. For the 0.5%S fuel, soluble material could be tightly attached in EC. Also mechanical losses or movements of EC during the extraction could also cause changes in the most refractory EC.

The actual samples were not exposed to any pre-treatment. The phenomenon related to the changes in the most refractory EC after extraction would deserve further studies. Besides, OC cannot be determined from extracted filters. Extractions are also time-consuming and they also increase risks for inhomogeneous PM. On the positive side, the automatic split determination could be used for all extracted samples.

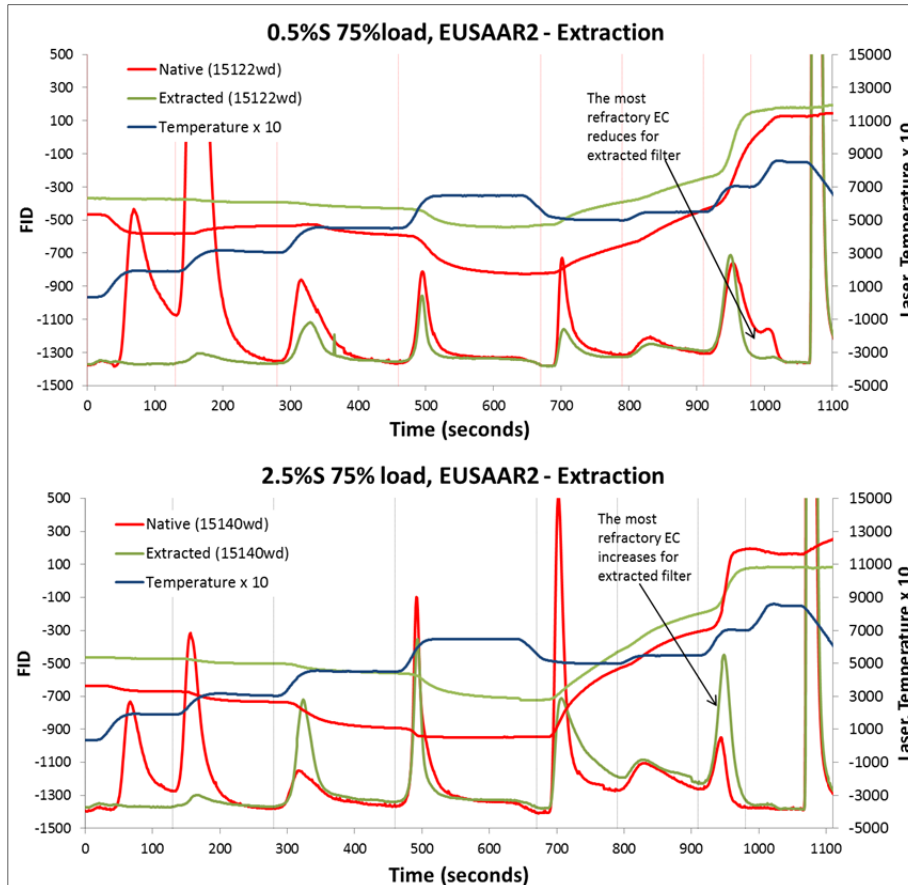


Figure 5.28. Examples of thermograms for 2.5%S and 0.5%S fuels at 75% engine load from native filters and from the same filters after washing with toluene and water.

### Choice of temperature program

Temperature programs studied were the EUSAAR2 with peak temperature of 650 °C and NIOSH 5040 with two peak temperatures (870 °C and 750 °C). Fuels contained constituents that are susceptible to induce premature evolving EC in the EC/OC analysis. Metal and sulphate contents were high for the 2.5%S and 0.5%S fuels, and two fuels contained oxygen (Bio30 and 2.5%S fuel).

Using the NIOSH870 program, a pre-oxygen split was observed for some samples (Figure 5.29). Reduced peak temperature of the NIOSH750 and EUSAAR2 programs alleviated the tendency towards pre-oxygen split. This also proves that the pre-oxygen split observed using NIOSH 5040 was not due to the oxygen leak in the instrument.

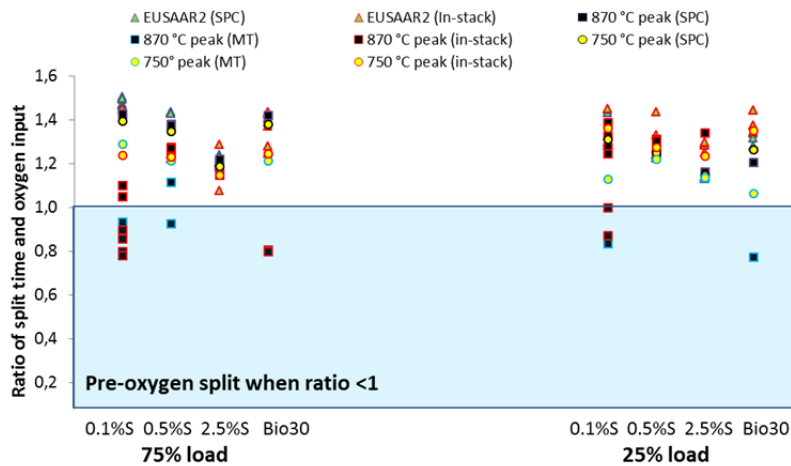


Figure 5.29. Pre-oxygen split was detected when using the NIOSH 5040 temperature program at 870 °C and 750 °C peak temperatures in inert phase. Pre-oxygen split was not detected at all when using the EUSAAR2 program (650 °C peak temperature in inert phase). Oxygen was introduced at 435 s in the NIOSH 5040 and at 670 s in the EUSAAR2

Comparison of the EC results obtained with three temperature programs is shown in Figure 5.30. The EC results were at the same level for the in-stack and the ISO 8178 diluted samples when using the same temperature program despite of differences in the sampling principles.

The EC results were clearly higher with the EUSAAR2 than with the NIOSH programs at high EC concentrations. The most substantial differences between the temperature programs (up to 5.5 mg/Sm<sup>3</sup>) were seen for the samples obtained with the 2.5%S and 0.5%S fuels, which contained substantially heavy organic compounds (asphaltenes), metal compounds, oxygen, sulphates and water.

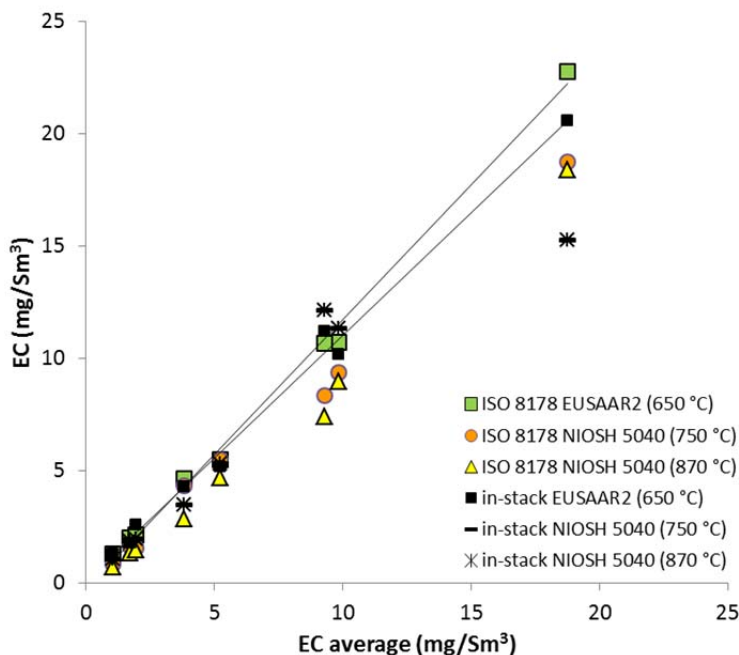


Figure 5.30. The EC results obtained using three programs for samples collected with the ISO 8178 and in-stack sampling.



Average standard deviation of the results obtained with three programs in one laboratory were below 1 mg/Sm<sup>3</sup> at concentrations below 5 mg/Sm<sup>3</sup> and below 3 mg/Sm<sup>3</sup> at higher concentrations.

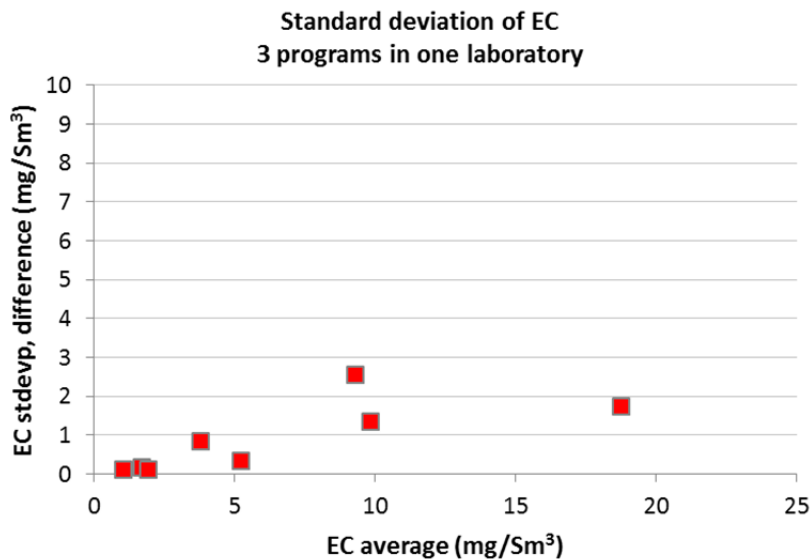


Figure 5.31. Average standard deviations of three programs (EUSAAR2 and modified NIOSH 5040 programs) in one laboratory.

The EUSAAR2 temperature program was selected for the round-robin. EUSAAR2 was deemed to alleviate risk of premature evolving EC with marine engine PM samples.

### Constant split time

Different split times and the EC results were obtained for seemingly similar thermograms in the EC part of the He/O<sub>2</sub> phase (Figure 5.24 and Appendix 2). When the EC results for the replicate tests were calculated using the same split times, indeed, good comparability of the EC results was achieved. Small changes in the laser signal (and split time) in the region of large output of carbon may lead to large changes in the EC results. A constant split of 750 s in the EUSAAR2 was selected to be tested as a quality assurance method in the round-robin (in addition to normal procedure).

### Composition of yellow punch after the EC/OC analysis

The punches for the 2.5%S and 0.5%S fuels at 75% load were yellow after the EUSAAR2 program (Figure 5.32).



Figure 5.32. Yellow/brownish punches for the 2.5%S fuel after the EC/OC temperature program. Typically punches should be white after the EC/OC analysis.

The yellow punch after the EUSAAR2 program for the 2.5%S fuel appeared to contain mainly vanadium, and also some calcium and nickel (see Appendix 3), which is in-line with the metal analysis results of PM samples (Chapter 5.4.5). Vanadium possesses a complex chemistry of coloured compounds, some of them are yellow, for example vanadium pentoxide (V<sub>2</sub>O<sub>5</sub>).

and vanadium sulphate ( $V_2(SO_4)_3$ ); these are also slightly soluble in water. The latter may form a green hydrate in moist air. Some ions formed by  $V_2O_5$  are blue and some are pale yellow salts containing  $VO_2$  centers (formed with strong acids). Colour of  $V_2O_3$  is black, while  $VO_2$  is dark blue.  $VO$  and  $V_2O_2$  are grey.  $V_2O_5$  catalyses conversion of  $SO_2$  to  $SO_3$  between 400 and 620 °C.  $V_2O_5$  catalyses oxidation of hydrocarbons and it is also used as catalyst in the  $NO_x$  reduction technology.  $V_2O_5$  decomposes at high temperature of 1750 °C (Shiju 2004)(Wikipedia, 6/2017).

#### 5.5.4 EC round-robin in three laboratories

Round-robin was conducted by three laboratories, **Lab a**, **Lab b** and **Lab c**. 10 sample filters and one blank filter were selected for the analyses (Table 5.6). Three punches were taken from each filter for each laboratory. Samples were analysed using the EUSAAR2 program with 60 seconds prolongation. In addition to auto/manual split typically used in laboratories, data was analysed using a constant split of 750 seconds (EUSAAR2 (CS)). **Lab c** used only automatic split in the EC analyses. In **Lab c** determination of the split point for one of three punches for the sample EC2 (0.1%S 25% load) and EC5 (0.5%S 25% load) showed split in the first temperature step of inert phase. These are regarded as **outliers** and the results are handled separately.

Table 5.6. Round-robin samples.

EC1_1	0.1 %S 75 %	EC7_1	2.5 %S 25 %
EC1_2	0.1 %S 75 %	EC7_2	2.5 %S 25 %
EC1_3	0.1 %S 75 %	EC7_3	2.5 %S 25 %
EC2_1	0.1 %S 25 %	EC8_1	Bio30 75 %
EC2_2	0.1 %S 25 %	EC8_2	Bio30 75 %
EC2_3	0.1 %S 25 %	EC8_3	Bio30 75 %
EC3_1	0.5 %S 25 %	EC9_1	Bio30 25 %
EC3_2	0.5 %S 25 %	EC9_2	Bio30 25 %
EC3_3	0.5 %S 25 %	EC9_3	Bio30 25 %
EC4_1	0.5 %S 75 %	EC10_1	0.1 %S 75 %
EC4_2	0.5 %S 75 %	EC10_2	0.1 %S 75 %
EC4_3	0.5 %S 75 %	EC10_3	0.1 %S 75 %
EC5_1	0.5 %S 25 %	EC11_1	reference
EC5_2	0.5 %S 25 %	EC11_2	reference
EC5_3	0.5 %S 25 %	EC11_3	reference
EC6_1	2.5 %S 75 %		
EC6_2	2.5 %S 75 %		
EC6_3	2.5 %S 75 %		

The EC results were higher in **Lab a** than those obtained in **Lab b** and **Lab c** for samples EC4 (0.5%S 75% load) and EC6 (2.5%S 75% load) (Figure 5.33). One of the most complicated thermograms was observed for sample EC4 (0.5 %S 75 %, see Chapter 5.5.2), and it was challenging to get a reliable split time automatically or manually. Laser signals for sample EC6 (2.5 %S 75 %) followed similar patterns as for EC4, but with less pronounced changes. Complicated laser signals in samples 4 and 6 are probable reasons for the differences in the EC results between laboratories. The drop in laser signal in the first temperature step of the inert phase was interpreted as start of pyrolysis in **Lab b** and **Lab c** (lower EC), while **Lab a** interpreted this as drying of wet filters (higher EC).

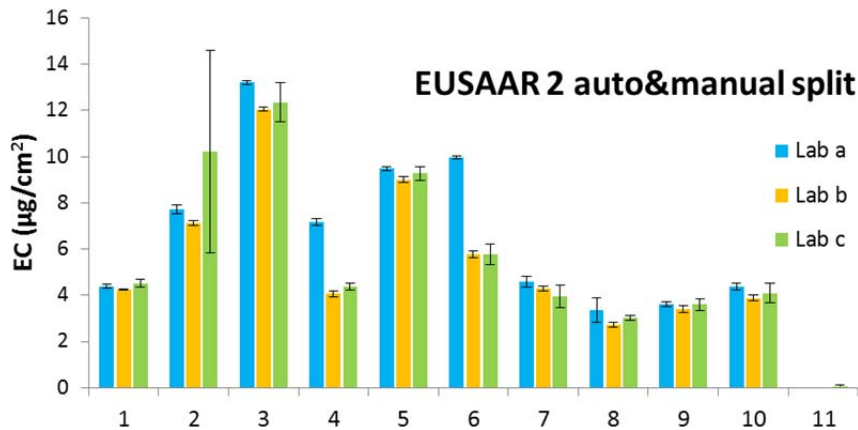


Figure 5.33. The EC results of the round-robin samples obtained in Lab a, Lab b and Lab c by using auto/manual split. Two outliers for **Lab c** excluded.

The minimum, maximum and average EC results observed in three laboratories are shown in Figure 5.34. The EC results were additionally calculated using the constant split of 750 s to inspect, if the differences in the EC results were based on the thermograms, or on the uncertainty in the optical laser signal determination of the split time. The results are shown both with and without the outliers obtained in **Lab c** for samples EC2 (0.1%S 25% load) and EC5 (0.5%S 25% load). Constant split method shows that the thermograms in the “EC part” of the EUSAAR2 program were similar for all samples in three laboratories. Even for the test runs regarded as outliers in **Lab c** showed reasonable results with the constant split of 750 s: EC2: 32.0, 13.3 and 7.1  $\mu\text{g}/\text{cm}^2$  with automatic split, while 7.3, 11.8 and 7.1  $\mu\text{g}/\text{cm}^2$  with constant split; EC5: 30.6, 9.1 and 9.5  $\mu\text{g}/\text{cm}^2$  with automatic split, while 8.6, 8.0 and 8.9  $\mu\text{g}/\text{cm}^2$  with constant split. The differences in the EC results were due to the differences in the interpretation of the thermograms and due to the uncertainty of the optical laser signal. Constant split time is suggested as a quality assurance method for difficult ship PM samples, to identify outliers and when the results are different for replicate samples.

Fig. 7 shows that the EC concentrations were lower at 75% load than at 25% load. EC was below 4.6  $\text{mg}/\text{m}^3$  at 75% engine load with all fuels, whereas it was even as high as 23  $\text{mg}/\text{m}^3$  at 25% engine load. The 2.5%S fuel showed the highest EC results at 75% engine load, but not at the 25% engine load. The 0.5%S residual fuel showed the highest EC results at the 25% load, while its EC results were lower than those for the 2.5%S fuel at the 75% engine load. The Bio30 fuel showed the lowest EC results, and the EC results were low also for the 0.1%S distillate fuel at both engine loads. The effect of load and fuel to the BC and EC results are discussed further in Chapter 5.6.

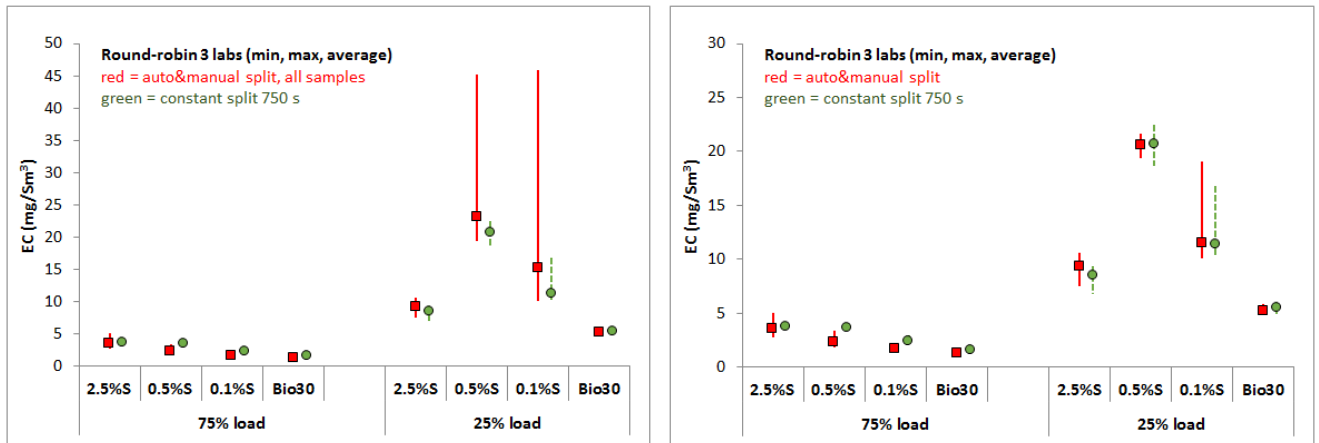


Figure 5.34. The EC results of the round-robin samples analysed in Lab a, Lab b and Lab c. Red markers show the EC results based on the optical split time determination and the green markers on the constant split time of 750 s. Left hand figure includes all three replicates of each sample. Right hand figure excludes two outliers in Lab c.

Some differences in the EC results between laboratories may originate from differences in the TC results. The TC results in **Lab c** were in most cases lower than TC in **Lab a** and **Lab b** (Figure 5.35). In **Lab c**, some samples seemed to be contaminated with OC (EC1\_2, EC2\_2 and EC3\_1), but the EC parts of thermograms were similar in all laboratories. **Lab c** had an older instrument than **Lab a** and **Lab b**, which may explain some of the differences.

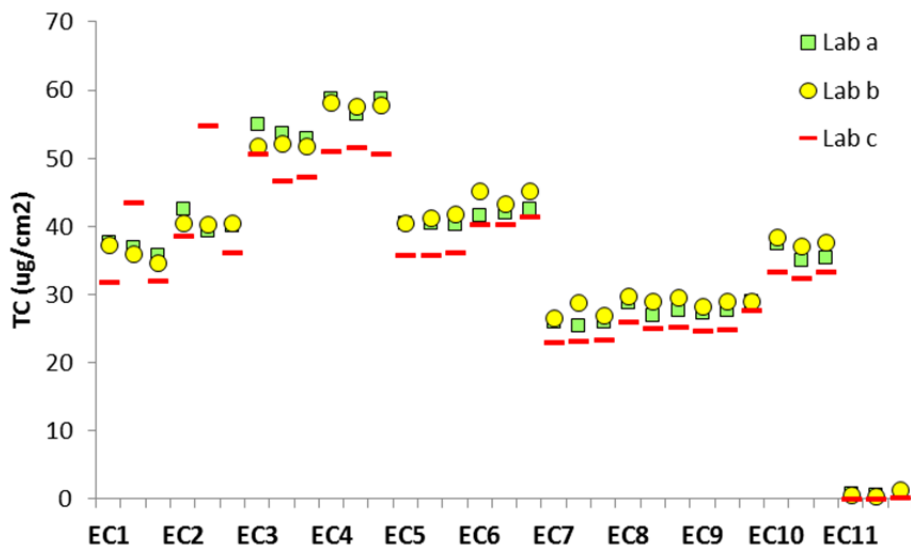


Figure 5.35. The TC results from the three laboratories in the round-robin, the EUSAAR2 program.

Spread of the results in three laboratories as mg/m<sup>3</sup> is shown in Figure 5.36. Standard deviations of EC within each laboratory were below 0.5 mg/Sm<sup>3</sup> with some exceptions in **Lab c** (deviation up to 6.3 mg/Sm<sup>3</sup>). Standard deviation is also presented for all EC results from three laboratories (nine results per sample excluding two outliers for **Lab c**). Standard deviation of EC in three laboratories was below 1 mg/Sm<sup>3</sup> for most samples with an average of 0.75 mg/m<sup>3</sup> (8.6%). The highest spread of the results was observed for the 0.1%S fuel at

25% load. Panteliadis (Panteliadis et al. 2015) found repeatability and reproducibility of EC to be 15 and 20% when using EUSAAR2 (20 and 26 % for NIOSH 5040).

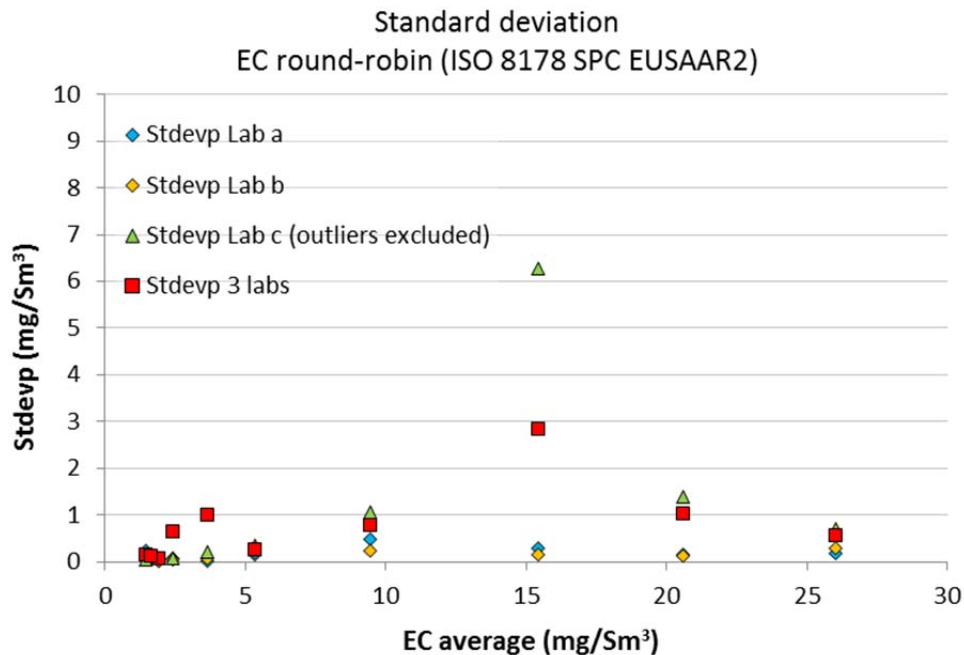


Figure 5.36. Standard deviation (mg/m<sup>3</sup>) of the round-robin EC results obtained within each laboratory and that of all results in three laboratories (red markers). Two outliers in Lab c are excluded.

EC average standard deviations within each laboratory were as follows:

- **Lab a**, average standard deviation of EC: 0.17 mg/m<sup>3</sup> (1.9%)
- **Lab b**, average standard deviation of EC: 0.13 mg/m<sup>3</sup> (1.5%)
- **Lab c**, average standard deviation of EC: 1.04 mg/m<sup>3</sup> (11.8%)
- Average standard deviation of EC in three laboratories: 0.75 mg/m<sup>3</sup> (8.6%)

## 5.6 BC results

### 5.6.1 Comparison of instruments

From the optical BC measurements, two parallel Smoke Meters and aethalometers were used. Smoke Meter AVL 415S was located underneath and AVL 415SE upside of the sampling point. For the underneath location, there is a risk of condensation of sulphuric acid in the instrument, while in the upside position there is a risk of losing a part of sample due to condensation. However, intercorrelation between AVL 415S and AVL 415SE was excellent showing that neither of the risks realised when using heated transfer lines and heated measuring chamber (Figure 5.37). Even for the 2.5%S fuel, good correlation between the two instruments was observed. Heated transfer lines and measuring chambers are not used for all Smoke Meters.

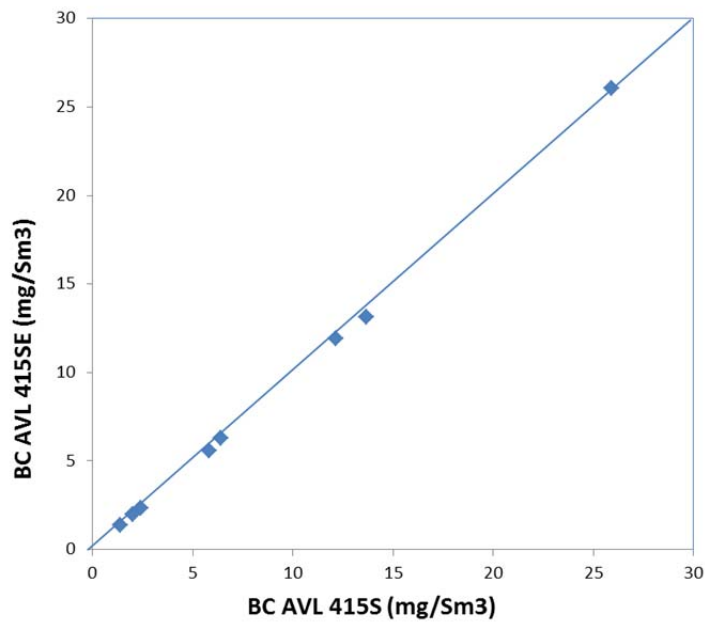


Figure 5.37. Intercorrelation between two Smoke Meters.

Intercorrelations between the BC results obtained with two aethalometers without pre-treatment were good for the other fuels than for the 0.5%S fuel. In this case, higher BC was observed for the AE33 than for the AE42 instrument (Figure 5.38). When CS or TD was used as pre-treatment, intercorrelation between two aethalometers was good also for the 0.5%S fuel. For 2.5%S fuel, the BC result obtained with AE33 was substantially low when using TD as pre-treatment.

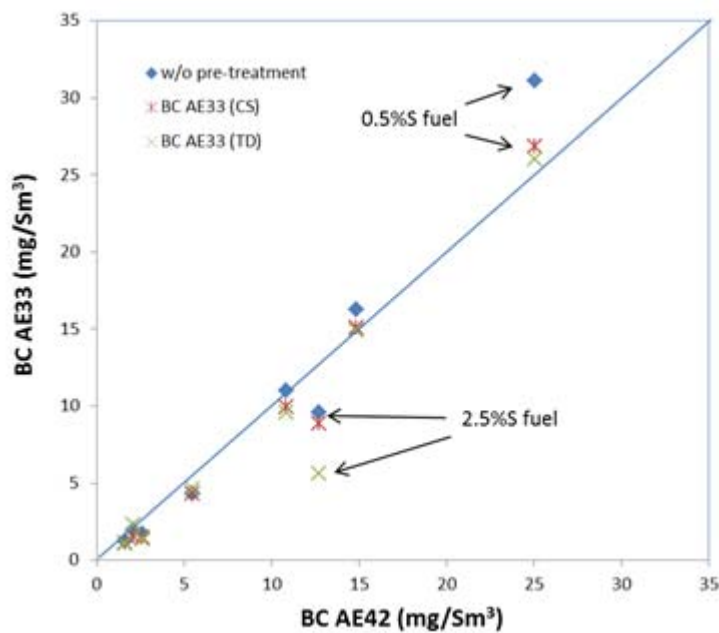


Figure 5.38. Intercorrelation between the BC results obtained with two aethalometers.

Figure 5.39 shows the BC results obtained with AVL 415SE (BC based on FSN, raw exhaust sampling), AVL MSS (BC based on PAS, low DR), MAAP and aethalometer AE33 (DR below 200), and the EC results (EUSAAR2, ISO 8178 SPC sampling).

The BC results obtained with AVL 415S, AVL MSS, AE33 and were relatively consistent with each other, and also close to the EC results. In most cases, the AVL 415S and AVL MSS showed the BC results close to each other. Both are easy-to-use instruments. AVL Smoke Meters require manual start of each measurement, while other instruments measure on-line.

At concentrations below  $10 \text{ mg/Sm}^3$ , spread between the BC results obtained with the other instruments than AE33 was small. At higher BC concentrations, spread in the BC results between instruments increased.

For the aethalometer AE33, the BC concentrations were often higher than those obtained with the other instruments. When CS pre-treatment was used before AE33, the comparability of the BC results with those obtained with the other instruments improved. CS did not significantly affect the BC results obtained with MAAP. Apparently, AE33 is sensitive towards positive bias due to the volatile compounds that can be removed by using CS pre-treatment of exhaust.

The most noticeable in Figure 5.39 were the low BC results obtained with MAAP at the highest BC concentrations.

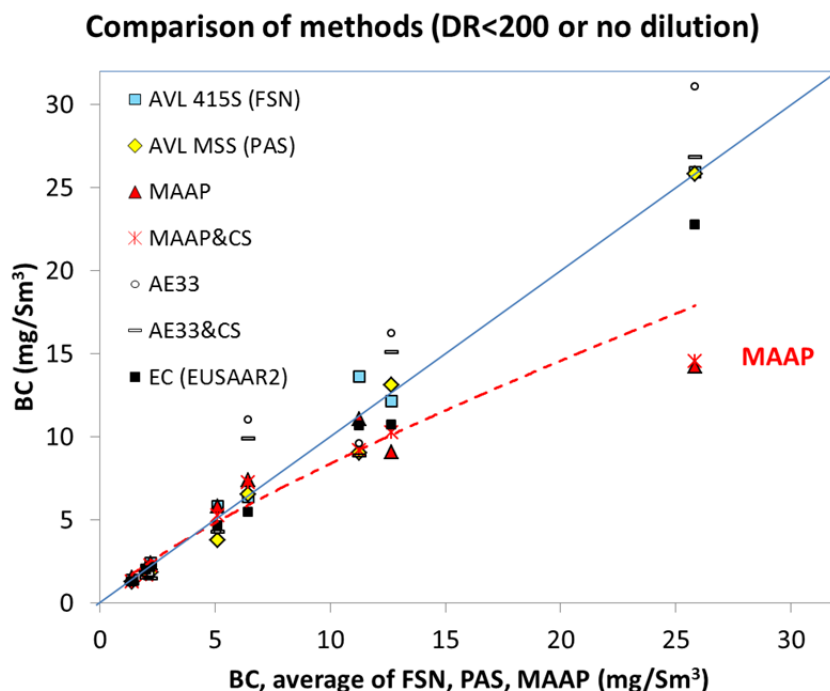


Figure 5.39. The BC results obtained with AVL 415S (FSN, raw exhaust), AVL MSS (PAS, low DR), MAAP and AE33 (DR below 200). The EC results were obtained using the EUSAAR2 program.

In addition to DRs below 200, DRs above 600 were used in the measurements with MAAP and the aethalometers (Figure 5.40). High DRs in the range of 1600–1800 could not be determined reliably, and the respective BC results are not quantitative. However, instruments in the same dilution line can be compared with each other. Interestingly, when dilution was sufficient, MAAP showed the BC results in the same range as aethalometers.

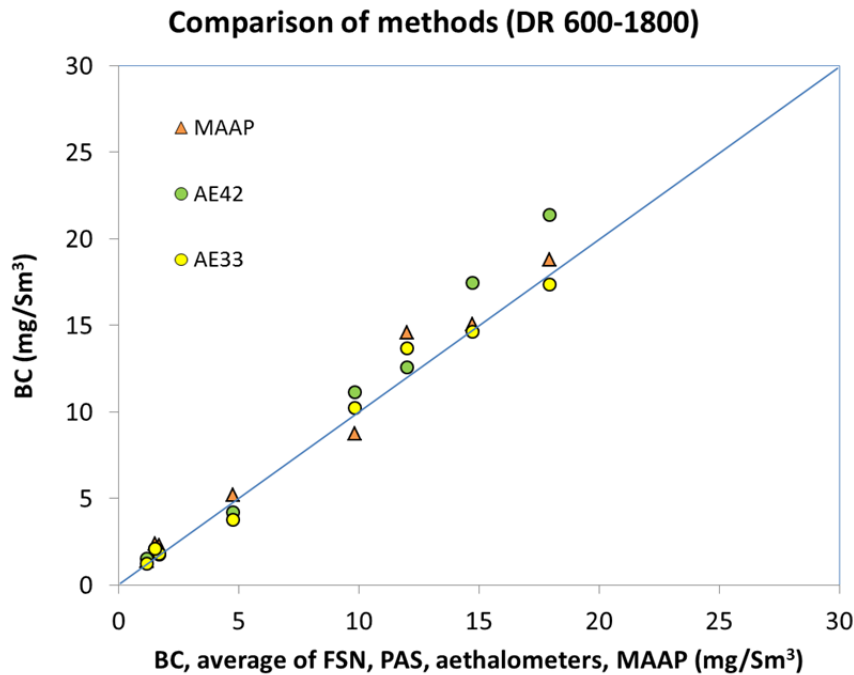


Figure 5.40. Comparison of the results obtained with instruments in the same dilution line. Tests with high DR of 600–1800.

**The reliable measurement range of MAAP is narrow.** Hyvärinen et al. (Hyvärinen et al. 2013) realised that MAAP underestimates BC already at concentrations higher than  $9 \mu\text{g}/\text{m}^3$  at 16.7 lpm. Furthermore, MAAP underestimates BC concentration by 30% when mass accumulation rate exceeds  $0.4 \mu\text{g}/\text{min}$ . Minimum DRs required to keep the BC concentrations in this range at two sample flow rates of MAAP are shown in Figure 5.41.

The BC mass accumulation rate of  $0.4 \mu\text{g}/\text{min}$  represents the BC concentration of  $24 \mu\text{g}/\text{m}^3$  in the diluted exhaust gas at MAAP sample flow rate of 16.7 lpm, and  $67 \mu\text{g}/\text{m}^3$  at sample flow rate of 6.0 lpm. When the BC concentration of the exhaust gas is  $25 \text{ mg}/\text{m}^3$ , DR of almost 400 is needed for MAAP at 6.0 lpm sample flow rate, and DR as high as 1100 at 16.7 lpm ( $1 \text{ m}^3/\text{h}$ ) sample flow rate. Flow rate (6 lpm) and averaging time (1 min) in our study alleviates challenges in staying in the reliable measurement range of MAAP.



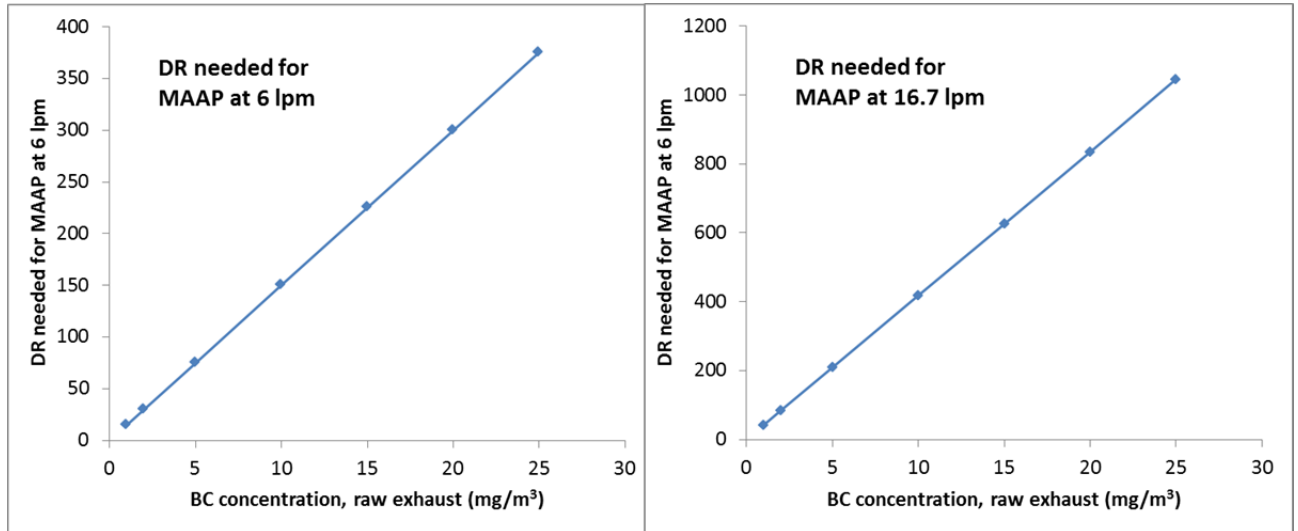


Figure 5.41. The dilution ratios needed to keep the BC mass accumulation rate below 0.4  $\mu\text{g}/\text{min}$  at 6 and 16.7 lpm sample flow rates of MAAP.

The BC concentration of 67  $\mu\text{g}/\text{Sm}^3$  in the diluted exhaust gas was exceeded in some engine load and fuel combinations at DRs below 200 (Table 5.7), particularly for the 0.5%S fuel at 25% engine load. The diluted BC concentrations at DR>600 were sufficiently low for MAAP. This explains the low BC concentrations obtained with MAAP at DR<200 when compared with the other instruments (Figure 5.39), while not at DR>600 (Figure 5.40).

Table 5.7. Maximum BC concentrations in diluted exhaust gas observed with aethalometers, MAAP and SP-AMS, whichever showed the highest BC concentrations.

	Fuel 0.1%S		Fuel 0.5%S		Fuel 2.5%S		Bio30	
<b>DR</b>	90-155	700-900	150-180	1600-1800	200-400	600-800	100-120	600-700
<b>Max BC<sup>a</sup></b>	125	14	183	13	35	28	93	13

<sup>a</sup> Observed maximum BC concentration ( $\mu\text{g}/\text{Sm}^3$ ) in diluted exhaust gas.

SP-AMS results were calculated using RIE=0.05 and CE=0.5. With these values the BC results were in reasonable agreement the BC results of optical measurements and EC for the 0.1%S, 0.5%S and Bio30 fuel, while larger difference was observed for the 2.5%S fuel. More variation between results was observed for higher BC concentrations when using 25% load. It can be that due to high organic loading the organic compounds interfere with the BC peaks causing increased uncertainty to results.

## 5.6.2 Summary of BC and impact of fuels and engine loads on BC

Figure 5.42 shows the BC and EC results by using different measurement methods. Comparability was relatively good between the BC results obtained with FSN based Smoke Meters (AVL 415S, AVL 415SE), PAS method (AVL MSS), aethalometers (AE42, AE33) and MAAP 5012. As MAAP underestimated BC at 25% engine load, those results are not shown in the Figure. The EC results from the ISO 8178 PM and in-stack sampling compared relatively well with the BC results when using the EUSAAR2 program, while NIOSH 5040 program resulted in slightly lower results.

Fuels and engine loads were rated in the same order with different instruments despite of the different measurement principles. Particularly when considering the uncertainty in dilution

ratios and high losses in the pre-treatment units, comparability of the BC results was reasonable.

One of the most critical issues for reliable BC measurements proved to be the test set-up. MAAP and aethalometers are designed for ambient BC measurements, and consequently high dilution ratios are needed when the BC concentrations are high. High dilution ratios are a source of uncertainty. Furthermore, special instrumentation and expertise needed for high dilution ratios are not practical for routine BC measurements.

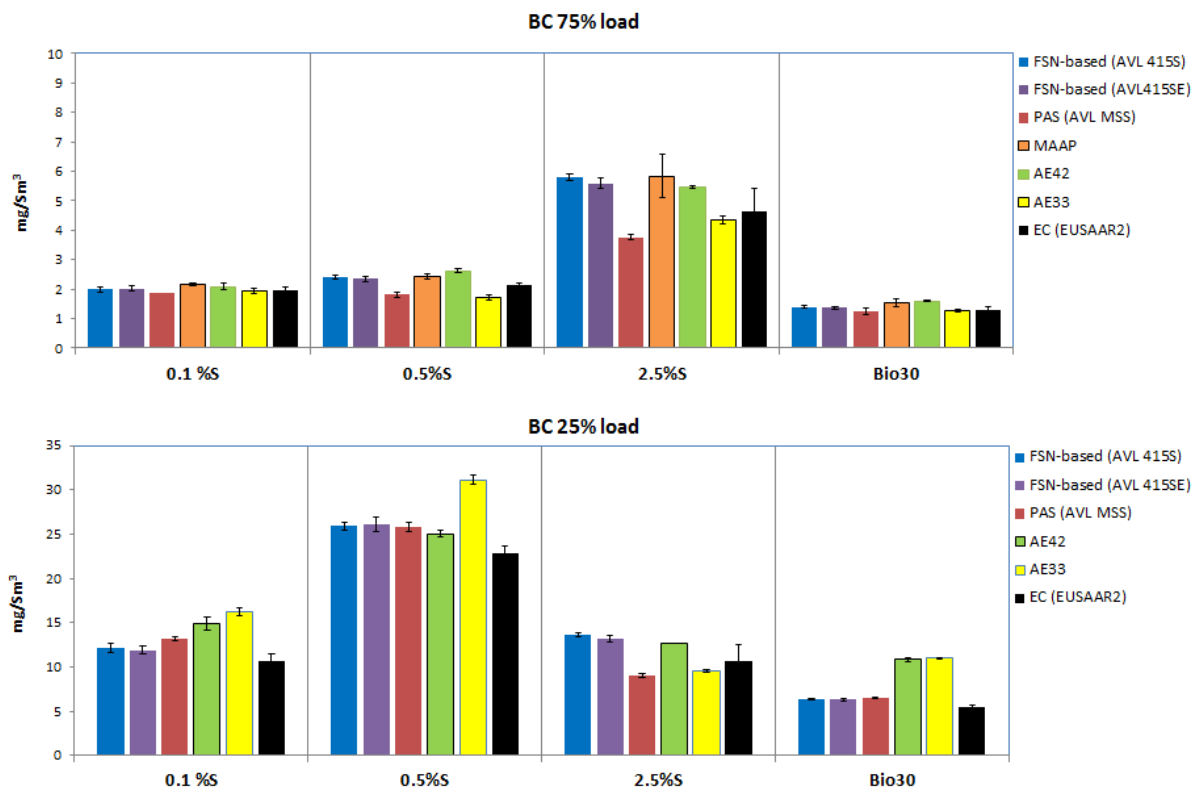


Figure 5.42. The BC concentrations measured with different instruments using DR below 200 or no dilution. EC analysed from filters is also shown. Error bars represent standard deviations.

The 2.5%S fuel resulted in the highest BC at 75% load, whereas the 0.5%S fuel showed the highest BC at 25% engine load. At 25% load, BC for the 2.5%S fuel was almost as low as that for the 0.1%S fuel. Certain metal oxides are known to catalytically enhance combustion of BC (Ristimäki et al. 2010, Sippula et al. 2014), which may explain the low BC result for the 2.5%S fuel at 25% load. The 0.5%S fuel was the second heaviest fuel after the 2.5%S fuel. The highest BC for the 0.5%S fuel at 25% load may be related to the heavy organic compounds of fuel combined with lower ash content of the 0.5%S fuel than that of the 2.5%S fuel.

Combustion temperature is higher at 75% than at 25% engine, which led to low overall BC concentrations. In this case, all fuels combusted so well that the role of catalytic metals in combustion was apparently overruled, and also BC for the 0.5%S fuel levelled out. The 2.5%S fuel was the heaviest of the tested fuels, and it contained the highest amount of ash and heavy organic compounds. E.g. asphaltene are more prone to incomplete combustion than the lighter hydrocarbons.

The BC concentrations were lower for the 0.1%S and Bio30 fuels than for the 2.5%S and 0.5%S fuels at both engine loads. Fuels containing distillates typically consist of lighter and cleaner-burning compounds than residual fuels. The lowest BC concentrations were

achieved with the oxygen-containing Bio30 fuel at both engine loads. Oxygen in fuel enhances combustion and reduces soot emissions from diesel engine (Murtonen et al. 2010; Aakko-Saksa et al. 2012; McGill et al. 2003).

The BC results (g/kWh and g/kg oil equivalent) rated the engine loads and fuels in the same order as the BC concentrations. BC was lower at 75% than at 25% engine load in all units studied: mass/Sm<sup>3</sup>, mass/kWh and mass/kg oil equivalent (Figure 5.43). In addition to the impact of engine load on the BC emissions, also role of fuels was substantial. At 75% load, BC varied from 1.4 to 5.8 mg/Sm<sup>3</sup> and at 25% load from 6.4 to 25.9 mg/Sm<sup>3</sup> (AVL 415S, based on FSN) depending on the fuel used.

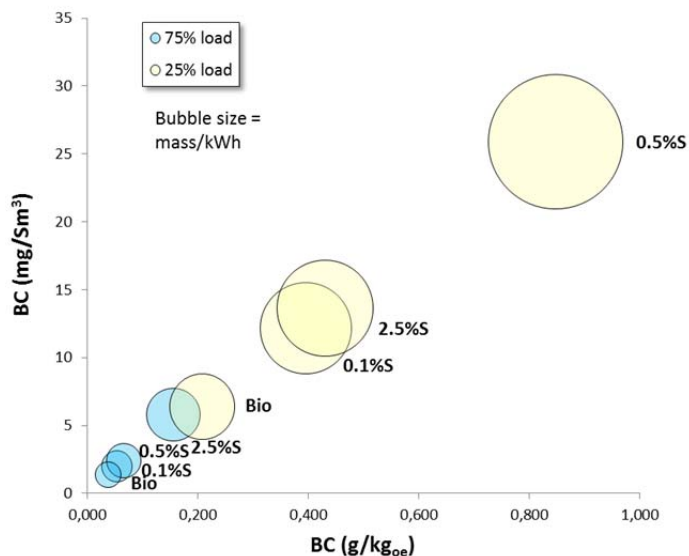


Figure 5.43. BC emissions in different units. BC presented here was measured with AVL 415S (based on FSN).

BC correlated to some extent with OC, CO and NO<sub>x</sub>. BC decreased to some extent when OC and CO decreased (Figure 5.44). However, for the 2.5%S fuel at 25% load, BC was not as high as the CO concentration would suggest. BC decreased with increasing NO<sub>x</sub> concentrations. However, this effect was mainly seen when the data points at 75% and 25% engine loads were compared with each other (two data groups rather than correlation).

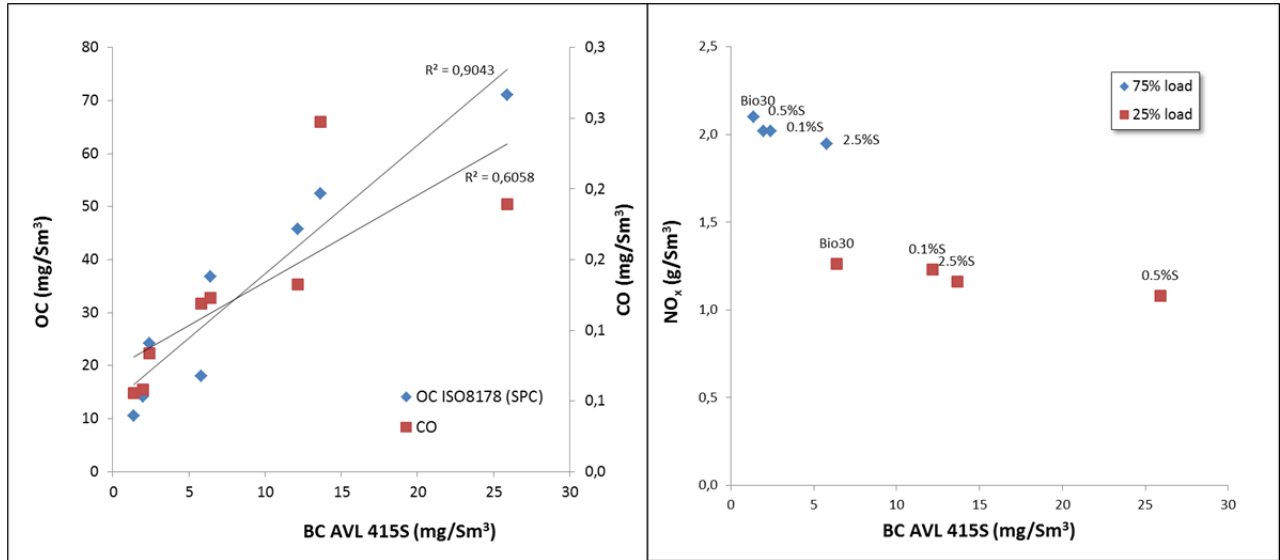


Figure 5.44. Correlation of BC (FSN-based, AVL 415S/SE) with the OC (EUSAAR2, ISO 8178 sampling with SPC), CO and  $\text{NO}_x$  concentrations.

### 5.6.3 Standard deviations

Standard deviations of the BC results for each instrument (Figure 5.45) were below  $0.5 \text{ mg/Sm}^3$  at BC concentrations below  $5 \text{ mg/Sm}^3$ , whereas spread was higher (up to  $1 \text{ mg/Sm}^3$ ) at higher BC concentrations. No major differences in the repeatability of different BC instruments were observed.

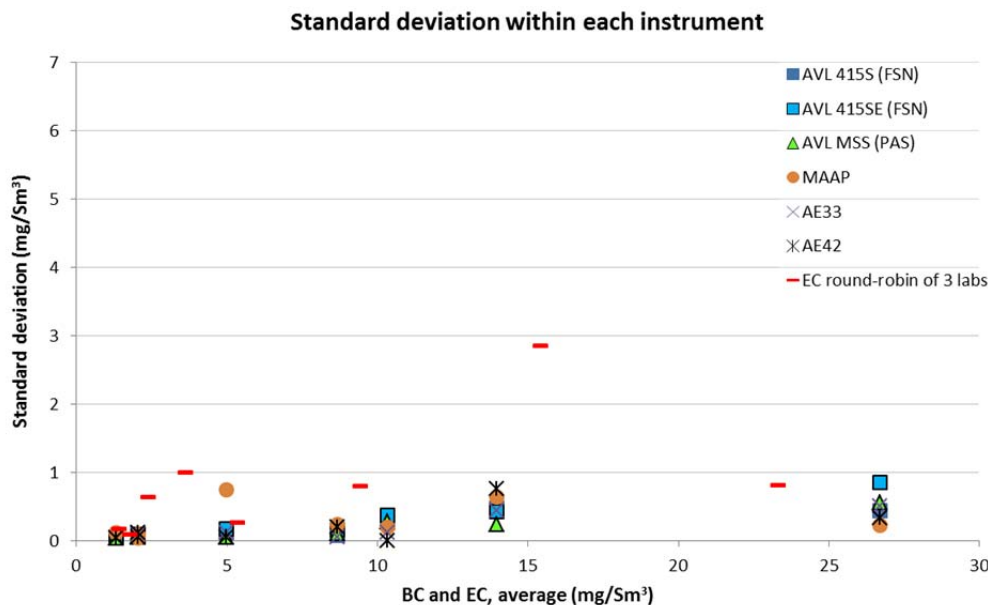


Figure 5.45. Standard deviations for each BC instrument and standard deviation of EC (EUSAAR2) in three laboratories.

Standard deviations of BC between six instruments were below  $1 \text{ mg/Sm}^3$  at BC concentrations below  $5 \text{ mg/Sm}^3$ , whereas deviations up to  $3 \text{ mg/Sm}^3$  were observed at higher BC concentrations. Standard deviations of BC were close to those observed for the EC results (Chapter 5.5).

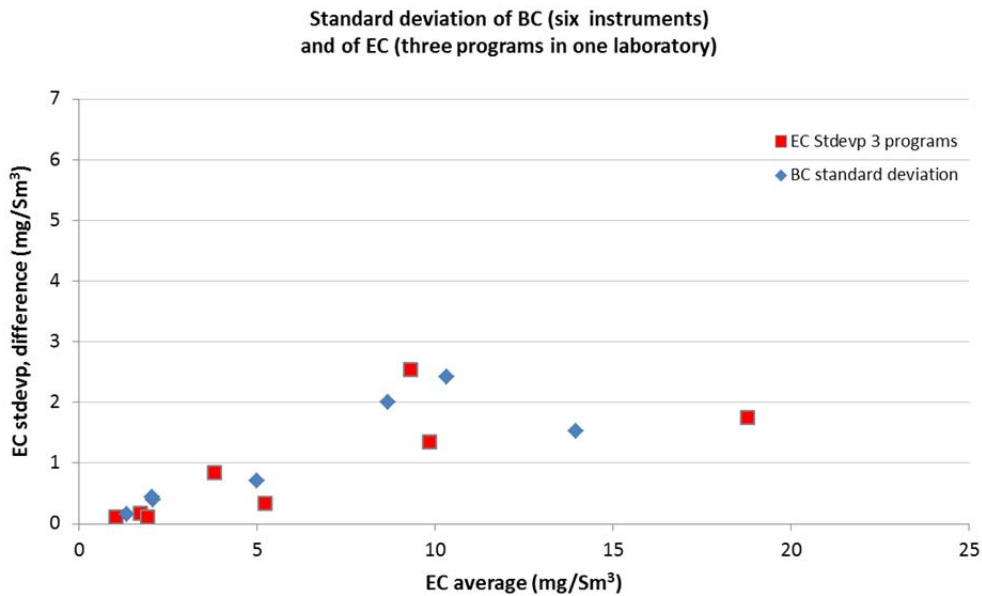


Figure 5.46. Standard deviations of BC between six instruments and of EC between three temperature programs.

Some of the major building blocks of uncertainty in the BC and EC measurements are shown in Figure 5.47. In addition to the measurement principle itself, dilution and sampling procedures accumulate substantial uncertainty.

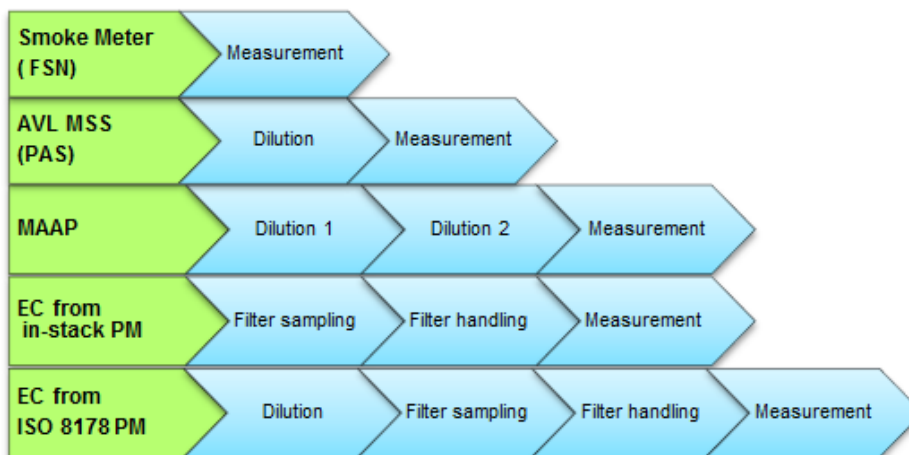


Figure 5.47. Examples of building blocks of uncertainty for the BC and EC measurements.

## 5.7 Brown carbon

Strong absorbance at the UV typically indicates high contribution of BrC, which absorbs light particularly at shorter UV wavelengths, e.g. at 370nm.

Intercorrelation between the aethalometers AE33 and AE42 at 370nm is shown in Figure 5.48. Substantially higher response at 370 nm was observed with AE33 than with AE42 for the 0.5%S fuel at 25% engine load. AE33's response at 370nm was reduced when CS was used as a pre-treatment unit to remove volatile of compounds of exhaust. This effect was pronounced for the 0.5%S fuel at 25% load. These results indicate that AE33 is sensitive

towards volatile compounds present in the exhaust from 0.5%S fuel leading to overestimated response at 370nm, when CS pre-treatment is not used.

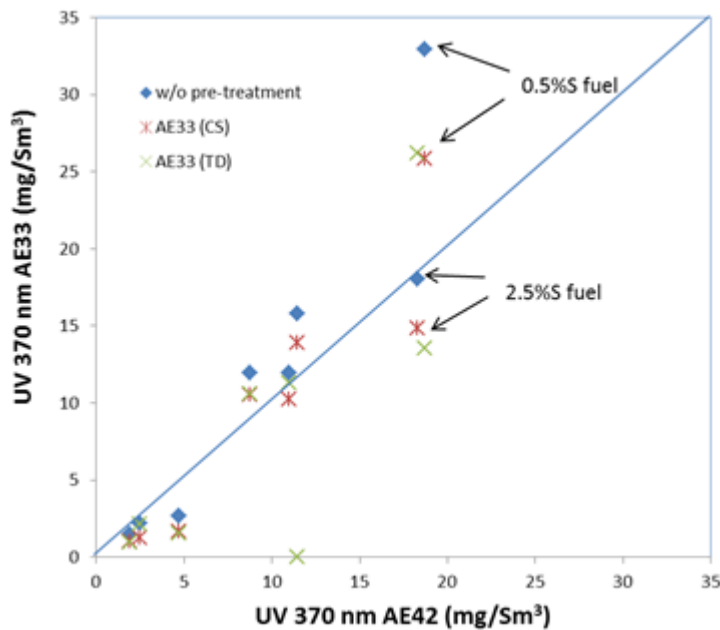


Figure 5.48. Intercorrelation between the response at UV obtained with two aethalometers.

For BrC, absorption decreases with increasing wavelength, while the light absorption of BC is only weakly dependent on wavelength (Yang et al. 2009, Andreae and Gelencser 2006, Lim et al. 2014, Collaud Coen et al. 2010, Yang et al. 2009). Figure 5.49 shows general view on the wavelength dependence given by AE33 for different fuels at 75% and 25% engine loads. Figure 5.50 shows the wavelength dependences observed with AE33 when diluted exhaust was untreated and when CS or TD pre-treatment was used.

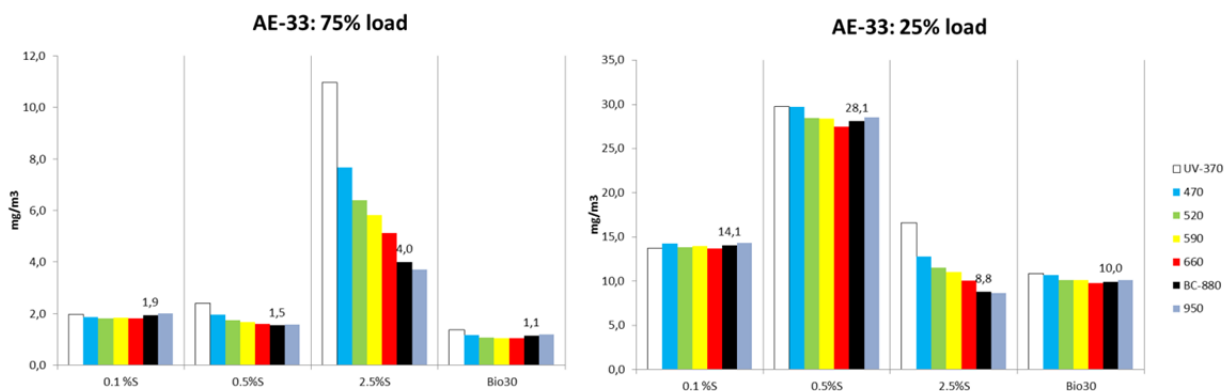


Figure 5.49. Wavelength dependence of absorbances measured with AE33.

The most substantial wavelength dependence was observed for the 2.5%S fuel, and some wavelength dependence also for the 0.5%S fuel. No substantial wavelength dependence was observed for the 0.1%S or Bio30 fuels.

For 2.5%S fuel, wavelength-dependence was strong with and without pre-treatment. Because CS or TD did not flatten the wavelength-dependence, the presence of conventional BrC was not evident. The constituents causing the wavelength dependence in this case may be heavy organic species, or inorganic species (e.g. metals). The overall absorbance reduced when TD was applied for the 2.5%S fuel at 25% engine load, while CS did not have such effect.

For the 0.5%S fuel, slight wavelength-dependence was observed with AE33, and this dependence also flattened when using CS or TD. At 75% load, magnitude of absorbance was not changed when pre-treatment was applied. Instead, at 25% engine load the absorbance decreased when CS or TD was used. This indicates that the samples contained organic material at 25% engine load, and at least some of it may be BrC.

For the 0.1%S or Bio30 fuels, not much wavelength-dependence was seen with or without CS or TD pre-treatment. This indicates that substantial amount of BrC was not present in these samples. CS and TD reduced the magnitude of absorbance at all wavelengths to some extent, which may be due to e.g. uncertainties in calculations of losses in the pre-treatment units.

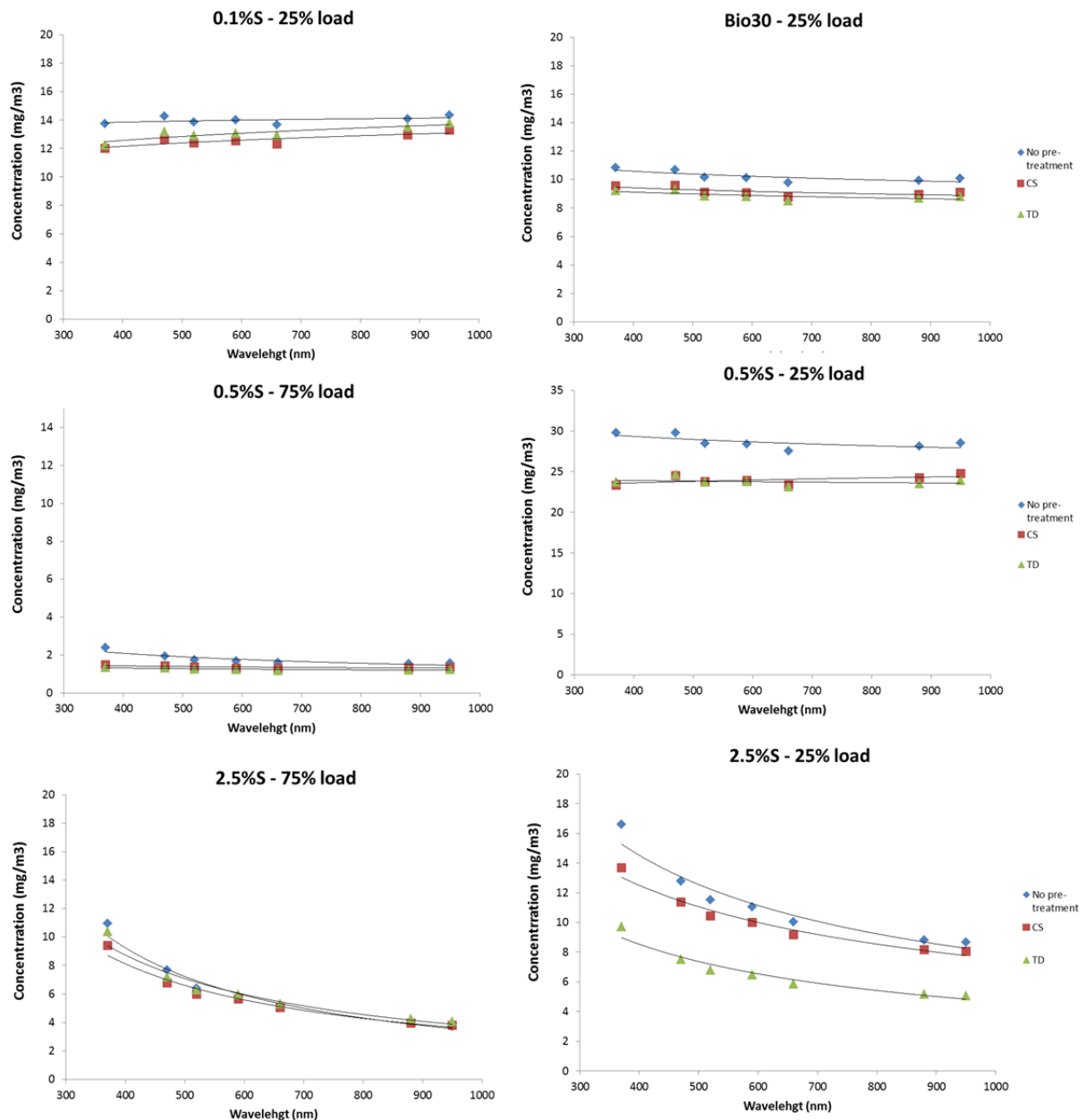


Figure 5.50. Wavelength dependence of absorption measured with AE33 with and without exhaust pre-treatment with CS and TD.

OC and BrC type material having absorbance at UV wavelength are shown in Figure 5.51. For the ISO 8178 diluted samples at 75% and 25% loads, higher OC fraction for the 0.5%S fuel than for the 2.5%S fuel was observed. However, the UV response (BrC) was lower for the 0.5%S fuel than for 2.5%S fuel at 75% engine load. This indicates that for the 0.5%S fuel, aerosols contained lighter organics (less BrC) than those for the 2.5%S fuel, which is supported by the in-stack OC results. At 25% engine load, the UV response (BrC) for the 0.5%S fuel was higher or close to that for the 2.5%S fuel.



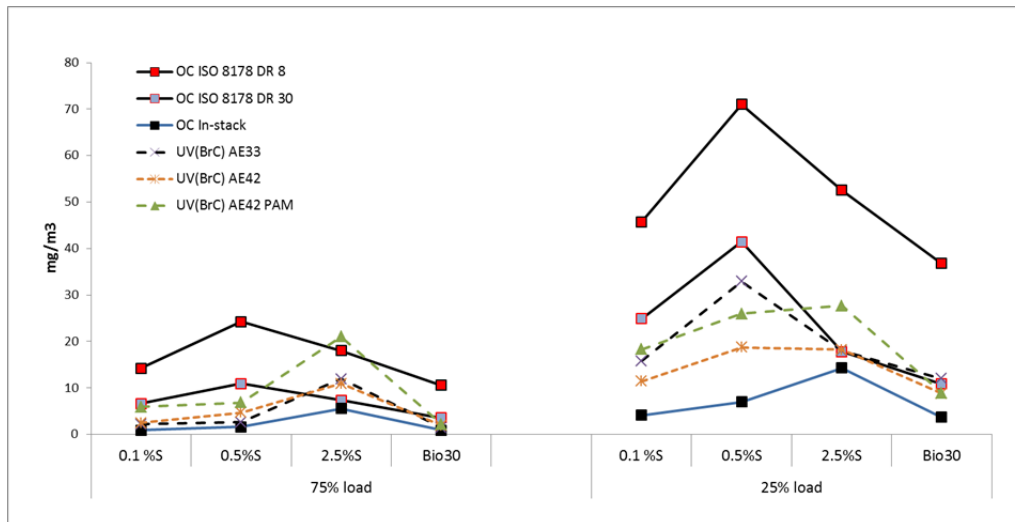


Figure 5.51. The OC concentrations (EUSAAR2) and BrC-type material having absorbance at UV wavelength (aethalometers).

## 5.8 Aged aerosol

Aging of aerosols at the atmosphere was simulated using a PAM chamber to oxidize the aerosol representing at least two day of aging in the atmosphere. For aged exhaust, the results are not quantitative due to the characteristics of measurements, such as high uncertainty related to DR and PM losses in the chamber. However, some general patterns of the results are preliminarily discussed here in qualitative terms.

The transformation of PM, e.g. change in size and optical properties when coating of particles become thicker due to condensation, during aging influences how the aerosol scatters or absorbs light (Lim et al. 2014, Collaud Coen et al. 2010, Yang et al. 2009). Sulphate aerosols or increase in particle size (from 0.1 towards 1.0  $\mu\text{m}$ ) lead to increased light scattering. Also, ammonium nitrate scatters light, whereas organonitrates can absorb solar radiation strongly, especially in short wavelengths (Zhang et al., 2011).

For aged exhaust, concentrations of sulphate were high, and so were the conversion percentages of  $\text{SO}_2$  to  $\text{SO}_4$ , roughly in a range of 10-20% (Figure 5.52). Calculated  $\text{SO}_2$  conversions to  $\text{SO}_4$  in primary PM (in-stack) are shown this Figure as a reference (see Chapter 5.4.3). Conversions were not calculated for the Bio30 fuel, because it contained only 4.3 mg/kg sulphur.

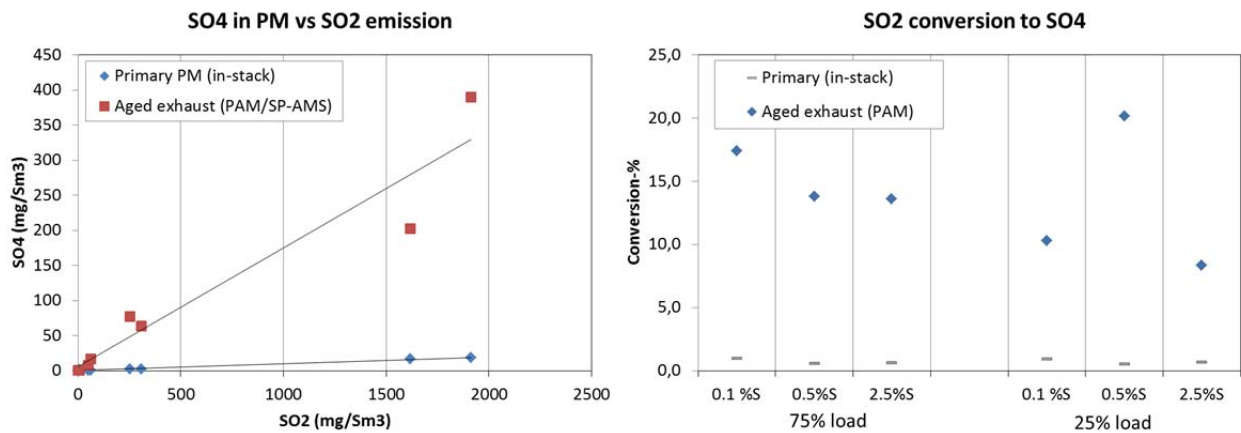


Figure 5.52.  $\text{SO}_2$  conversion to  $\text{SO}_4$  in aged aerosol (secondary PM). Conversion of  $\text{SO}_2$  to  $\text{SO}_4$  in primary PM (in-stack sampling) shown as reference (see Chapter 5.4.3).

Figure 5.53 represents ratios of organics, sulphates, nitrates and ammonia in the aged exhaust and the BC concentrations obtained with the optical instruments. Substantially high ratios of organics and sulphates to BC were observed for the 0.1%S, 0.5%S and 2.5%S fuels. For primary exhaust, the respective ratios of organics (in-stack) and BC were only around 1, and for sulphates (in-stack) and BC below 4.

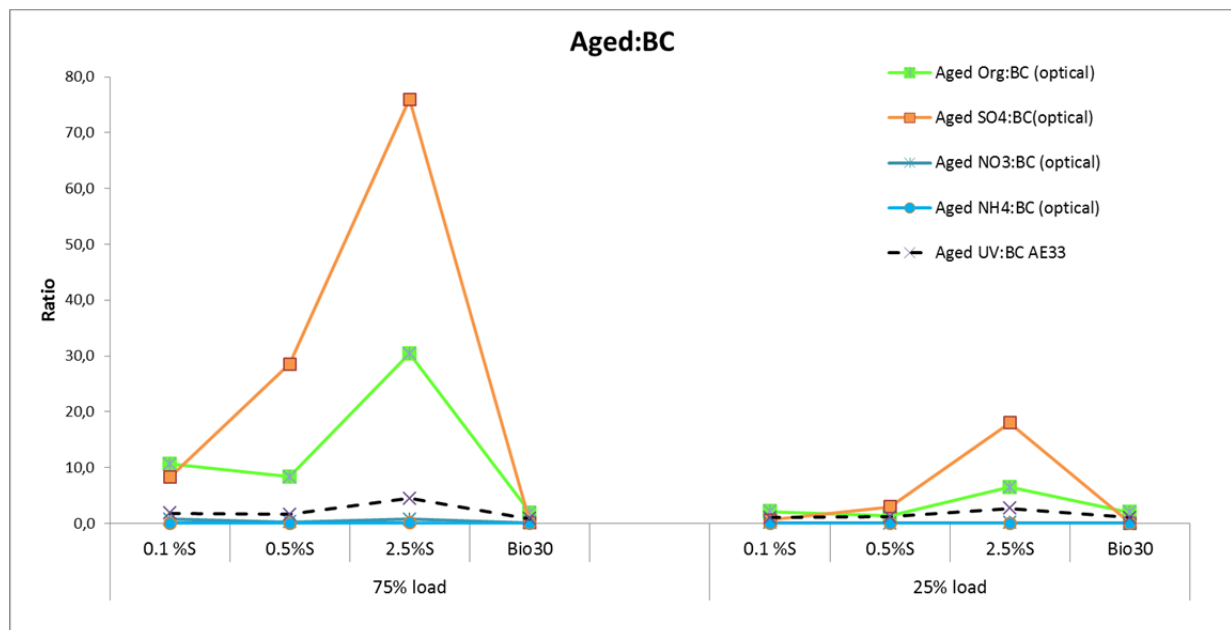


Figure 5.53. Ratio of components in the aged exhaust and the BC results obtained with the optical instruments.

Due to high ionization efficiency and subsequent fragmentation in SP-AMS it is not possible to identify individual organic compounds in the exhaust. However formed organic fragments can be further divided to subgroups representing the common organic families (e.g. hydrocarbons, oxidated hydrocarbons etc.). An example of SO, CHN, CHO and CH families present in the aged aerosols (PAM) is shown in Figure 5.54. Following names are used in figure:

- CH=hydrocarbon,
- SO=sulphur containing fragments
- CHO=fragment with composition  $C_xH_yO$ ,
- CHOgt1=  $C_xH_yO_z$ , where z is greater than 1
- CHN=organic compound containing  $C_xH_yN$ ,

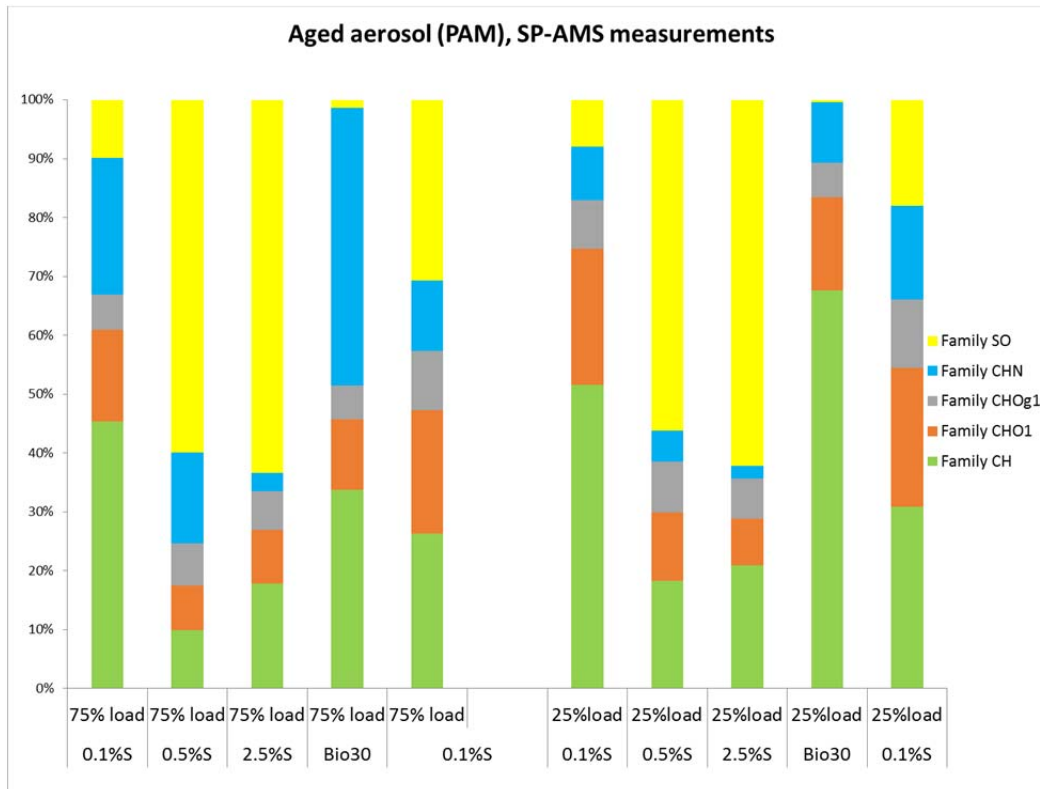


Figure 5.54. An example of SO, CHN, CHO and CH families present in the aged aerosols after PAM, SP-AMS measurements.

## 5.9 Particle sizing and volatility

### 5.9.1 Particle number size distributions

Number size distributions were measured using porous tube diluter (PTD) dilution setup with total dilution ratios  $< 200$ . The dilution setup coupling PTD diluter and residence time chamber allows nucleation and condensation of semivolatile gaseous compounds during dilution, and it has been shown to mimic atmospheric dilution and nucleation mode formation in vehicle measurements (Keskinen & Rönkkö 2010; Rönkkö et al. 2006). Number size distribution results were combined from two devices, SMPS and NanoSMPS, making the transition in 30-50 nm size class. The combined number size distributions for 75% load and 25% load measured with SMPS and NanoSMPS are shown in Figure 5.55. Standard deviations for the size distributions are marked with the shaded areas. During the measurement with IFO at 75% load, one clearly differing distribution was measured that broadened the standard deviation but only minimally the average distribution. The same results are shown in logarithmic scale in Figure 5.56 to better illustrate the different particle

modes and especially soot mode in  $>100\text{nm}$  size that is almost invisible in linear plots. During the measurement days for heavy fuel oil and intermediate fuel oil, a discrepancy was seen between the absolute levels of number concentrations measured by SMPS and NanoSMPS and for this reason, in Figure 5.56 only particle size and shapes of the distributions are compared using SMPS and NanoSMPS results.

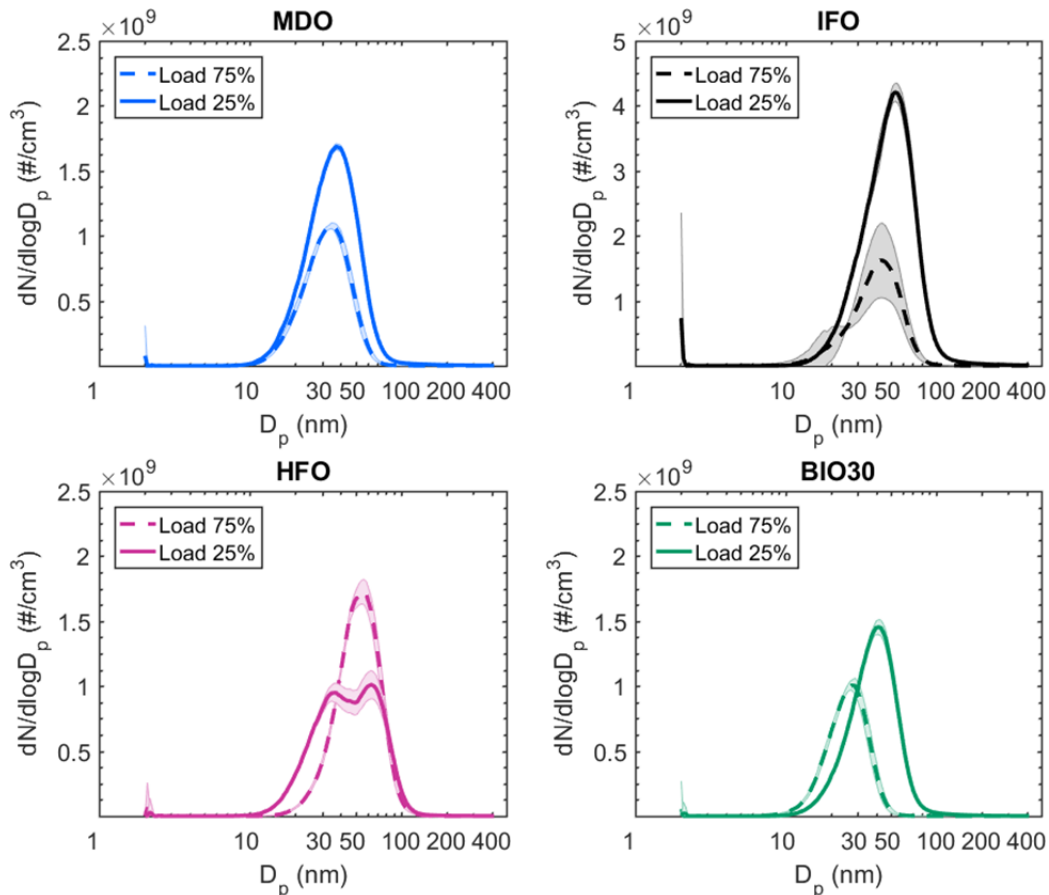


Figure 5.55. Number size distributions for 75% load and 25% load measured with SMPS and NanoSMPS. Standard deviations are marked as shaded areas around the distributions.

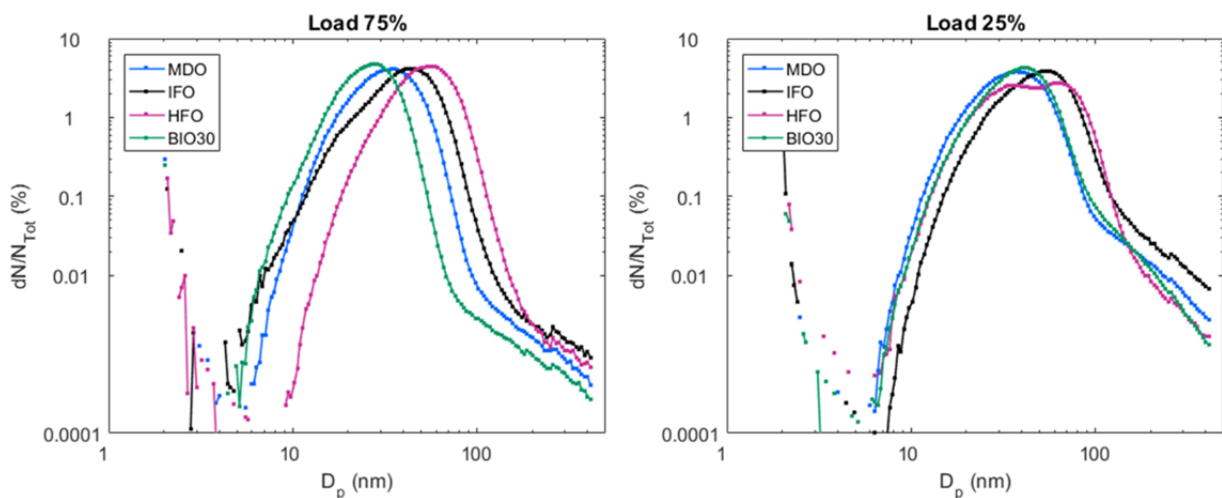


Figure 5.56. Number size distributions for 75% load and 25% load measured with SMPS and NanoSMPS. Y-axis is in logarithmic scale. Number size distributions have been normalized by the measured total particle number.

Diesel engines typically emit particles that can be seen in the particle size distribution as one, two or three separate modes. Soot mode particles consist of agglomerates that can have semivolatile condensates on them. Nucleation mode particles in ship emissions usually consist of volatile compounds such as water, sulphur compounds and hydrocarbons but can also include fuel ash components and soot spherules (eg. Fridell et al., 2008).

For all the tested fuels at both load points, the size distributions showed pronounced nucleation modes with peaks in particle sizes between 20 and 70 nm. High nucleation modes have been observed also in previous studies considering particle emissions from marine engines (eg. Anderson et al., 2015; (Kasper et al. 2007). For HFO at 25% load, the size distribution contained two elevated modes with peaks at 30 nm and 70 nm. Nucleation mode particles are generally thought to consist of volatile sulphuric and hydrocarbon compounds that have either formed particles of their own by nucleation or condensed on existing seed particles. In the case of high ash content in fuel, also species in fuel ash may contribute to nucleation mode formation (Lyyräinen et al. 1999).

At 75% load, the mean diameter of the nucleation mode particles seemed to increase as the fuel sulphur content increased. The diameters corresponding to the peaks in the number size distributions ranged from 28 nm for BIO30 to 55 nm for HFO. At 25% load the dependence of mean particle size on fuels sulphur content was less obvious and peak diameters were generally larger. The peak diameters were around 40 nm for MDO and BIO30 and around 55 nm for IFO. For HFO, two pronounced modes were seen in addition to the soot mode with peak diameters around 35 nm and 65 nm. The volatility tests described in section 1.8.2 showed that also for HFO at 75% load, the nucleation mode actually contained two separate modes.

### 5.9.2 Total particle number

Total particle number was measured using a CPC that measures particles between 7 nm and 1  $\mu\text{m}$ . Particle number was measured after PTD dilution and two additional bridge diluters were used before the CPC to decrease the concentration below the upper detection range of the instrument. The instrument was not available for the MDO measurements in the beginning and in the end of the campaign, but for other fuels, results are shown in Figure 5.57.

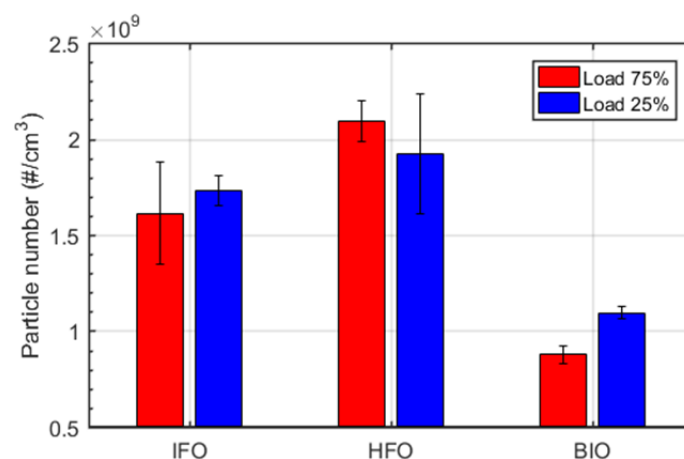


Figure 5.57. Total particle number measured by CPC.

The measured total particle numbers were between  $0.8\text{--}2.1 \times 10^9$   $1/\text{cm}^3$  for all of the studied fuels. Highest concentrations were measured for heavy fuel oil and lowest for the biofuel blend. For IFO and HFO, the used engine load had only moderate effect on the number concentration, or at least the differences were inside the standard deviations of the measurement. For the biofuel blend, number concentration was higher at low load. This was also indicated for MDO by the SMPS measurements.

### 5.9.3 Particle volatility

Volatility of the particles was studied using thermal treatment with either catalytic stripper or thermodenuder. Catalytic stripper was used in constant temperature of 350 °C. Thermodenuder was used either in constant temperature of 265 °C or to measure temperature ramps. During the ramps, TD was first heated to a target temperature of 300 °C and then let to cool, while simultaneously measuring particle size distributions. The results are shown in Figure 5.58 and Figure 5.59 for 75% load and 25% load, respectively. The particle number size distributions were corrected for size-dependent diffusion and thermoforetic particle losses in TD and CS.

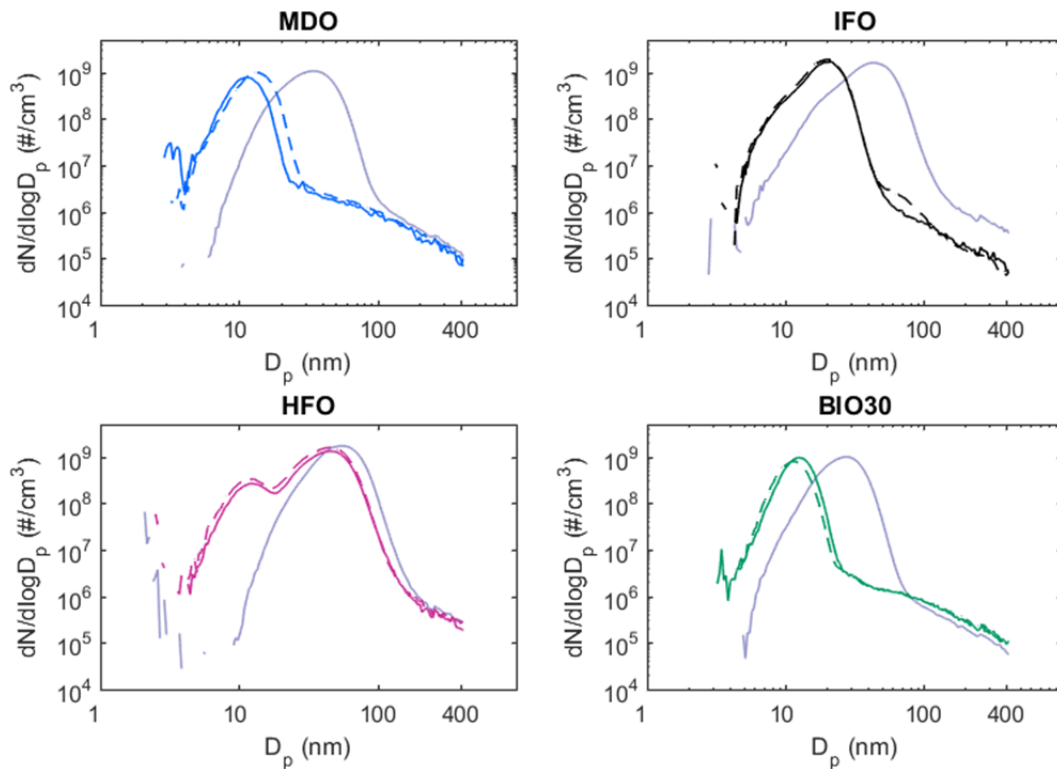


Figure 5.58. Number size distributions of all particles (grey line) and non-volatile particle size distributions measured with thermodenuder (TD) and catalytic stripper (CS) at 75% load. Solid line marks non-volatile particles measured after thermodenuder and dotted line non-volatile particles measured after catalytic stripper.

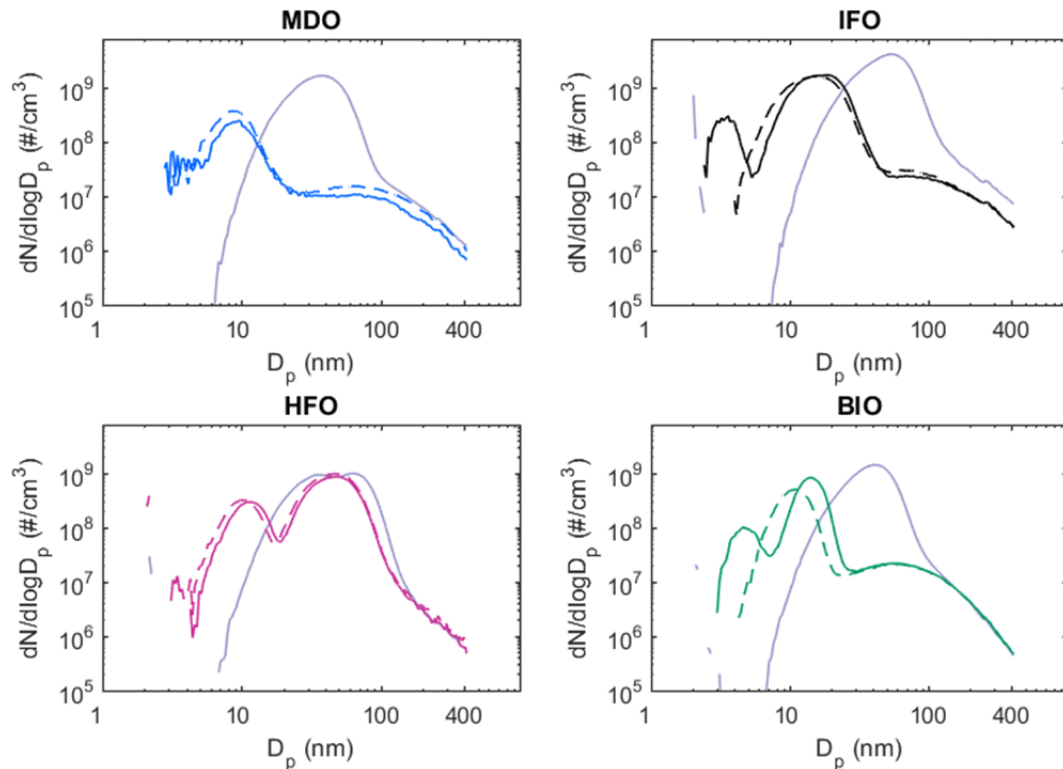


Figure 5.59. Number size distributions of all particles (grey line) and non-volatile particle size distributions measured with thermodenuder (TD) and catalytic stripper (CS) at 25% load. Solid line marks non-volatile particles measured after thermodenuder and dotted line non-volatile particles measured after catalytic stripper.

The non-volatile number size distributions show that in all of the studied cases, the thermal treatment reduced the mean size of the nucleation mode particles. However, the nucleation mode particles were not completely volatile and they included a non-volatile core that was seen in 20–30 nm size for IFO and around 10 nm size for other fuels. For HFO, particularly the first of the two pronounced modes included a high share of volatile condensates. For the second mode, evaporation of volatile condensates was only moderate and the peak of the mode was reduced to around 50 nm size in thermal treatment. Due to the shrinking of the nucleation mode particles, the peaks of soot mode particles are better visible in the size distributions measured after CS and TD, especially at 25% load where soot mode concentrations were higher. More discussion related to the nucleation mode particle composition have been presented in Ntziachristos et al. 2016.

The behaviour of the particle modes was similar at both load points, only the exact particle diameters and concentrations varied. Only in the cases of IFO and biofuel blend at 25% load, the measurements with TD and CS suggested different behaviour of the nucleation mode particles. At first look, the thermodenuder measurements (solid lines in Figure 5.59) indicated that the nucleation mode would include two types of solid particles, ones in 10–20 nm size class and others in only 3–4 nm size. However, by looking at the evolution of the particle size distributions during thermodenuder ramps, it was likely that the active carbon lining in thermodenuder was not able to remove all of the volatile compounds during these two measurements. In this case, the volatile gases could again nucleate or condensate during cooling of the sample.

According to the current understanding, the particle in diameters larger than 30 nm in TD or CS treated exhaust sample is considered as soot mode and contributes to BC measurements made by e.g. SP-AMS or optical methods.

Figure 5.60 shows the fraction of particle volume after thermal treatment with catalytic stripper. It could be seen that at low load the fractions of non-volatile particulate volume was higher. With HFO the fraction of non-volatile particle volume was observed to be highest, 55-60% of total particle volume. For other fuels the fraction of non-volatile particle volume varied between 10-40%.

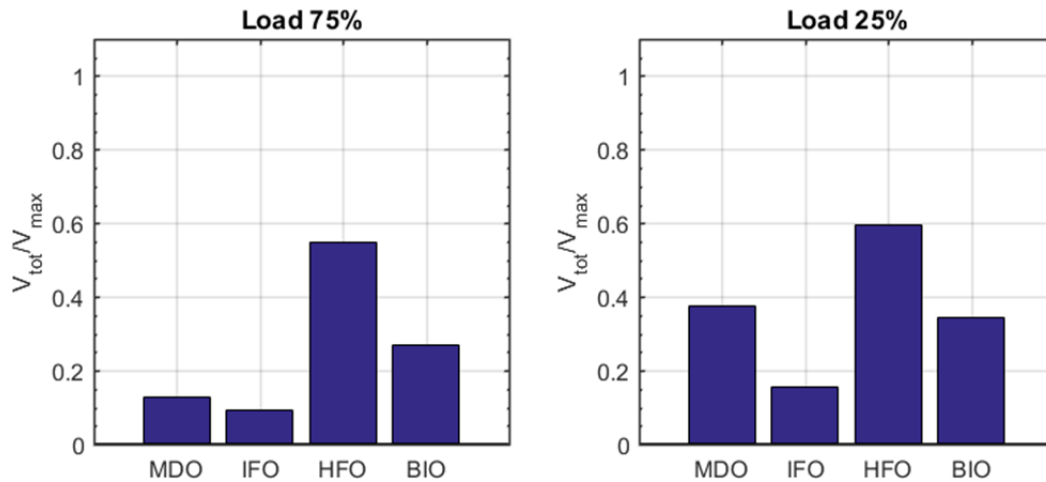


Figure 5.60. Remaining fraction of particle volume after thermal treatment with catalytic stripper at 350°C. Particle volumes were calculated from particle number size distributions between 2-414 nm.

Figure 5.61 show the thermodenuder temperature ramps for all the fuels and at both load conditions. In the figure the remaining particle volume is shown as a function of thermodenuder temperature. The thermodenuder was let to cool to a temperature of 45 °C that is used as reference for the particle volume. The volatility of the particles depended on fuel; with MDO most of the particulate matter evaporated at temperatures below 150 °C, while with HFO evaporation was more gradual and non-volatile particle fraction did not reach stable level.



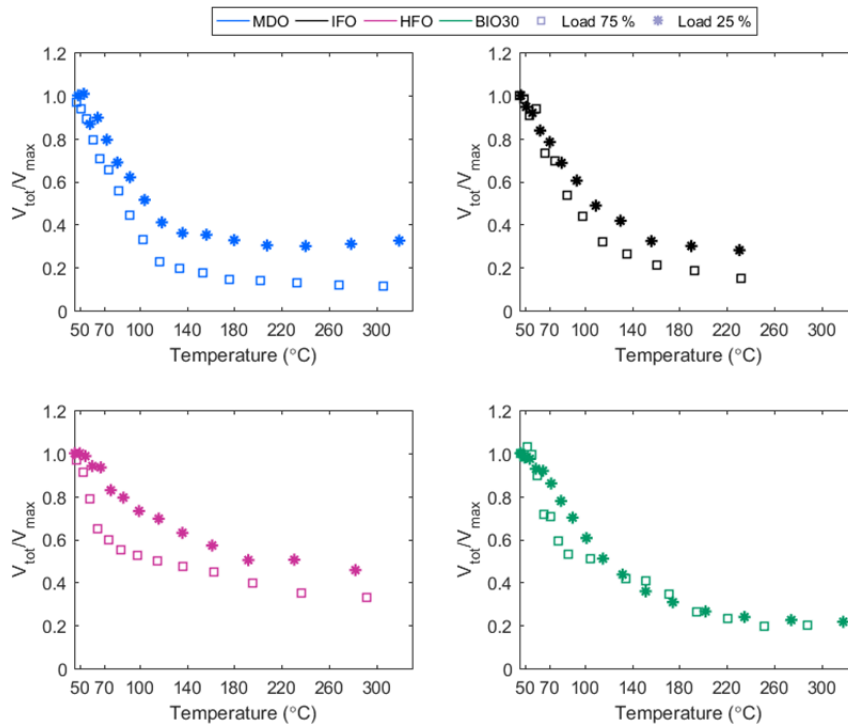


Figure 5.61 Fraction of remaining particle volume during thermodenuder ramps.

#### 5.9.4 Emission factors for soot mode particle number

Soot mode particle emission factors were determined different methods from particle size distributions measured by SMPS. These methods are:

1. Modal fit to measurement data without thermal treatment (soot mode w/o treatment)
2. Modal fit to measurement data with catalytic stripper (soot mode, CS). The catalytic stripper removes semi-volatile compounds from particles. This should enable a more accurate fit.
3. Number emissions of particles larger than 60nm, 80nm, and 100nm in diameter, calculated from distributions measured after CS (>60 nm, CS; >80 nm, CS; >100 nm, CS)

The modal fittings were done by fitting lognormal distributions to the measured SMPS data, using least squares method (LSN) (eg. Hussein et al. 2005) and the Solver optimisation tool in Excel. For HFO, 3 modes were fitted, for other fuels 2 modes were fitted. Results for soot mode particle number emission factors can be seen in Figure 5.62 and Figure 5.63.

The results show that using a constant particle size as definition for soot mode generally underestimates the number of soot particles, except for HFO for which the size distribution is tri-modal and the size range of particles larger than 60 nm is significantly affected by particles other than soot mode.

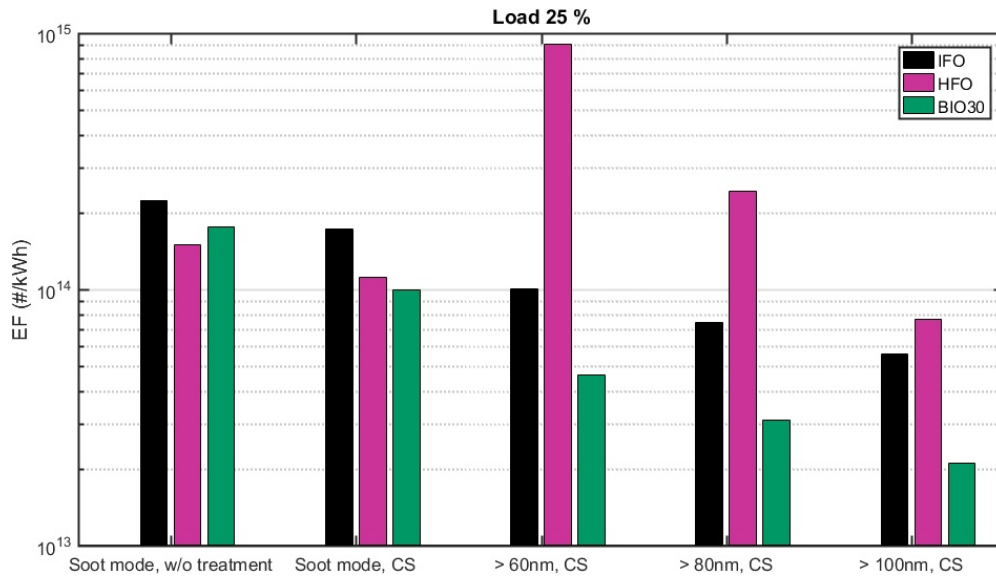


Figure 5.62 Emission factors for soot mode particle number at 25% load, determined by different methods from size distribution data.

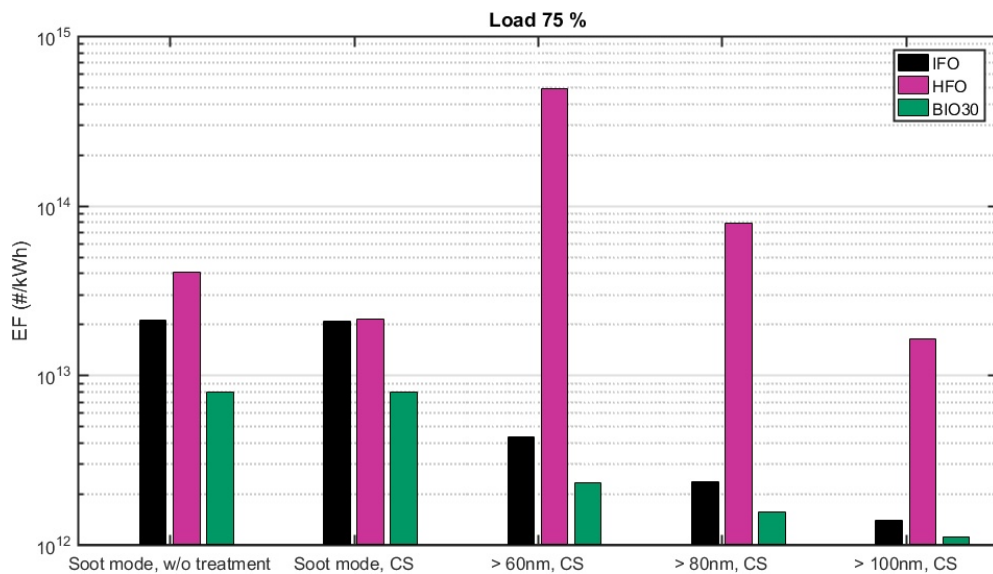


Figure 5.63 Emission factors for soot mode particle number at 75% load, determined by different methods from size distribution data.

In Figure 5.64 the soot mode particle number emission factors (Mode 3) are compared to particle number emission factors determined for other modes (Mode 1 and Mode 2) and for total particle number emission factors (All particles). It can be seen that the total particle number emission factor is almost totally dominated by other than soot mode particles.

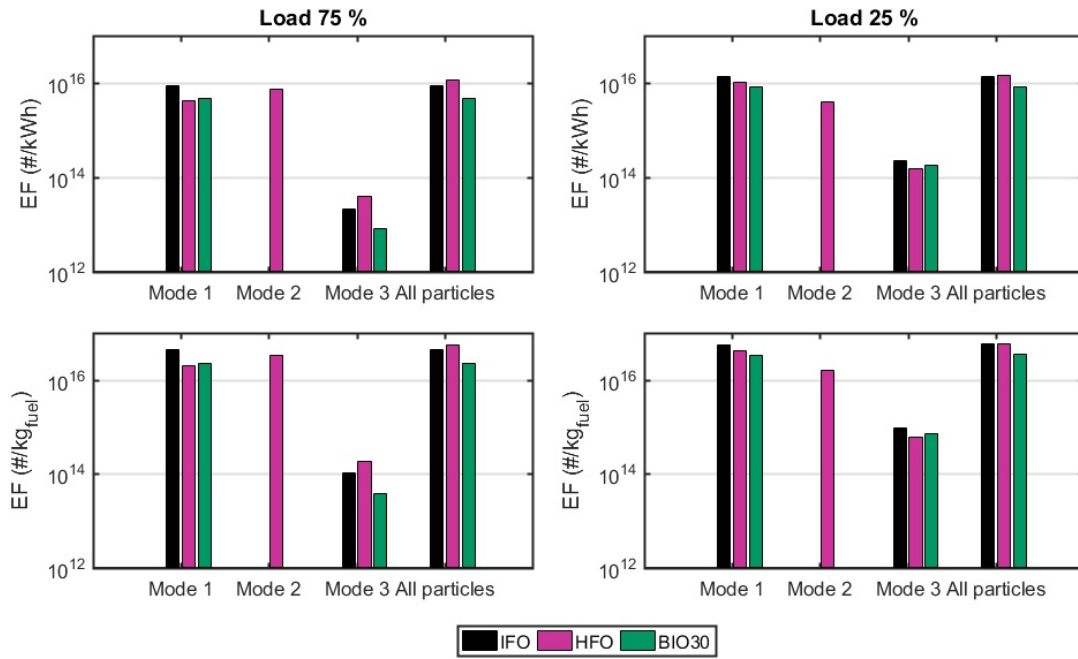


Figure 5.64. Particle number emission factors for measurements without CS (Kuittinen et al. manuscript in prep.)

## 6 Discussion and conclusions

The BC measurements from a 1.6-MW ship engine (Wärtsilä Vasa 4R32 LN) at 75% and 25% engine loads were conducted in VTT's engine laboratory using several BC measurement techniques. Fuels with 0.1%, 0.5% and 2.5% sulphur contents were used, as well as a biofuel blend (Bio30). To complement the BC results, a comprehensive setup of state-of-the-art instrumentation was used to characterize chemical composition and physical properties of the particulate emissions as well as main gaseous emissions.

In the WP1 laboratory measurements, the BC instruments representing optical, refractive and thermal-optical methods were employed. From the four IMO's candidate methods, Photo-Acoustic Spectroscopy (PAS, AVL MSS), MAAP and Filter Smoke Number (Smoke Meters AVL 415S and AVL 415SE) methods were covered, while Laser Induced Incandescence (LII) was not included in the measurements. In addition, BC was analysed with aethalometers (AE33, AE42). EC was analysed from filter samples obtained with ISO 8178 and in-stack collections. Pegasor PPS was used to analyse PM (on-line). Chemical composition and physical characteristics of PM were analysed. In-depth measurements covered e.g. PM size distribution, volatility, hygroscopicity, secondary aerosol formation potential were analysed using state-of-the-art methods including SP-AMS, SMPS and PSM.

### Feasibility of different methods for routine BC measurements from ships?

Smoke meters (FSN) sample directly from the raw exhaust and AVL MSS (PAS) has manufacturer's own dilution system using low dilution ratios, whereas MAAP and aethalometers are designed for ambient BC measurements and thus high DRs are needed to obtain suitable BC concentrations from diesel engine exhaust. **The need for dilution is the critical factor distinguishing the BC instruments and having consequences on the complexity of the test set-up, and on the reliability of the BC results.** The main pros and cons of the dilution principles are shown in Table 6.1.

Table 6.1. Pros and cons of different sampling alternatives for the BC measurements. Old ship engine using residual fuel is assumed.

Sampling for BC measurements	Pros	Cons
<b>Raw exhaust sampling</b> (FSN)	<ul style="list-style-type: none"> <li>No need for pressurised air</li> <li>Simple installation</li> <li>No uncertainty of dilution ratio</li> </ul>	<ul style="list-style-type: none"> <li>Condensation of sample gas to be avoided</li> </ul>
<b>Instrument's own dilution, low dilution ratio</b> AVL MSS (PAS)	<ul style="list-style-type: none"> <li>Low risk of condensation of the sample gas</li> <li>Simple system to use</li> <li>Manufacturer has developed calibrations and quality assurance</li> </ul>	<ul style="list-style-type: none"> <li>Pressurized air needed, or option with an internal dilution air pump.</li> <li>Filtration and drying of the dilution air</li> <li>More complex than raw sampling</li> <li>Increases uncertainties</li> </ul>
<b>High dilution ratios DR&gt;&gt;100</b> (MAAP, aethalometers)	Good for research (qualitative) purposes	<ul style="list-style-type: none"> <li>Not for routine BC measurements</li> <li>Complicated test set-up</li> <li>High uncertainties due to high DR.</li> </ul>

Despite of the differences in the BC measurement principles, **the comparability was relatively good between the BC results** based on FSN (AVL 415S, AVL 415SE), PAS (AVL MSS), aethalometers (AE42, AE33) and MAAP 5012 (at sufficiently high DRs). EC results from the ISO 8178 PM and in-stack sampling compared also relatively well with the BC results, when the prolonged EUSAAR2 protocol was used. Fuels and engine loads were rated in the same order with different instruments despite of the different measurement principles. Standard deviation of the BC results between six instruments was  $<1 \text{ mg/Sm}^3$  at BC concentrations below  $5 \text{ mg/Sm}^3$ , and up to  $3 \text{ mg/Sm}^3$  at higher BC concentrations.

Standard deviation for each individual BC instrument was  $<0.5 \text{ mg/Sm}^3$  and up to  $1 \text{ mg/Sm}^3$ , respectively.

FSN is a standardised method designed for exhaust emission measurements. The FSN method is robust, easy to use and measures directly from the raw exhaust gas. BC is calculated based on FSN. PAS method was studied using the AVL MSS instrument consisting of sensor and conditioning units for dilution, and calibrations were designed by manufacturer. AVL MSS provided a continuous on-line measurement of the BC concentration. **Both of these IMO candidate methods (FSN, PAS) seemed practical for the routine BC measurements from ships, while MAAP was not practical** (the same applies to aethalometers). MAAP is designed for ambient aerosol measurements, and thus high dilution ratios associated with high uncertainties were needed. Furthermore, narrow measurement range of MAAP is easily exceeded. If MAAP is used, the diluted BC concentrations and sample flow should be reported and inspected against the reliable measurement range.

EC is not a commensurable definition with BC, but it is often discussed along with the BC results. The EC measurement was challenging from marine engine PM filters. In this work, EUSAAR2 with prolongation was selected for round-robin. Spread in the EC results between three temperature programs in one laboratory was higher ( $<3 \text{ mg/Sm}^3$ ) than that between three laboratories using one temperature program ( $<1 \text{ mg/Sm}^3$ ). When considering EC for measurements from ships, one of the bottlenecks concerns lack of small robust PM sampling systems.

Main findings in the SEA-EFFECTS BC project of the feasibility of different measurement methods for the ship BC measurements are shown in Table 6.2. In addition, other findings are commented, e.g. the CS and TD pre-treatment options to remove volatile constituents from exhaust. The PPS-M operated without problems with all fuels tested, and correlated with the in-stack PM-results.

Table 6.2. Main findings for methods applicable for old ships using residual fuels.

Measurement	Comment	Outcome
BC, FSN	Raw exhaust sampling. Robust.	<b>Feasible</b> for routine measurements.
BC, PAS	<b>On-line.</b>	<b>Feasible</b> for routine measurements
BC, MAAP (and aethalometers)	<b>On-line.</b> High dilution ratio and heated diluters needed. Narrow range.	Not recommended for routine measurements.
EC	Filter sampling, laboratory analysis. <ul style="list-style-type: none"> <li>• ISO 8178 (dilution). Commercial systems are large and heavy.</li> <li>• In-stack installation complicated.</li> </ul>	Not recommended for routine measurements.
<b>PM and gases</b>		
PM, Pegasor PPS	Low DR. <b>On-line.</b>	Potential for further development.
Gaseous: FTIR (Gasmeter)	CO, CO <sub>2</sub> , methane, NO, NO <sub>2</sub> , N <sub>2</sub> O, NH <sub>3</sub> , aldehydes etc. <b>On-line.</b>	<b>Feasible.</b>
Gaseous: micro-hotplate	Trial with a sensor for total HC. <b>On-line.</b>	Potential for further development.
HC(Spectral Engines)	E.g. methane, ethane, propane. <b>On-line.</b>	Potential for further development.
<b>Note:</b> Sample pre-treatment with CS or TD is potential, but increases system complexity (high losses to be accounted for). Materials compatible with acids for high sulphur fuels are needed.		

### The effect of fuel and engine load on the BC emission from an old ship engine

The BC emission was dependent on both engine load and fuel properties, but not directly on the sulphur content of fuel. The BC emission was substantially higher at 25% load than at

75% load. The 2.5%S fuel showed the highest BC emission at 75% load, whereas its BC emission was relatively low at 25% load. Certain metals present in the 2.5%S fuel may catalytically enhance combustion of BC at 25% load. The 0.5%S fuel showed the highest BC emission at 25% load, while at 75% load its BC emission was low (close to that for the 0.1%S and Bio30 fuels). This indicates better combustion of fuel at higher temperature (75% engine load) even without the catalytic effect of metals. Even at 0.5% sulphur level fuel may contain BC precursors depending on crude oil and processing technology. The BC emissions for the 0.1%S and Bio30 fuels were low. The lowest BC was observed for the Bio30 fuel presumably basing on its oxygen content. Fuels containing distillates typically consist of lighter hydrocarbons than the residual fuels. The load and fuel dependences observed for the BC emissions in this study are characteristic for the old engine studied equipped with a mechanical injection system. Engines equipped with modern injection systems are less sensitive towards fuel properties, by default.

In opposite to the BC emission, the PM emission was strongly dependent on fuel sulphur content. For 2.5%S fuel, PM contained high share of sulphates, organic carbon, metals and oxygen associated with water and oxides, while share of BC was low for all fuels. Higher concentration of heavy PAHs in PM were found for the 0.5%S and 2.5%S fuels than for the 0.1%S and Bio30 fuels.

### **Glance on the in-depth analyses**

In this project a vast amount of in-depth data was generated, and its analysis deserves further efforts in addition to the publications presented so far. For example, information of particle sizes and their volatility is valuable in the development of the BC measurement instruments. From particle sizing measurements, some conclusions were already drawn. For all the tested fuels at both engine loads, the smallest “nucleation” mode particles were observed. At 75% load, the mean diameter of these particles increases along with fuel sulphur content (28 nm Bio30; 55 nm 2.5%S). At 25% load, the mean particle size was generally larger (40-55 nm), and less dependent on fuel. The total particle numbers were  $0.8\text{--}2.1 \times 10^9 \text{ 1/cm}^3$ , the highest for 2.5%S fuel and the lowest for the biofuel blend. Volume of the non-volatile particles was higher at low than at high engine load, and the highest for the 2.5%S fuel (55-60%, for other fuels 10-40%). For the 0.1%S fuel, the PM evaporated below 150 °C, while with the 2.5%S fuel evaporation was more gradual. For the 2.5%S fuel the particle size distribution was tri-modal differently from the other fuels.

Also aged exhaust was studied in detail besides the fresh exhaust. These results will give a comprehensive view to contribute in the discussion of the parameters affecting the global warming. A glance on the fractions (e.g. organics:BC) is given in this report, but the processing of in-depth data will continue. The results obtained enlighten also the health impact of ship emissions (e.g. particle sizing and analyses of PAHs and metals). The outcome of WP1 was taken into account in validation of the measurements on-board a ship in WP2 (Timonen et al. 2017).

## References

---

- Aakko, P. & Nylund, N.-O., 2003. Particle emissions at moderate and cold temperatures using different fuels. Society of Automotive Engineers, [Special Publication] SP, SP-1809(724), pp.279–296.
- Aakko-Saksa, P. et al., 2012. Future Combustion technology for synthetic and renewable fuels in compression ignition engines (REFUEL), Aalto University publication series SCIENCE + TECHNOLOGY 21/2012,
- Aakko-Saksa, P. et al., 2016. CIMAC Paper 068 Black carbon measurements using different marine fuels. 28th CIMAC World Congress.
- ACEA et al., 2006. World-wide fuel charter WWFC. (Fourth Edition), p.68.
- Amanatidis, S. et al., 2013. Evaluation of an oxidation catalyst (“catalytic stripper”) in eliminating volatile material from combustion aerosol. *Journal of Aerosol Science*, 57, pp.144–155. Available at: <http://dx.doi.org/10.1016/j.jaerosci.2012.12.001>.
- Arnott, W.P. et al., 2005. Towards Aerosol Light-Absorption Measurements with a 7-Wavelength Aethalometer: Evaluation with a Photoacoustic Instrument and 3-Wavelength Nephelometer. *Aerosol Science and Technology*, 39(September 2015), pp.17–29.
- Bauer, J.J. et al., 2009. Characterization of the sunset semi-continuous carbon aerosol analyzer. *Journal of the Air & Waste Management Association* (1995), 59(7), pp.826–833.
- Barneto, A.G. et al., 2014. Journal of Analytical and Applied Pyrolysis Thermogravimetric monitoring of oil refinery sludge. *Journal of Analytical and Applied Pyrolysis*, 105, pp.8–13. Available at: <http://dx.doi.org/10.1016/j.jaap.2013.09.007>.
- Birch, M.E. & Cary, R.A., 1996. Elemental carbon-based method for monitoring occupational exposures to particulate diesel exhaust. *Aerosol Science and Technology*, 25(3), pp.221–241.
- Bond, T.C. et al., 2013. Bounding the role of black carbon in the climate system: A scientific assessment. *Journal of Geophysical Research Atmospheres*, 118(11), pp.5380–5552.
- Carbone, S. et al., 2015. Characterization of trace metals on soot aerosol particles with the SP-AMS: Detection and quantification. *Atmospheric Measurement Techniques*, 8(11), pp.4803–4815.
- Cavalli, F. et al., 2010. Toward a standardised thermal-optical protocol for measuring atmospheric organic and elemental carbon: the EUSAAR protocol. *Atmospheric Measurement Techniques*, 3(1), pp.79–89.
- Chang, D. & Gerpen, J., 1997. Fuel Properties and Engine Performance for Biodiesel Prepared from Modified Feedstocks. SAE Technical Paper. SAE Technical Paper Series, 971684.
- Collaud Coen, M. et al., 2010. Minimizing light absorption measurement artifacts of the Aethalometer: Evaluation of five correction algorithms. *Atmospheric Measurement Techniques*, 3(2), pp.457–474.
- Drinovec, L. et al., 2015. The “dual-spot” Aethalometer: An improved measurement of aerosol black carbon with real-time loading compensation. *Atmospheric Measurement Techniques*, 8(5), pp.1965–1979.
- Durbin, T.D. & Norbeck, J.M., 2002. Effects of Biodiesel Blends and Arco EC-Diesel on Emissions from Light Heavy-Duty Diesel Vehicles. *Env. Sci. & Technol.*, 36, pp.1686–

1691.

- Graboski, M.S. & McCormick, R.L., 1998. Combustion of fat and vegetable oil derived fuels in diesel engines. *Prog. Energy Combust. Sci.*, 24, pp.126–164.
- Grimaldi, C.N. et al., 2002. Common Rail HSDI Diesel Engine Combustion and Emissions with Fossil / Bio-Derived Fuel Blends. (724).
- Hansen, A. D. A., Rosen, H., and Novakov, T.: The aethalometer – an instrument for the real-time measurement of optical absorption by aerosol particles, *Sci. Total Environ.*, 36, 191–196, 1984.
- Happonen, M. et al., 2013. Diesel exhaust emissions and particle hygroscopicity with HVO fuel-oxygenate blend. *Fuel*, 103, pp.380–386. Available at: <http://dx.doi.org/10.1016/j.fuel.2012.09.006>.
- Hellen, G., 2015. Black Carbon Emissions - Latest news from IMO.
- Hussein, T., Maso, M. D., Petäjä, T., Koponen, I. K., Paatero, P., Aalto, P. P., Hämeri, K., Kulmala, M. (2005). Evaluation of an automatic algorithm for fitting the particle number size distributions. *Boreal Environ.*, (October), 337–355.
- Hyvärinen, A.P. et al., 2013. Correction for a measurement artifact of the Multi-Angle Absorption Photometer (MAAP) at high black carbon mass concentration levels. *Atmospheric Measurement Techniques*, 6(1), pp.81–90.
- IPCC, 2013. CLIMATE CHANGE 2013 T. F. Stocker et al., eds., Cambridge University Press, Cambridge, United Kingdom and New York, NY, USA.
- Jung, J. et al., 2011. The effects of accumulated refractory particles and the peak inert mode temperature on semi-continuous organic carbon and elemental carbon measurements during the CAREBeijing 2006 campaign. *Atmospheric Environment*, 45(39), pp.7192–7200. Available at: <http://dx.doi.org/10.1016/j.atmosenv.2011.09.003>.
- Kanaya et al. (2008) Mass concentrations of black carbon measured by four instruments in the middle of Central East China in June 2006. *Atmos. Chem. Phys.*, 8, 7637–7649, 2008.
- Kang, E., Toohey, D. W., & Brune, W. H. (2011) Dependence of SOA oxidation on organic aerosol mass concentration and OH exposure: experimental PAM chamber studies” *Atmospheric Chemistry and Physics*, 11(4), 2011, pp. 1837-1852, doi:10.5194/acp-11-1837-2011.
- Karanasiou, A. et al., 2011. On the quantification of atmospheric carbonate carbon by thermal/optical analysis protocols. *Atmospheric Measurement Techniques*, 4(11), pp.2409–2419.
- Karanasiou, A. et al., 2015. Thermal-optical analysis for the measurement of elemental carbon ( EC ) and organic carbon ( OC ) in ambient air a literature review.
- Karjalainen, P. et al., 2016. Time-resolved characterization of primary particle emissions and secondary particle formation from a modern gasoline passenger car. *Atmospheric Chemistry and Physics*, 16(13), pp.8559–8570.
- Kasper, A., Aufdenblatten, S., Forss, A., Mohr, M., & Burtscher, H. (2007). Particulate Emissions from a Low-Speed Marine Diesel Engine. *Aerosol Science and Technology*, 41(September 2014), 24–32. doi:10.1080/02786820601055392.
- Keskinen, J., & Rönkkö, T. (2010). Can real-world diesel exhaust particle size distribution be reproduced in the laboratory? A critical review. *Journal of the Air & Waste Management Association* (1995), 1245–1255. doi:10.3155/1047-3289.60.10.1245.



- Kuittinen, N., Karjalainen, P., Aakko-Saksa, P., Timonen, H., Simonen, P., Mylläri, F., Wihersaari, H., Keskinen, J., Rönkkö, T. (2017). Exhaust particle characteristics and number emission factors for marine diesel engine using different fuels. (manuscript in prep.).
- Lack, D.A. et al., 2014. Characterizing elemental, equivalent black, and refractory black carbon aerosol particles: A review of techniques, their limitations and uncertainties. *Analytical and Bioanalytical Chemistry*, 406(1), pp.99–122.
- Lappi, M.K. & Ristimäki, J.P., 2017. Evaluation of thermal optical analysis method of elemental carbon for marine fuel exhaust. *Journal of the Air & Waste Management Association* ISSN: (In press).
- Lim, S. et al., 2014. Absorption and scattering properties of organic carbon versus sulfate dominant aerosols at Gosan climate observatory in Northeast Asia. *Atmospheric Chemistry and Physics*, 14(15), pp.7781–7793. Available at: <http://www.atmos-chem-phys.net/14/7781/2014/acp-14-7781-2014.html> <http://www.atmos-chem-phys.net/14/7781/2014/>.
- Lipsky, E.M. & Robinson, A.L., 2006. Effects of dilution on fine particle mass and partitioning of semivolatile organics in diesel exhaust and wood smoke. *Environmental Science and Technology*, 40(1), pp.155–162.
- Long, C.M., Nascarella, M.A. & Valberg, P.A., 2013. Carbon black vs . black carbon and other airborne materials containing elemental carbon : Physical and chemical distinctions. *Environmental Pollution*, 181, pp.271–286. Available at: <http://dx.doi.org/10.1016/j.envpol.2013.06.009>.
- Lyyräinen, J., Jokiniemi, J., Kauppinen, E. and Joutsensaari, J. (1999). Aerosol characterisation in medium-speed diesel engines operating with heavy fuels. *Journal of Aerosol Science*, 30(6), 771-784.
- Maenhaut, W. 2009. Principles of thermal methods for the detection and differentiation of EC and OC, intercomparison results. In the Kuhlbusch, T. et al., JRC Scientific and Technical Reports by “Measurement of Elemental and Organic Carbon in Europe. Report of the preparatory workshop for a future standard measurement method”. JRC 54045. DOI 10.2788/34791. © European Communities, 2009.
- McCormick, R. et al., 2001. Impact of Biodiesel Source Material and Chemical Structure on Emissions of Criteria Pollutants from a Heavy-Duty Engine. *Env. Sci. & Technol.*, 35(9), pp.1742–1747.
- McGill, R. et al., 2003. Emission Performance of Selected Biodiesel Fuels. SAE Technical Paper Series, 2003-01–18.
- Mejía-Centeno, I., Martínez-Hernández, A. & Fuentes, G.A., 2007. Effect of low-sulfur fuels upon NH<sub>3</sub> and N<sub>2</sub>O emission during operation of commercial three-way catalytic converters. *Topics in Catalysis*, 42–43(1–4), pp.381–385.
- Murtonen, T., Aakko-Saksa, P., Kuronen, M., Mikkonen, S., Lehtoranta, K. 2010. Emissions with heavy-duty diesel engines and vehicles using FAME, HVO and GTL fuels with and without DOC+POC aftertreatment. *SAE International Journal of Fuels and Lubricants*, 2(2), pp.147–166.
- Murtonen, T. et al., 2012. Emission reduction potential with paraffinic renewable diesel by optimizing engine settings or using oxygenate. *SAE Technical Papers*, 9.
- Needham, 1991. Dieselnet. (<https://dieselnet.com/>), accessed December 2016.
- Neste, 1987. Öljykattilalaitoksen käyttö- ja suunnittelutietoa (In Finnish),
- Ntziachristos, L., Saukko, E., Lehtoranta, K., Rönkkö, T., Timonen, H., Simonen, P., &

- Karjalainen, P. 2016. Impact of sampling conditions and procedure on particulate matter emissions from a marine diesel engine. CIMAC Congress 2010.
- Nylund, N.O., Aakko, P., Mikkonen, S. and Niemi, A., 1997. Effects of Physical and Chemical Properties of Diesel Fuel on NO<sub>x</sub> Emissions of Heavy-Duty Diesel Engines. Society of Automotive Engineers, (Technical Paper 972997), p.11.
- Onasch, T. B., Trimborn, A., Fortner, E. C., Jayne, J. T., Kok, G. L., Williams, L. R., Davidovits, P., and Worsnop, D. R.: Soot Particle Aerosol Mass Spectrometer: Development, Validation, and Initial Application, *Aerosol Science and Technology*, 46, 804-817, 10.1080/02786826.2012.663948, 2012.
- Ortega, A. M. et al., 2013. Secondary organic aerosol formation and primary organic aerosol oxidation from biomass burning smoke in a flow reactor during FLAME-3” *Atmospheric Chemistry and Physics Discussions*, 13(5), 2013, pp. 13799-13851, doi:10.5194/acpd-13-13799-2013.
- Panteliadis, P. et al., 2015. ECOC comparison exercise with identical thermal protocols after temperature offset correction - Instrument diagnostics by in-depth evaluation of operational parameters. *Atmospheric Measurement Techniques*, 8(2), pp.779–792.
- Petzold, A. et al., 2013. Recommendations for reporting black carbon measurements. *Atmospheric Chemistry and Physics*, 13(16), pp.8365–8379.
- Petzold, A., Kramer, H. & Scölliner, M., 2002. Continuous Measurement of Atmospheric Black Carbon Using a Multi-Angle Absorption Photometer. *Environ. Sci. & Pollout, Res.*, 4, p.78–82.
- Quinn, P. et al., 2011. AMAP, 2011. The impact of black carbon on Arctic climate., Available at: <http://forskningbasen.deff.dk/Share.external?sp=S39b23054-f90c-4eb7-885a-846f62d83a76&sp=Sau>.
- Ramana, M. V. & Devi, A., 2016. CCN concentrations and BC warming influenced by maritime ship emitted aerosol plumes over southern Bay of Bengal. *Scientific Reports*, 6(August), p.30416. Available at: <http://www.nature.com/articles/srep30416>.
- Ristimäki, J., Hellen, G. & Lappi, M., 2010. Chemical and physical characterization of exhaust particulate matter from a marine medium speed diesel engine. CIMAC Congress 2010, Paper # 73, p.11.
- Rostedt, A. et al., 2014. Characterization and Response Model of the PPS-M Aerosol Sensor. *Aerosol Science and Technology*, 6826(September), pp.37–41.
- Rönkkö, T., Virtanen, A., Vaaraslahti, K., Keskinen, J., Pirjola, L., & Lappi, M. 2006. Effect of dilution conditions and driving parameters on nucleation mode particles in diesel exhaust: Laboratory and on-road study. *Atmospheric Environment*, 40, 2893–2901. doi:10.1016/j.atmosenv.2006.01.002
- Rönkkö, T. et al., 2011. "Diesel Exhaust Nanoparticle Volatility Studies by a New Thermodenuder with Low Solid Nanoparticle Losses" Abstracts in the 15th ETH. In Conference on Combustion Generated Nanoparticles, 26-29 June, 2011, Zürich, Switzerland.
- Saarikoski, S. et al., 2008. Sources of organic carbon in fine particulate matter in northern European urban air. *Atmospheric Chemistry and Physics*, 8, pp.6281–6295.
- Saarikoski, S. et al., 2017. Investigating the chemical species in submicron particles emitted by city buses. *Aerosol Science and Technology*, 51(3), pp.317–329. Available at: <http://dx.doi.org/10.1080/02786826.2016.1261992>.

- Sharp, C.A., Howell, S.A. & Jobe, J., 2000. The Effect of Biodiesel Fuels on Transient Emissions from Modern Diesel Engines, Part I Regulated Emissions and Performance. SAE Technical Paper Series, 2000-01-19.
- Shiju, N.R., 2004. Supported vanadium oxide catalysts in oxidation and oxidative dehydrogenation reactions: structure and catalytic properties.
- Sippula, O. et al., 2014. Particle emissions from a marine engine: Chemical composition and aromatic emission profiles under various operating conditions. *Environmental Science and Technology*, 48(19), pp.11721–11729.
- Stuart, D.D., 2010. Acid Dewpoint Temperature Measurement and Its Use in Estimating Sulfur Trioxide Concentration. *Analysis Division Symposium*, pp.12–24.
- Suominen, A., 2011. Emission control and fuels for marine sector. Future fuels for engine power plants seminar, Helsinki, 22 November 2011.
- Timonen, H., Aakko-Saksa, P., Kuittinen, N., Karjalainen, P., Murtonen, T., Lehtoranta, K., Vesala, H., Bloss, M., Saarikoski, S., Koponen, P., Piimäkorpi, P. and Rönkkö, T. 2017. Black carbon measurement validation onboard (SEA-EFFECTS BC WP2), Research Report VTT-R-04493-17.
- Viana, M. et al., 2007. Comparative analysis of organic and elemental carbon concentrations in carbonaceous aerosols in three European cities. *Atmospheric Environment*, 41, pp.5972–5983.
- Viidanoja, J. et al., 2002. Organic and black carbon in PM<sub>2.5</sub> and PM<sub>10</sub>: 1 year of data from an urban site in Helsinki, Finland. *Atmospheric Environment*, 36, pp.3183–3193.
- Wentzel, M. et al., 2003. Transmission electron microscopical and aerosol dynamical characterization of soot aerosols. *Journal of Aerosol Science*, 34(10), pp.1347–1370.
- Winther, M. et al., 2014. Emission inventories for ships in the arctic based on satellite sampled AIS data. *Atmospheric Environment*, 91, pp.1–14. Available at: <http://dx.doi.org/10.1016/j.atmosenv.2014.03.006>.
- Yang, M. et al., 2009. Attribution of aerosol light absorption to black carbon, brown carbon, and dust in China &ndash; interpretations of atmospheric measurements during EAST-AIRE. *Atmospheric Chemistry and Physics Discussions*, 8(2), pp.10913–10954.
- Zhang, X. L., Lin, Y. H., Surratt, J. D., Zotter, P., Prevot, A. S. H., and Weber, R. J.: Light-absorbing soluble organic aerosol in Los Angeles and Atlanta: A contrast in secondary organic aerosol, *Geophysical Research Letters*, 38, ArtnL2181010.1029/2011gl049385, 2011.

## Appendix 1. Results in different units

Average concentrations (mass per Sm <sup>3</sup> ).			75% load				25% load			
			0.1% S	0.5% S	2.5% S	Bio30	0.1% S	0.5% S	2.5% S	Bio30
NO <sub>x</sub>		g/Sm <sup>3</sup>	2,0	2,0	2,0	2,1	1,2	1,1	1,2	1,3
HC		g/Sm <sup>3</sup>	0,1	0,1	0,1	0,1	0,2	0,1	0,1	0,1
CO		g/Sm <sup>3</sup>	0,1	0,1	0,1	0,1	0,1	0,2	0,2	0,1
CO <sub>2</sub>		g/Sm <sup>3</sup>	117	118	123	117	97	97	105	97
O <sub>2</sub> (dry)		%	11,7	12,4	12,5	12,2	13,2	13,9	13,9	13,8
H <sub>2</sub> O	FTIR	g/Sm <sup>3</sup>	50	49	42	52	43	43	38	44
NO <sub>2</sub>	FTIR	mg/Sm <sup>3</sup>	51	26	15	49	37	9	9	35
CH <sub>4</sub>	FTIR	mg/Sm <sup>3</sup>	1,3	0,5	1,0	1,1	2,4	6,0	5,8	2,2
N <sub>2</sub> O	FTIR	mg/Sm <sup>3</sup>	<2	2,4	2,1	<2	<2	2,2	2,4	<2
NH <sub>3</sub>	FTIR	mg/Sm <sup>3</sup>	<2	<2	<2	<2	<2	<2	<2	<2
SO <sub>2</sub>	FTIR	mg/Sm <sup>3</sup>	63	307	1912	5	51	254	1618	2
C <sub>2</sub> H <sub>4</sub>	FTIR	mg/Sm <sup>3</sup>	2,9	5,7	2,1	3,3	4,2	6,3	0,9	4,7
HCHO	FTIR	mg/Sm <sup>3</sup>	<2	3,5	3,6	2,0	2,8	3,3	3,0	4,4
CH <sub>3</sub> CHO	FTIR	mg/Sm <sup>3</sup>	<2	<2	<2	<2	<2	<2	<2	<2
PM	ISO 8178 (SPC)	mg/Sm <sup>3</sup>	20,5	43,7	152,9	17,9	63,5	102,9	134,2	52,5
PM	EN 13284-1 (in-stack)	mg/Sm <sup>3</sup>	9,5	15,8	99,8	6,9	25,5	55,9	134,6	14,8
PM	PPS-M	mg/Sm <sup>3</sup>	1,2	13,7	109,0	1,1	11,6	25,0	101,5	8,0
BC	AVL 4155	mg/Sm <sup>3</sup>	2,0	2,4	5,8	1,4	12,1	25,9	13,6	6,4
BC	AVL 415SE	mg/Sm <sup>3</sup>	2,0	2,3	5,6	1,4	11,9	26,1	13,1	6,3
BC	AVL MSS	mg/Sm <sup>3</sup>	1,9	1,8	3,8	1,3	13,1	25,8	9,0	6,5
BC	MAAP	mg/Sm <sup>3</sup>	2,2	2,4	5,8	1,5	er	er	11,1	er
BC	AE33	mg/Sm <sup>3</sup>	1,9	1,7	4,4	1,3	16,2	31,1	9,6	11,0
BC	AE42	mg/Sm <sup>3</sup>	2,1	2,6	5,5	1,6	14,9	25,1	12,7	10,8
EC	PM: ISO 8178 (SPC)EUSAAR2	mg/Sm <sup>3</sup>	2,0	2,1	4,6	1,3	10,7	22,8	10,7	5,5
EC	PM: in-stack, EN 13284-1EUSAAR2	mg/Sm <sup>3</sup>	1,8	2,6	4,3	1,3	10,2	20,6	11,2	5,2
PM: mSD4		mg/Sm <sup>3</sup>	0,9	2,6	18,3	1,1	0,7	2,1	16,4	0,2
PM: H <sub>2</sub> SO <sub>4</sub>		mg/Sm <sup>3</sup>	0,2	4,0	38,5	0,7	0,0	1,1	15,9	0,7
PM: NO <sub>3</sub>		mg/Sm <sup>3</sup>	0,1	0,0	0,3	0,1	0,4	0,3	0,1	0,2
PM: PO <sub>4</sub> , Br, Cl, F		mg/Sm <sup>3</sup>	0,2	0,0	0,0	0,1	0,3	0,1	0,1	0,2
PM: heavy OC		mg/Sm <sup>3</sup>	0,9	1,6	5,6	0,9	4,1	7,0	14,3	3,7
PM: light OC		mg/Sm <sup>3</sup>	13,3	22,6	12,4	9,7	41,6	64,0	38,2	33,1
PM: metals		mg/Sm <sup>3</sup>	0,6	1,1	8,9	0,5	0,8	1,4	10,9	0,7
PM: EC		mg/Sm <sup>3</sup>	2,0	2,1	4,6	1,3	10,7	22,8	10,7	5,5
Rest of PM		mg/Sm <sup>3</sup>	2,4	9,6	64,2	3,6	4,8	4,1	27,7	8,2
Ca		mg/Sm <sup>3</sup>	0,4	0,3	0,5	0,2	0,5	0,7	1,0	0,4
Fe		mg/Sm <sup>3</sup>	0,0	0,1	0,3	0,0	0,1	0,1	0,1	0,0
Mg		mg/Sm <sup>3</sup>	0,0	0,0	0,1	0,0	0,0	0,0	0,0	0,0
Mo		mg/Sm <sup>3</sup>	0,0	0,0	0,0	0,0	0,0	0,1	0,0	0,1
Na		mg/Sm <sup>3</sup>	0,0	0,1	0,4	0,0	0,0	0,2	0,1	0,1
Ni		mg/Sm <sup>3</sup>	0,0	0,1	1,7	0,0	0,0	0,1	1,4	0,0
P		mg/Sm <sup>3</sup>	0,0	0,0	0,0	0,0	0,0	0,1	0,1	0,0
V		mg/Sm <sup>3</sup>	0,0	0,1	5,9	0,0	0,0	0,0	8,1	0,0
benz(a)anthracene*		µg/Sm <sup>3</sup>	2,0	2,7	0,6	0,7	1,9	3,5	2,6	1,2
chrysene*		µg/Sm <sup>3</sup>	3,2	5,2	3,9	1,7	3,9	7,8	6,8	2,9
benzo(b)fluoranthene*		µg/Sm <sup>3</sup>	0,8	1,2	0,6	0,3	0,5	1,4	1,1	0,5
benzo(k)fluoranthene*		µg/Sm <sup>3</sup>	0,6	0,9	0,3	0,4	0,5	1,0	0,7	0,5
benzo(a)pyrene*		µg/Sm <sup>3</sup>	0,1	0,3	0,1	0,0	0,1	1,0	0,3	0,1
indeno(1,2,3-cd)pyrene*		µg/Sm <sup>3</sup>	0,0	0,2	0,0	0,0	0,0	0,4	0,3	0,1
dibenz(a,h)anthracene*		µg/Sm <sup>3</sup>	0,0	0,2	0,1	0,0	0,0	0,4	0,3	0,0
PAH7		µg/Sm <sup>3</sup>	6,9	10,8	5,8	3,2	7,1	15,6	12,3	5,5

Sm<sup>3</sup> = Volumetric flow in standardized conditions, 273.15 K and 101325 Pa.

**Average emissions (mass per kg oil equivalent).**

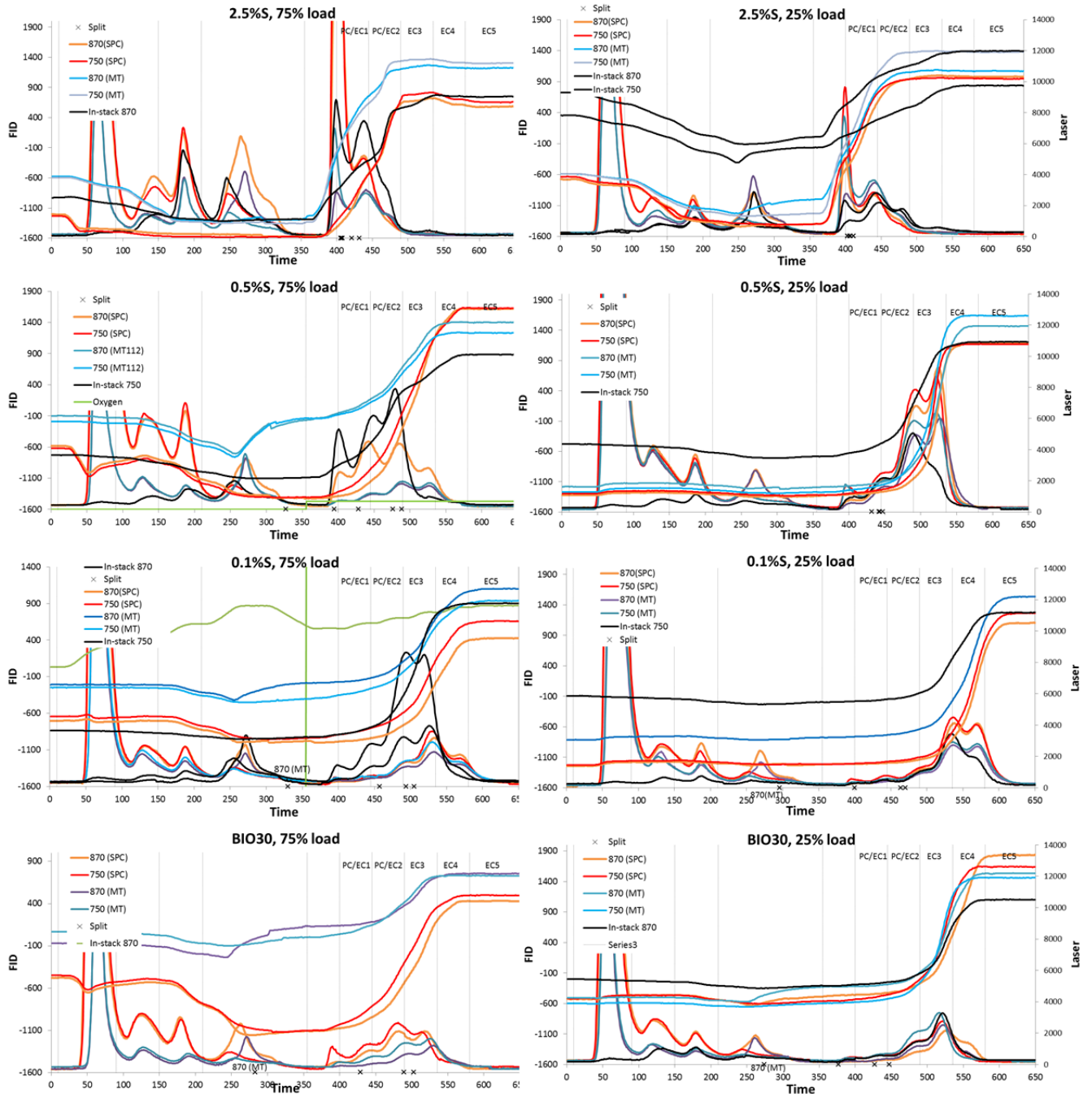
		75% load				25% load				
		0.1% S	0.5% S	2.5% S	Bio30	0.1% S	0.5% S	2.5% S	Bio30	
NO <sub>x</sub>	g/kgoe	54,1	54,2	52,3	56,0	39,9	35,3	36,7	40,8	
HC	g/kgoe	2,5	1,5	1,8	2,3	5,5	3,4	3,6	4,5	
CO	g/kgoe	1,6	2,3	3,2	1,5	4,3	6,2	7,8	4,0	
CO <sub>2</sub>	g/kgoe	3152	3180	3303	3140	3149	3176	3298	3139	
O <sub>2</sub> (dry)	%	11,7	12,4	12,5	12,2	13,2	13,9	13,9	13,8	
H <sub>2</sub> O	FTIR	g/kgoe	1335	1332	1133	1389	1404	1393	1184	1426
NO <sub>2</sub>	FTIR	mg/kgoe	1378	694	406	1303	1195	282	276	1126
CH <sub>4</sub>	FTIR	mg/kgoe	36	14	26	28	78	197	182	72
N <sub>2</sub> O	FTIR	mg/kgoe	<50	64	56	<50	<50	73	76	<50
NH <sub>3</sub>	FTIR	mg/kgoe	bd	bd	bd	bd	bd	bd	bd	
SO <sub>2</sub>	FTIR	mg/kgoe	1692	8264	51208	138	1649	8294	51056	55
C <sub>2</sub> H <sub>4</sub>	FTIR	mg/kgoe	79	154	56	89	135	207	28	152
HCHO	FTIR	mg/kgoe	<50	94	96	52	90	107	93	143
CH <sub>3</sub> CHO	FTIR	mg/kgoe	<50	<50	<50	<50	<50	<50	<50	
PM	ISO 8178 (SPC)	mg/kgoe	551	1175	4094	480	2065	3366	4235	1703
PM	EN 13284-1 (in-stack)	mg/kgoe	255	425	2674	185	828	1827	4248	481
PM	PPS-M	mg/kgoe	33	369	2917	30	379	817	3203	260
BC	AVL 415S	mg/kgoe	53	65	155	37	395	847	430	208
BC	AVL 415SE	mg/kgoe	54	63	150	37	388	853	415	205
BC	AVL MSS	mg/kgoe	51	49	101	34	427	844	285	211
BC	MAAP	mg/kgoe	58	65	156	41	295	466	350	240
BC	AE33	mg/kgoe	52	46	116	34	529	1017	302	357
BC	AE42	mg/kgoe	56	71	146	43	484	819	401	352
EC	PM: ISO8178 (SPC)EUSAAR2	mg/kgoe	53	57	124	34	348	744	336	178
EC	PM: in-stack, EN 13284-1EUSAAR2	mg/kgoe	48	69	114	35	332	673	354	167
PM: mSO <sub>4</sub>	mg/kgoe	25	71	490	30	22	68	518	8	
PM: H <sub>2</sub> SO <sub>4</sub>	mg/kgoe	6	107	1031	17	0	35	500	23	
PM: NO <sub>3</sub>	mg/kgoe	2,8	0,1	8,7	1,7	12,7	11,4	2,1	5,2	
PM: PO <sub>4</sub> , Br, Cl, F	mg/kgoe	4,5	0,5	0,0	3,8	10,3	3,4	2,6	6,9	
PM: heavy OC	mg/kgoe	24	43	149	24	134	229	452	120	
PM: light OC	mg/kgoe	357	609	332	259	1354	2094	1205	1074	
PM: metals	mg/kgoe	15	28	240	14	28	47	345	23	
PM: EC	mg/kgoe	53	57	124	34	348	744	336	178	
Rest of PM	mg/kgoe	64	258	1719	96	156	133	873	266	
Ca	mg/kgoe	10,2	9,3	13,4	5,3	16,8	22,9	30,4	12,6	
Fe	mg/kgoe	0,7	3,9	6,8	0,7	1,9	2,0	4,6	1,4	
Mg	mg/kgoe	0,3	0,3	2,2	0,0	0,3	1,6	1,5	0,3	
Mo	mg/kgoe	1,0	0,7	0,0	0,0	1,5	3,3	0,0	1,7	
Na	mg/kgoe	0,6	3,7	11,1	0,0	1,0	7,6	3,2	3,5	
Ni	mg/kgoe	0,0	3,7	45,9	0,1	0,0	3,3	44,2	0,0	
P	mg/kgoe	0,5	0,6	0,5	0,6	1,5	3,4	1,8	1,6	
V	mg/kgoe	0,2	1,7	158,0	0,7	0,3	1,6	255,0	0,7	
benz(a)anthracene*	µg/kgoe	54,6	73,4	16,2	19,9	62,3	115,1	80,6	37,8	
chrysene*	µg/kgoe	86,9	138,9	105,2	45,3	125,9	254,0	213,4	95,0	
benzo(b)fluoranthene*	µg/kgoe	20,8	33,2	16,5	8,9	16,7	44,3	34,4	17,2	
benzo(k)fluoranthene*	µg/kgoe	15,3	23,1	9,1	9,6	15,0	31,4	21,1	15,4	
benzo(a)pyrene*	µg/kgoe	2,0	6,8	1,7	0,5	4,6	32,3	8,2	4,3	
indeno(1,2,3-cd)pyrene*	µg/kgoe	0,9	4,4	1,1	0,4	1,2	11,7	10,3	1,8	
dibenz(a,h)anthracene*	µg/kgoe	0,4	4,6	1,5	0,1	0,4	12,7	9,0	0,5	
PAH7	µg/kgoe	184,5	290,1	155,0	86,8	231,4	510,9	388,0	177,3	

**Average emissions (mass per kWh).**

			75% load				25% load			
			0.1%S	0.5%S	2.5%S	Bio30	0.1%S	0.5%S	2.5%S	Bio30
NO <sub>x</sub>	ISO 8178	g/kWh	11,0	11,1	10,9	11,3	9,4	8,5	8,9	9,5
HC	ISO 8178	g/kWh	0,50	0,31	0,38	0,46	1,29	0,81	0,87	1,04
CO	ISO 8178	g/kWh	0,32	0,46	0,66	0,30	1,02	1,49	1,89	0,93
CO <sub>2</sub>	ISO 8178	g/kWh	642	650	686	633	745	766	798	730
O <sub>2</sub> (dry)	ISO 8178	%	11,7	12,4	12,5	12,2	13,2	13,9	13,9	13,8
H <sub>2</sub> O	FTIR	g/kWh	272	272	235	280	332	336	287	332
NO <sub>2</sub>	FTIR	mg/kWh	281	142	84	263	283	68	67	262
CH <sub>4</sub>	FTIR	mg/kWh	7,3	2,8	5,4	5,7	18,5	47,6	44,1	16,8
N <sub>2</sub> O	FTIR	mg/kWh	<10	13,0	11,6	<10	11,9	17,5	18,5	11,0
NH <sub>3</sub>	FTIR	mg/kWh	bd	bd	bd	bd	bd	bd	bd	bd
SO <sub>2</sub>	FTIR	mg/kWh	345	1690	10638	28	390	1939	12356	13
C <sub>2</sub> H <sub>4</sub>	FTIR	mg/kWh	16,1	31,4	11,5	18,0	32,0	49,9	6,8	35,4
HCHO	FTIR	mg/kWh	<10	19,2	20,0	10,5	21,2	25,8	22,6	33,2
CH <sub>3</sub> CHO	FTIR	mg/kWh	<10	<10	<10	<10	<10	<10	<10	<10
PM	ISO 8178 (SPC)	mg/kWh	112	240	851	97	488	811	1025	396
PM	EN 13284-1 (in-stack)	mg/kWh	52	87	555	37	196	440	1028	112
PM	PPS-M	mg/kWh	7	76	606	6	90	197	775	60
BC	AVL 415S	mg/kWh	11	13	32	8	93	204	104	48
BC	AVL 415SE	mg/kWh	11	13	31	7	92	205	100	48
BC	AVL MSS	mg/kWh	10	10	21	7	101	203	69	49
BC	MAAP	mg/kWh	12	13	32	8	70	112	85	56
BC	AE33	mg/kWh	11	9	24	7	125	245	73	83
BC	AE42	mg/kWh	11	14	30	9	114	197	97	82
EC	PM: ISO8178 (SPC)EUSAAR2	mg/kWh	11	12	26	7	82	179	81	41
EC	PM: in-stack, EN 13284-1EUSAAR2	mg/kWh	10	14	24	7	78	162	86	39
PM: mSO <sub>4</sub>		mg/kWh	5,0	14,5	101,9	6,0	5,3	16,4	125,5	1,8
PM: H <sub>2</sub> SO <sub>4</sub>		mg/kWh	1,1	21,9	214,1	3,5	0,0	8,5	121,1	5,2
PM: NO <sub>3</sub>		mg/kWh	0,6	0,0	1,8	0,3	3,0	2,7	0,5	1,2
PM: PO <sub>4</sub> , Br, Cl, F		mg/kWh	0,9	0,1	0,0	0,8	2,4	0,8	0,6	1,6
PM: heavy OC		mg/kWh	5,0	8,8	31,0	4,9	31,7	55,1	109,4	28,0
PM: light OC		mg/kWh	72,8	124,6	69,1	52,2	320,1	504,7	291,6	250,0
PM: metals		mg/kWh	3,1	5,8	49,8	2,9	6,5	11,3	83,5	5,3
PM: EC		mg/kWh	10,8	11,8	25,9	6,9	82,3	179,4	81,4	41,4
Rest of PM		mg/kWh	13,1	52,8	357,1	19,3	37,0	32,1	211,2	61,8
Ca		mg/kWh	2,1	1,9	2,8	1,1	4,0	5,5	7,3	2,9
Fe		mg/kWh	0,1	0,8	1,4	0,1	0,4	0,5	1,1	0,3
Mg		mg/kWh	0,1	0,1	0,5	0,0	0,1	0,4	0,4	0,1
Mo		mg/kWh	0,2	0,1	0,0	0,0	0,4	0,8	0,0	0,4
Na		mg/kWh	0,1	0,8	2,3	0,0	0,2	1,8	0,8	0,8
Ni		mg/kWh	0,0	0,8	9,5	0,0	0,0	0,8	10,7	0,0
P		mg/kWh	0,1	0,1	0,1	0,1	0,3	0,8	0,4	0,4
V		mg/kWh	0,0	0,3	32,8	0,1	0,1	0,4	61,7	0,2
benz(a)anthracene*		µg/kWh	11,13	15,02	3,37	4,01	14,72	27,73	19,50	8,79
chrysene*		µg/kWh	17,70	28,40	21,84	9,13	29,77	61,22	51,64	22,10
benzo(b)fluoranthene*		µg/kWh	4,24	6,79	3,42	1,79	3,96	10,68	8,32	4,00
benzo(k)fluoranthene*		µg/kWh	3,12	4,73	1,90	1,93	3,54	7,56	5,11	3,58
benzo(a)pyrene*		µg/kWh	0,40	1,38	0,35	0,11	1,09	7,78	1,99	1,00
indeno(1,2,3-cd)pyrene*		µg/kWh	0,19	0,89	0,22	0,08	0,28	2,81	2,48	0,41
dibenz(a,h)anthracene*		µg/kWh	0,07	0,94	0,30	0,02	0,09	3,06	2,18	0,12
PAH7		µg/kWh	37,58	59,33	32,20	17,51	54,73	123,13	93,90	41,26

## Appendix 2. Example of thermograms using NIOSH 5040

Examples of thermograms using NIOSH 5040 program with 870 and 750 °C peak temperatures in the inert phase.



### Appendix 3. Yellow punch after the EC/OC analysis

Native loaded filter punch (Näyte 2), yellow punch after thermo-optical analysis (Näyte 1) and blank punch (Näyte 3) were analysed using a scanning electron microscope (SEM) and energy-dispersive X-ray spectroscopy (EDS), and back-scattered electrons (BE), which detects carbon (C) and heavier elements. Lighter elements and low concentrations (<0,5%) may not be detected.



For yellow punch (1) mainly vanadium (V) and slightly calcium (Ca) and nickel (Ni) were observed besides quartz filter elements (Si and O). Loaded punch (2) contains sulphur (S), vanadium and slightly calcium (Ca) and nickel (Ni) besides quartz filter elements (Si, O).

